KIT
Karlsruhe Institute of Technology

Analysis and Optimization of Convolutional Neural Network Architectures

Master Thesis of

Martin Thoma

Department of Computer Science
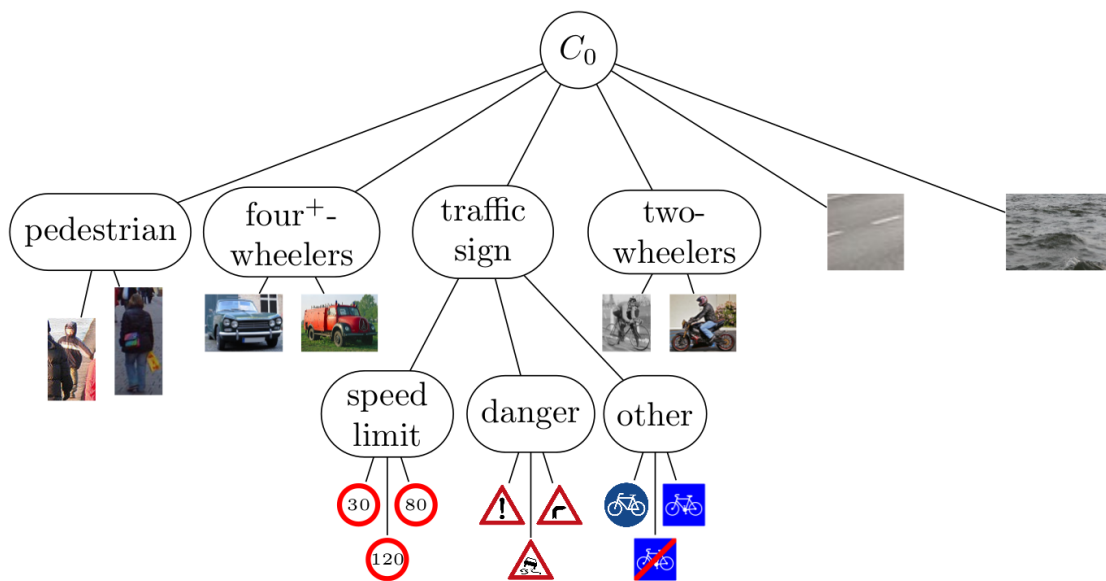Institute for Anthropomatics
and
FZI Research Center for Information Technology

Reviewer: Prof. Dr.–Ing. R. Dillmann
Second reviewer: Prof. Dr.–Ing. J. M. Zöllner
Advisor: Dipl.–Inform. Michael Weber

Research Period: 03. May 2017 – 03. August 2017

www.kit.edu

Analysis and Optimization of Convolutional Neural Network Architectures

by
Martin Thoma

Master Thesis
August 2017

Affirmation

Ich versichere wahrheitsgemäß, die Arbeit selbstständig angefertigt, alle benutzten Hilfs-mittel vollständig und genau angegeben und alles kenntlich gemacht zu haben, was aus Arbeiten anderer unverändert oder mit Abänderungen entnommen wurde.

Karlsruhe,   *Martin Thoma*
August 2017

Abstract

Convolutional Neural Networks (CNNs) dominate various computer vision tasks since Alex Krizhevsky showed that they can be trained effectively and reduced the top-5 error from $26.2\,\%$ to $15.3\,\%$ on the ImageNet large scale visual recognition challenge. Many aspects of CNNs are examined in various publications, but literature about the analysis and construction of neural network architectures is rare. This work is one step to close this gap. A comprehensive overview over existing techniques for CNN analysis and topology construction is provided. A novel way to visualize classification errors with confusion matrices was developed. Based on this method, hierarchical classifiers are described and evaluated. Additionally, some results are confirmed and quantified for CIFAR-100. For example, the positive impact of smaller batch sizes, averaging ensembles, data augmentation and test-time transformations on the accuracy. Other results, such as the positive impact of learned color transformation on the test accuracy could not be confirmed. A model which has only one million learned parameters for an input size of $32 \times 32 \times 3$ and 100 classes and which beats the state of the art on the benchmark dataset Asirra, GTSRB, HASYv2 and STL-10 was developed.

Zusammenfassung

Modelle welche auf Convolutional Neural Networks (CNNs) basieren sind in verschiedenen Aufgaben der Computer Vision dominant seit Alex Krizhevsky gezeigt hat dass diese effektiv trainiert werden können und er den Top-5 Fehler in dem ImageNet large scale visual recognition challenge Benchmark von 26.2% auf 15.3% drücken konnte. Viele Aspekte von CNNs wurden in verschiedenen Publikationen untersucht, aber es wurden vergleichsweise wenige Arbeiten über die Analyse und die Konstruktion von Neuronalen Netzen geschrieben. Diese Masterarbeit stellt einen Schritt dar um diese Lücke zu schließen. Eine umfassende Überblick über Analyseverfahren und Topologielernverfahren wird gegeben. Ein neues Verfahren zur Visualisierung der Klassifikationsfehler mit Konfusionsmatrizen wurde entwickelt. Basierend auf diesem Verfahren wurden hierarchische Klassifizierer eingeführt und evaluiert. Zusätzlich wurden einige bereits in der Literatur beschriebene Beobachtungen wie z.B. der positive Einfluss von kleinen Batch-Größen, Ensembles, Erhöhung der Trainingsdatenmenge durch künstliche Transformationen (Data Augmentation) und die Invarianzbildung durch künstliche Transformationen zur Test-Zeit (Test-time transformations) experimentell bestätigt. Andere Beobachtungen, wie beispielsweise der positive Einfluss gelernter Farbraumtransformationen konnten nicht bestätigt werden. Ein Modell welches weniger als eine Millionen Parameter nutzt und auf den Benchmark-Datensätzen Asirra, GTSRB, HASYv2 und STL-10 den Stand der Technik neu definiert wurde entwickelt.

Acknowledgment

This work can be cited the following way:

```
@MastersThesis{Thoma:2017,
    Title      = {Analysis and Optimization of Convolutional Neural Network
                   Architectures},
    Author     = {Martin Thoma},
    School     = {Karlsruhe Institute of Technology},
    Year       = {2017},

    Address    = {Karlsruhe, Germany},
    Month      = jun,
    Type       = {Masters's Thesis},

    Keywords   = {machine learning; artificial neural networks;
                   classification; supervised learning; CNNs},
    Url        = {https://martin-thoma.com/msthesis/}
}
```

A DVD with a digital version of this master thesis and the source code as well as the used data is part of this work.

Contents

1. Introduction

Computer vision is the academic field which aims to gain a high-level understanding of the low-level information given by raw pixels from digital images.

Robots, search engines, self-driving cars, surveillance agencies and many others have applications which include one of the following six problems in computer vision as sub-problems:

- **Classification**:[1] The algorithm is given an image and k possible classes. The task is to decide which of the k classes the image belongs to. For example, an image from a self-driving cars on-board camera contains either `paved road`, `unpaved road` or `no road`: Which of those given three classes is in the image?

- **Localization**: The algorithm is given an image and one class k. The task is to find bounding boxes for all instances of k.

- **Detection**: Given an image and k classes, find bounding boxes for all instances of those classes.

- **Semantic Segmentation**: Given an image and k classes, classify each pixel.

- **Instance segmentation**: Given an image and k classes, classify each pixel as one of the k classes, but distinguish different instances of the classes.

- **Content-based Image Retrieval**: Given an image x and n images in a database, find the top u images which are most similar to x.

There are many techniques to approach those problems, but since AlexNet [KSH12] was published, all of those problems have high-quality solutions which make use of Convolutional Neural Networks (CNNs) [HZRS15a, LAE$^+$16, RFB15, DHS16, SKP15].

Today, most neural networks are constructed by rules of thumb and gut feeling. The architectures evolved and got deeper, more hyperparameters were added. Although there are methods for analyzing CNNs, those methods are not enough to determine all steps in the development of network architectures without gut feeling. A detailed introduction to CNNs as well as nine methods for analysis of CNNs is given in Chapter 2.

---

[1]Classification is also called *identification* if the classes are humans. Another name is *object recognition*, although the classes can be humans and animals as well.

Despite the fact that most researchers and developers do not use topology learning, a couple of algorithms have been proposed for this task. Five classes of topology learning algorithms are introduced in Chapter 3.

When datasets and the number of classes are large, evaluating a single idea how to improve the network can take several weeks just for the training. Hence the idea of building a hierarchy of classifiers which allows to split the classification task into various sub-tasks that can easily be combined is evaluated in Chapter 4.

Confusion Matrix Ordering (CMO), the hierarchical classifier, 9 types of hyperparameters and label smoothing are evaluated in Chapter 5.

This work focuses on classification problems to keep the presented ideas as pure and simple as possible. The described techniques are relevant to all six described computer vision problems due to the fact that Encoder-Decoder architectures are one component of state-of-the-art algorithms for all six of them.

2. Convolutional Neural Networks

In the following, it is assumed that the reader knows what a multilayer perceptron (MLP) is and how they are designed for classification problems, what activation functions are and how gradient descent works. In case the reader needs a refresher on any of those topics, I recommend chapter 4.3 and 4.4 of [Tho14a] as well as [LBH15].

This chapter introduces linear image filters in Section 2.1, then standard layer types of CNNs are explained in Section 2.2. The layer block pattern is described in Section 2.3, transition layers in Section 2.4 and nine ways to analyze CNNs are described in Section 2.5.

2.1. Linear Image Filters

A *linear image filter* (also called a *filter bank* or a *kernel*) is an element $F \in \mathbb{R}^{k_w \times k_h \times d}$, where k_w represents the filter's width, k_h the filter's height and d the number of input channels. The filter F is convolved with the image $I \in \mathbb{R}^{w \times h \times d}$ to produce a new image I'. The output image I' has only one channel. Each pixel $I'(x, y)$ of the output image gets calculated by point-wise multiplication of one filter element with one element of the original image I:

$$I'(x, y) = \sum_{i_x = 1 - \lceil \frac{k_w}{2} \rceil}^{\lfloor \frac{k_w}{2} \rfloor} \sum_{i_y = 1 - \lceil \frac{k_h}{2} \rceil}^{\lfloor \frac{k_h}{2} \rfloor} \sum_{i_c = 1}^{d} I(x + i_x, y + i_y, i_c) \cdot F(i_x, i_y, i_c)$$

This procedure is explained by Figure 2.1. It is essentially a discrete convolution.
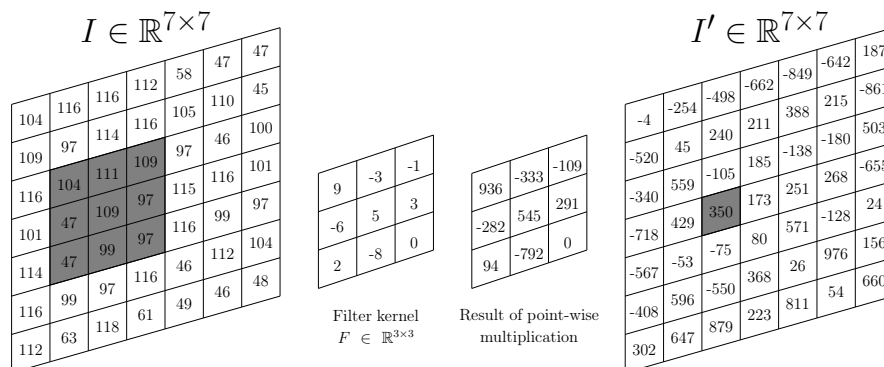

Figure 2.1.: Visualization of the application of a linear $k \times k \times 1$ image filter. For each pixel of the output image, k^2 multiplications and k^2 additions of the products have to be calculated.

One important detail is how boundaries are treated. There are four common ways of boundary treatment:

- **don't compute**: The image I' will be smaller than the original image. $I' \in \mathbb{R}^{(w-k_w+1)\times(h-k_h+1)\times d_3}$, to be exact.

- **zero padding**: The image I is padded by zeros where the filter would access elements which do not exist. This will result in edges being detected at the border if the border pixels are not black, but doesn't need any computation.

- **nearest**: Repeat the pixel which is closest to the boundary.

- **reflect**: Reflect the image at the boundaries.

Common tasks that can be done with linear filters include edge detection, corner detection, smoothing, sharpening, median filtering, box filtering. See Figure A.1 for five examples.

Please note that the result of a filtering operation is again an image. This means filters can be applied successively. While each pixel after one filtering operation with a 3×3 filter got influenced by $3 \cdot 3 = 9$ pixels of the original image, two successively applied 3×3 filters increase the area of the original image which influenced the output. The output is then influenced by 25 pixel. This is called the *receptive field*. The kind of pattern which is detected by a filter is called a *feature*. The bigger the receptive field is, the more complex can features get as they are able to consider more of the original image. Instead of taking one 5×5 filter with 25 parameters, one might consider to take two successive 3×3 filters with $2 \cdot (3 \cdot 3) = 18$ parameters. The 5×5 filter is a strict superset of possible filtering operations compared to the two 3×3 filters, but the relevance of this technique will become clear in Section 2.2.

2.2. CNN Layer Types

While the idea behind deep MLPs is that *feature hierarchies* capture the important parts of the input more easily, CNNs are inspired by the idea of *translational invariance*: Many features in an image are translationally invariant. For example, if a car is developed, one could try to detect it by its parts [FGMR10]. But then there are many positions at which the wheels could be. Combining those, it is desirable to capture low-level, translationally invariant features at lower layers of an artificial neural network (ANN) and in higher layers high-level features which are combinations of the low-level features.

Also, models should utilize the fact that the pixels of images are ordered. One way to use this is by learning image filters in so called *convolutional layers*.

While MLPs vectorize the input, the input of a layer in a CNN are *feature maps*. A feature map is a matrix $m \in \mathbb{R}^{w \times h}$, but typically the width equals the height ($w = h$). For an RGB

input image, the number of feature maps is $d = 3$. Each color channel is a feature map.

Since AlexNet [KSH12] almost halved the error in the ImageNet challenge, CNNs are state-of-the-art in various computer vision tasks.

Traditional CNNs have three important building tools:

- Convolutional layers with a non-linear activation function as described in Section 2.2.1,

- pooling layers as described in Section 2.2.2 and

- normalization layers as described in Section 2.2.4.

2.2.1. Convolutional Layers

Convolutional layers take several feature maps as input and produce n feature maps[1] as output, where n is the number of filters in the convolution layer. The filter weights of the linear convolutions are the parameters which are adapted to the training data. The number n of filters as well as the filter's size $k_w \times k_h$ are hyperparameters of convolutional layers. Sometimes, it is denoted as $n@k_w \times k_h$. Although the filter depth is usually omitted in the notation, the filters are of dimension $k_w \times k_h \times d^{(i-1)}$, where $d^{(i-1)}$ is the number of feature maps of the input layer $(i-1)$.

Another hyperparameter of convolution layers is the stride $s \in \mathbb{N}_{\geq 1}$ and the padding. Padding (usually zero-padding [SCL12, SEZ$^+$13, HZRS15a]) is used to make sure that the size of the feature maps doesn't change.

The hyperparameters of convolutional layers are

- the number of filters $n \in \mathbb{N}_{\geq 1}$,

- $k_w, k_h \in \mathbb{N}_{\geq 1}$ of the filter size $k_w \times k_h \times d^{(i-1)}$,

- the activation function of the layer (see Table B.3) and

- the stride $s \in \mathbb{N}_{\geq 1}$

Typical choices are $n \in \{32, 64, 128\}$, $k_w = k_h = k \in \{1, 3, 5, 11\}$ such as in [KSH12, SZ14, SLJ$^+$15], rectified linear unit (ReLU) activation and $s = 1$.

The concept of weight sharing is crucial for CNNs. This concept was introduced in [WHH$^+$89]. With weight sharing, the filters can be learned with stochastic gradient descent (SGD) just like MLPs. In fact, every CNN has an equivalent MLP which computes the same function if only the flattened output is compared.

---

[1] also called *activation maps* or *channels*

This is easier to see when the filtering operation is denoted formally:

$$o^{(i)}(\mathbf{x}) = b + \sum_{j=1}^{k} w_{ij} \cdot \mathbf{x}_j \qquad \text{with } i \in \{\,1,\ldots,w\,\} \times \{\,1,\ldots,h\,\} \times \{\,1,\ldots,d\,\} \qquad [2.1]$$

$$o^{(x,y,z)}(I) = b + \sum_{i_x=1-\lceil \frac{k_w}{2} \rceil}^{\lfloor \frac{k_w}{2} \rfloor} \sum_{i_y=1-\lceil \frac{k_h}{2} \rceil}^{\lfloor \frac{k_h}{2} \rfloor} \sum_{i_c=1}^{d} F_z(i_x, i_y, i_c) \cdot I(x+i_x, y+i_y, i_c) \qquad [2.2]$$

$$\text{with a bias } b \in \mathbb{R}, \ x \in \{\,1,\ldots,w\,\}, \ y \in \{\,1,\ldots,h\,\} \ \text{and} \ z \in \{\,1,\ldots,d\,\}$$

One can see that most weights of the equivalent MLP are zero and many weights are equivalent. Hence the advantage of CNNs compared to MLPs is the reduction of parameters. The effect of fewer parameters is that less training data is necessary to get suitable estimations for those. This means a MLP which is able to compute the same functions as a CNN will likely have worse results on the same dataset, if a CNN architecture is suitable for the dataset.

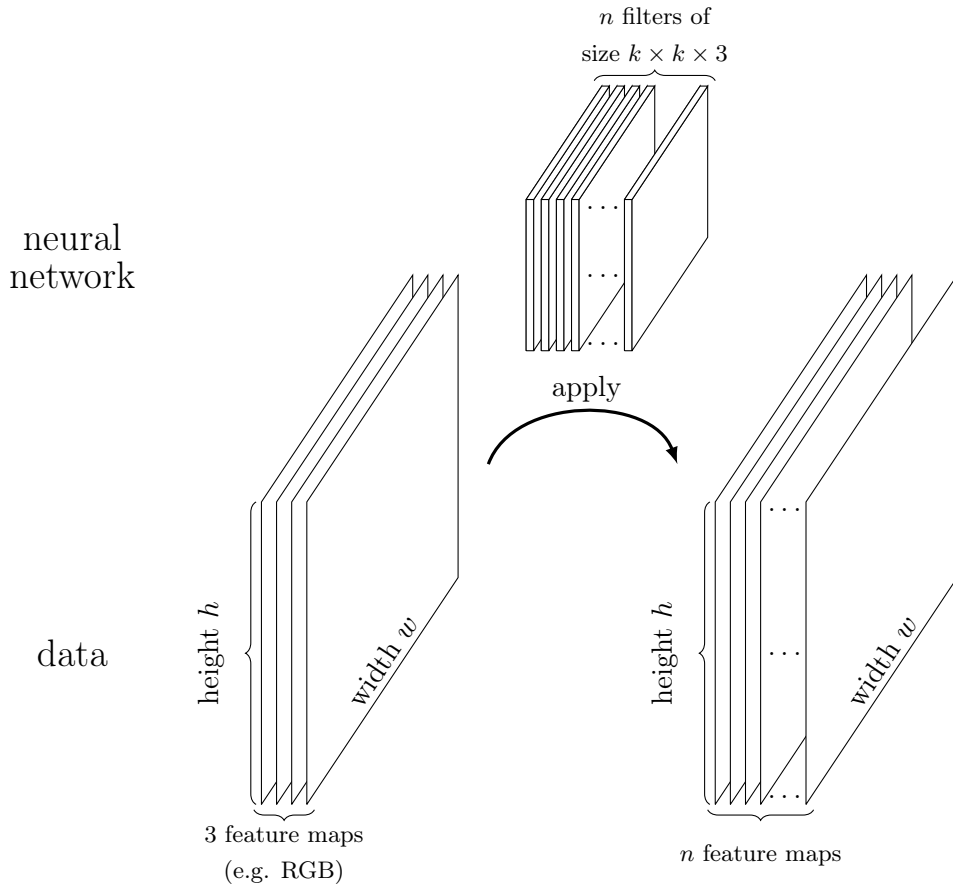See Figure 2.2 for a visualization of the application of a convolutional layer.

Figure 2.2.: Application of a single convolutional layer with n filters of size $k \times k \times 3$ with stride $s = 1$ to input data of size width $\times$ height with three channels.

A convolutional layer with n filters of size $k_w \times k_h$ and `SAME` padding after $d^{(i-1)}$ feature maps of size $s_x \times s_y$ has $n \cdot d^{(i-1)} \cdot (k_w \cdot k_h)$ parameters if no bias is used. In contrast, a fully connected layer which produces the same output size and does not use a bias would have $n \cdot d^{(i-1)} \cdot (s_x \times s_y)^2$ parameters. This means a convolutional layer has drastically fewer parameters. One the one hand, this means it can learn less complex decision boundaries. On the other hand, it means fewer parameters have to be learned and hence the optimization procedure needs fewer examples and the optimization objective is simpler.

It is particularly interesting to notice that even a convolutional layer of 1×1 filters does learn a linear combination of the d input feature maps. This can be used for dimensionality reduction, if there are fewer 1×1 filters in a convolutional layer than input feature maps. Another insight recently got important: Every fully connected layer has an equivalent convolutional layer which has the same weights.[2] This way, one can use the complete classification network as a very complex non-linear image filter which can be used for semantic segmentation.

A fully connected layer with $d \in \mathbb{N}_{\geq 1}$ inputs and $n \in \mathbb{N}_{\geq 1}$ nodes can be interpreted as a convolutional layer with an input of shape $1 \times 1 \times d$ and n filters of size 1×1. This will produce an output shape $1 \times 1 \times n$. Every single output is connected to all of the inputs.

When a convolutional layer is followed by a fully connected layer, it is necessary to vectorize to feature maps. If the 1×1 convolutional filter layer is applied to the vectorized output, it is completely equivalent to a fully connected layer. However, the vectorization can be omitted if a convolution layer without padding and a filter size equal to the feature maps size is applied. This was used by [LSD15].

2.2.2. Pooling Layers

Pooling summarizes a $p \times p$ area of the input feature map. Just like convolutional layers, pooling can be used with a stride of $s \in \mathbb{N}_{>1}$. As $s \geq 2$ is the usual choice, pooling layers are sometimes also called *subsampling layers*. Typically, $p \in \{\, 2, 3, 4, 5 \,\}$ and $s = 2$ such as for AlexNet [KSH12] and VGG-16 [SZ14].

The type of summary for the set of activations A varies between the functions listed in Table 2.1, spatial pyramid pooling as introduced in [HZRS14] and generalizing pooling functions as introduced in [LGT16].

---

[2]But convolutional layers only have equivalent fully connected layers if the output feature map is 1×1

Name	Definition	Used by
Max pooling	$\max \{\, a \in A \,\}$	[BPL10, KSH12]
Average / mean pooling	$\frac{1}{|A|} \sum_{a \in A} a$	LeNet-5 [LBBH98] and [KSlB$^+$10]
ℓ_2 pooling	$\sqrt{\sum_{a \in A} a^2}$	[Le13]
Stochastic pooling	*	[ZF13]

Table 2.1.: Pooling types for a set A of activations $a \in \mathbb{R}$.
(*) For stochastic pooling, each of the $p \times p$ activation values a_i in the pooling region gets picked with probability $p_i = \frac{a_i}{\sum_{a_j \in A} a_j}$. This assumes the activations a_i are non-negative.

Pooling is applied for three reasons: To get local translational invariance, to get invariance against minor local changes and, most important, for data reduction to $\frac{1}{s^2}$th of the data by using strides of $s > 1$.

See Figure 2.3 for a visualization of max pooling.
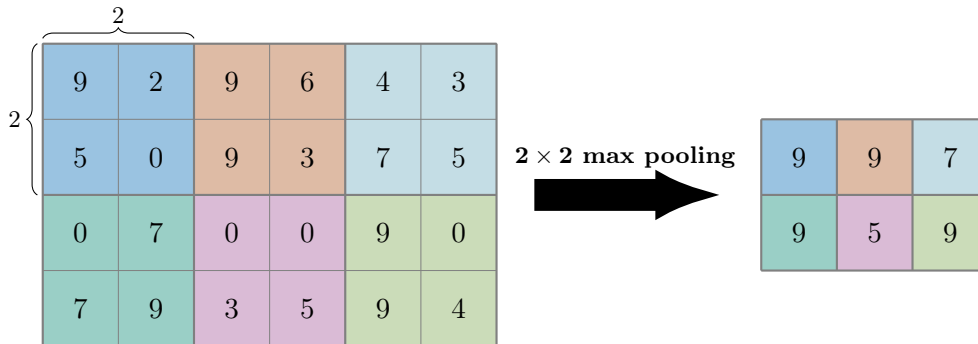
Figure 2.3.: 2×2 max pooling applied to a feature map of size 6×4 with stride $s = 2$ and padding.

Average pooling of $p \times p$ areas with stride s can be replaced by a convolutional layer. If the input of the pooling layer are $d^{(i-1)}$ feature maps, the convolutional layer has to have $d^{(i-1)}$ filters of size $p \times p$ and stride s. The ith filter has the values

$$\begin{pmatrix} \frac{1}{p^2} & \cdots & \frac{1}{p^2} \\ \vdots & \ddots & \vdots \\ \frac{1}{p^2} & \cdots & \frac{1}{p^2} \end{pmatrix}$$

for the dimension i and the zero matrix

$$\begin{pmatrix} 0 & \cdots & 0 \\ \vdots & \ddots & \vdots \\ 0 & \cdots & 0 \end{pmatrix}$$

for all other dimensions $i = 1, \ldots, d^{(i-1)}$.

2.2.3. Dropout

Dropout is a technique used to prevent overfitting and co-adaptations of neurons by setting the output of any neuron to zero with probability p. It was introduced in [HSK+12] and is well-described in [SHK+14].

A Dropout layer can be implemented as follows: For an input in of any shape s, a tensor of the same shape $D \in \{0, 1\}^s$ is sampled, where each element d_i is sampled independently from a Bernoulli distribution. The results are element-wise multiplied to calculate the output out of the Dropout layer:

$$\text{out} = D \odot \text{in} \qquad \text{with } d_i \sim B(1, p)$$

where $\odot$ is the Hadamard product

$$(A \odot B)_{i,j} := (A)_{i,j}(B)_{i,j}$$

Hence every value of the input gets set to zero with a dropout probability of p. Typically, Dropout is used with $p = 0.5$. Layers closer to the input usually have a lower dropout probability than later layers. In order to keep the expected output at the same value, the output of a dropout layer is multiplied with $\frac{1}{1-p}$ when dropout is enabled [Las17, tf-16b]. At inference time, dropout is disabled.

Dropout is usually only applied after fully connected layers, but not after convolutional layers as it usually increases the test error as pointed out in [GG16].

Models which use Dropout can be interpreted as an ensemble of models with different numbers of neurons in each layer, but also with weight sharing.

Conceptually similar are DropConnect and networks with stochastic depth. DropConnect [WZZ+13] is a generalization of Dropout, which sets weights to zero in contrast to setting the output of a neuron to zero. Networks with stochastic depth as introduced in [HSL+16] dropout only complete layers. This can be done by having Residual networks which have one identity connection and one residual feature connection. Hence the residual features can be dropped out and the identity connection remains.

2.2.4. Normalization Layers

One problem when training deep neural networks is *internal covariate shift*: While the parameters of layers close to the output are adapted to some input produced by lower layers, those lower layers parameters are also adapted. This leads to the parameters in the upper layers being worse. A very low learning rate has to be chosen to adjust for the fact that the input features might drastically change over time.

One way to approach this problem is by normalizing mini-batches as described in [IS15]. A Batch Normalization layer with d-dimensional input $x = (x^{(1)}, \ldots, x^{(d)})$ is first normalized point-wise to

$$\hat{x}^{(k)} = \frac{x^{(k)} - \bar{x}^{(k)}}{\sqrt{s'[x^{(k)}]^2 + \varepsilon}}$$

with $\bar{x}^{(k)} = \frac{1}{m} \sum_{i=1}^{m} x_i^{(k)}$ being the sample mean and $s'[x^{(k)}]^2 = \frac{1}{m} \sum_{i=1}^{m} (x_i^{(k)} - \bar{x}^{(k)})$ the sample variance where $m \in \mathbb{N}_{\geq 1}$ is the number of training samples per mini-batch, $\varepsilon > 0$ being a small constant to prevent division by zero and $x_i^{(k)}$ is the activation of neuron k for training sample i.

Additionally, for each activation $x^{(k)}$ two parameters $\gamma^{(k)}, \beta^{(k)}$ are introduced which scale and shift the feature:

$$y^{(k)} = \gamma^{(k)} \cdot \hat{x}^{(k)} + \beta^{(k)}$$

In the case of fully connected layers, this is applied to the activation, before the non-linearity is applied. If it is applied after the activation, it harms the training in early stages. For convolution, only one γ and one β is learned per feature map.

One important special case is $\gamma^{(k)} = \sqrt{s'[x^{(k)}]^2 + \varepsilon}$ and $\beta^{(k)} = \bar{x}^{(k)}$, which would make the Batch Normalization layer an identity layer.

During evaluation time,[3] the expected value and the variance are calculated once for the complete dataset. An unbiased estimate of the empirical variance is used.

The question where Batch Normalization layers (BN) should be applied and for which reasons is still open. For Dropout, it doesn't matter if it is applied before or after the activation function. Considering this, the possible options for the order are:

1. CONV / FC $\rightarrow$ BN $\rightarrow$ activation function $\rightarrow$ Dropout $\rightarrow \ldots$
2. CONV / FC $\rightarrow$ activation function $\rightarrow$ BN $\rightarrow$ Dropout $\rightarrow \ldots$
3. CONV / FC $\rightarrow$ activation function $\rightarrow$ Dropout $\rightarrow$ BN $\rightarrow \ldots$
4. CONV / FC $\rightarrow$ Dropout $\rightarrow$ BN $\rightarrow$ activation function $\rightarrow \ldots$

The authors of [IS15] suggest to use Batch Normalization before the activation function as in Items 1 and 4. Batch Normalization after the activation lead to better results in `https://github.com/ducha-aiki/caffenet-benchmark/blob/master/batchnorm.md`

Another normalization layer is Local Response Normalization as described in [KSH12], which includes ℓ_2 normalization as described in [WWQ13]. Those two normalization layers, however, are superseded by Batch Normalization.

---

[3]also called *inference time*

2.3. CNN Blocks

This section describes more complex building blocks than simple layers. CNN blocks act similar to a layer, but they are themselves composed of layers.

2.3.1. Residual Blocks

Residual blocks as introduced in [HZRS15a] are a milestone in computer vision. They enabled the computer vision community to go from about 16 layers as in VGG 16-D (see Appendix D.3) to several hundred layers. The key idea of deep residual networks (ResNets) as introduced in [HZRS15a] is to add an identity connection which skips two layers. This identity connection adds the feature maps onto the other feature maps and thus requires the output of the input layer of the residual block to be of the same dimension as last layer of the residual block.

Formally, it can be described as follows. If x_i are the feature maps after layer i and x_0 is the input image, H is a non-linear transformation of feature maps, then

$$y = H(x)$$

describes a traditional CNN. Note that this could be multiple layers. A residual block as visualized in Figure 2.4 is described by

$$y = H(x) + x$$

In [HZRS15a], they only used residual skip connections to skip two layers. Hence, if $\text{conv}_i(x_i)$ describes the application of the convolutional layer i to the input x_i without the nonlinearity, then such a residual block is

$$x_{i+2} = \text{conv}_{i+1}(\text{ReLU}(\text{conv}_i(x_i))) + x_i$$
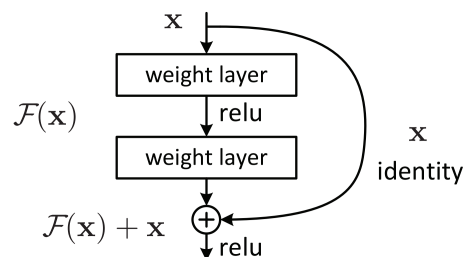
Figure 2.4.: ResNet module
Image source: [HZRS15a]

[HM16] provides some insights why deep residual networks are successful.

2.3.2. Aggregation Blocks

Two common ways to add more parameters to neural networks are increasing their depth by adding more layers or increasing their width by adding more neurons / filters. Inception blocks [AM15] implicitly started a new idea which was explicitly described in [XGD+16] as "ResNeXt block": Increasing the cardinality $C \in \mathbb{N}_{\geq 1}$. By cardinality, the authors describe the concept of having C small convolutional networks with the same topology but different weights. This concept is visualized in Figure 2.5. Please note that Figure 2.5 does not combine aggregation blocks with residual blocks as the authors did.
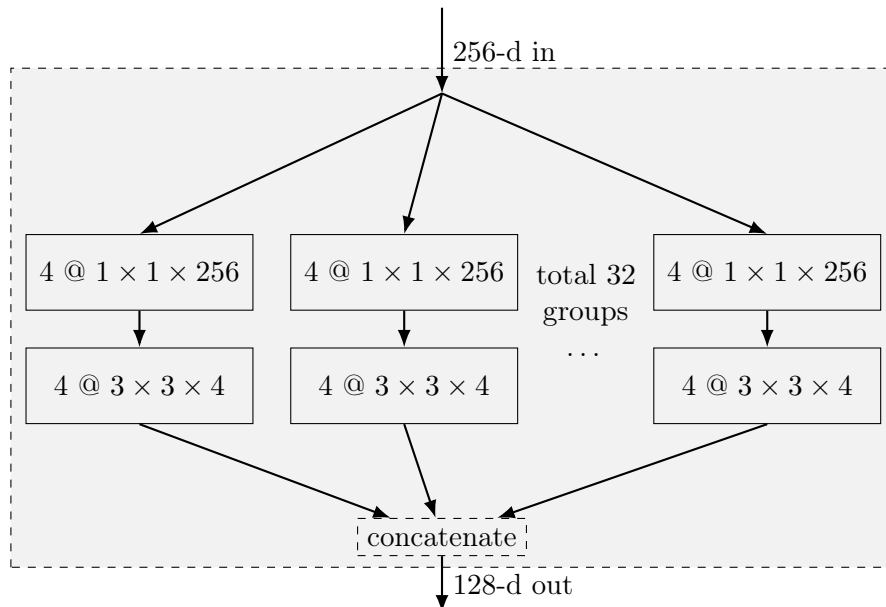
Figure 2.5.: Aggregation block with a cardinality of $C = 32$. Each of the 32 groups is a 2-layer convolutional network. The first layer receives 256 feature maps and applies four 1×1 filters to it. The second layer applies four 3×3 filters. Although every group has the same topology, the learned weights are different. The outputs of the groups are concatenated.

The hyperparameters of an aggregation block are:

- The topology of the group members.

- The cardinality $C \in \mathbb{N}_{\geq 1}$. Note that a cardinality of $C = 1$ is equivalent in every aspect to using the group network without an aggregation block.

2.3.3. Dense Blocks

Dense blocks are collections of convolutional layers which are introduced in [HLW16]. The idea is to connect each convolutional layer directly to subsequent convolutional layers. Traditional CNNs with L layers and one input layer have L connections between layers, but dense blocks have $\frac{L(L+1)}{2}$ connections between layers. The input feature maps are concatenated in depth. According to the authors, this prevents features from being re-learned and allows much fewer filters per convolutional layer. Where AlexNet and VGG-16 have several hundred filters per convolutional layer (see Tables D.2 and D.3), the authors used only on the order of 12 feature maps per layer.

A dense block is visualized in Figure 2.6.
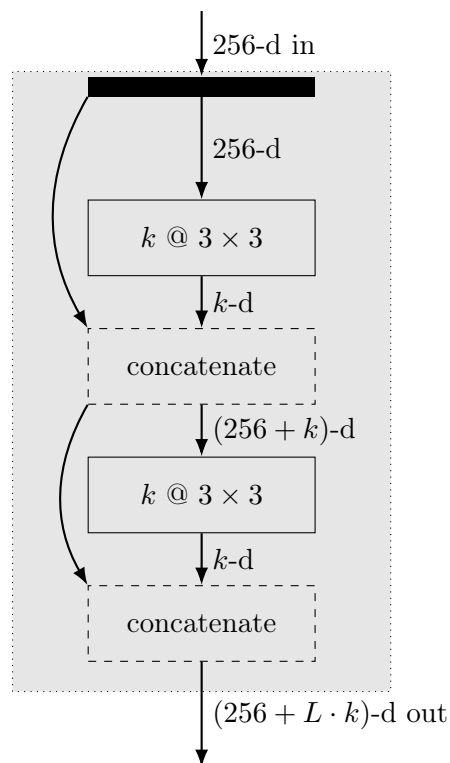
Figure 2.6.: Dense block with $L = 2$ layers and a growth factor of k.

Dense block have five hyperparameters:

- The activation function being used. The authors use ReLU.

- The size $k_w \times k_h$ of filters. The authors use $k_w = k_h = 3$.

- The number of layers L, where $L = 2$ is a simple convolutional layer.

- The number k of filters added per layer (called *growth rate* in the paper)

It might be necessary use 1×1 convolutions to reduce the number of $L \cdot k$ feature maps.

2.4. Transition Layers

Transition layers are used to overcome constraints imposed by resource limitations or architectural design choices. One constraint is the number of feature maps (see Appendix C.3 for details). In order to reduce the number of feature maps while still keeping as much relevant information as possible in the network, a convolutional layer i with k_i filters of the shape $1 \times 1 \times k_{i-1}$ is added. The number of filters k_i directly controls the number of generated feature maps.

In order to reduce the dimensionality (width and height) of the feature maps, one typically applies pooling.

Global pooling is another type of transition layer. It applies pooling over the complete feature map size to shrink the input to a constant 1×1 feature map and hence allows one network to have different input sizes.

2.5. Analysis Techniques

CNNs have dozens of hyperparameters and ways to tune them. Although there are automatic methods like random search [BB12], grid search [LBOM98], gradient-based hyperparameter optimization [MDA15] and Hyperband [LJD+16] some actions need a manual investigation to improve the model's quality. For this reason, analysis techniques which guide developers and researchers to the important hyperparameters are necessary. In the following, nine diagnostic techniques are explained.

A machine learning developer has the following choices to improve the model's quality:

(I1) Change the problem definition (e.g., the classes which are to be distinguished)

(I2) Get more training data

(I3) Clean the training data

(I4) Change the preprocessing (see Appendix B.1)

(I5) Augment the training data set (see Appendix B.2)

(I6) Change the training setup (see Appendices B.3 to B.5)

(I7) Change the model (see Appendices B.6 and B.7)

The preprocessing is usually not changed in modern architectures. However, this still leaves six very different ways to improve the classifier. Changing the training setup and the model each have too many possible choices to explore them completely. Thus, techniques are necessary to guide the developer to changes which are most promising to improve the model.

For all of the following methods, it is important to use only the training set and the validation set.

2.5.1. Qualitative Analysis by Example

The most basic analysis technique which should always be used is looking at examples which the network correctly predicted with a high certainty and what the classifier got wrong with a high certainty. Those examples can be arranged by applying t-SNE [MH08].

One the one hand, this might reveal errors in the training data. Most of the time, training data is manually labeled by humans who make mistakes. If a model is fit to those errors, its quality decreases.

On the other hand, this can show differences in the distribution of validation data which are not covered by the training set and thus indicate the need to collect more data.

2.5.2. Confusion Matrices

A *confusion matrix* is a matrix $(c)_{ij} \in \mathbb{N}_{\geq 0}^{K \times K}$, where $K \in \mathbb{N}_{\geq 2}$ is the number of classes, which contains all correct and wrong classifications. The item c_{ij} is the number of times items of class i were classified as class j. This means the correct classification is on the diagonal c_{ii} and all wrong classifications are of the diagonal. The sum $\sum_{i=1}^{K} \sum_{j=1}^{K} c_{ij}$ is the total number of samples which were evaluated and $\frac{\sum_{i=1}^{K} c_{ii}}{\sum_{i=1}^{K} \sum_{j=1}^{K} c_{ij}}$ is the accuracy.

The sums $r(i) = \sum_{j=1}^{K} c_{ij}$ of each class i are worth being investigated as they show if the classes are skewed. If the number of samples of one class dominates the data set, then the classifier can get a high accuracy by simply always prediction the most common class. If the accuracy of the classifier is close to the a priory probability of the most common class, techniques to deal with skewed classes might help.

An automatic criterion to check for this problem is

$$\text{accuracy} \leq \frac{\max(\{\, r(i) \mid i = 1, \ldots, k \,\})}{\sum_{i=1}^{k} r(i)} + \varepsilon$$

where ε is a small value to compensate the fact that some examples might be correct just by chance.

Other values which should be checked are the class-wise sensitivities:

$$s(k) = \frac{\#\ \text{correctly identified instances of class } k}{\#\ \text{instances of class } k} = \frac{c_{kk}}{r(k)} \in [0, 1]$$

If $s(i)$ is much lower than $s(j)$, it is an indicator that more or cleaner training data is necessary for $s(i)$.

The class-wise confusion

$$f_{\text{confusability}}(k_1, k_2) = \frac{c_{k_1 k_2}}{\sum_{j=1}^{K} c_{k_1 j}}$$

indicates if class k_1 gets often classified as class k_2. The highest values here can indicate if two classes should be merged or a specialized model for separating those classes could improve the overall system.

2.5.3. Validation Curves: Accuracy, loss and other metrics

Validation curves display a hyperparameter (e.g., the training epoch) on the horizontal axis and a quality metric on the vertical axis. Accuracy, error $= (1 - \text{accuracy})$ or loss are typical quality metrics. Other quality metrics can be found in [OHIL16].

In case that the number of training epochs are used as the examined hyperparameter, validation curves give an indicator if training longer improves the model's performance. By

plotting the error on the training set as well as the error on a validation set, one can also estimate if overfitting might become a problem. See Figure 2.7 for an example.
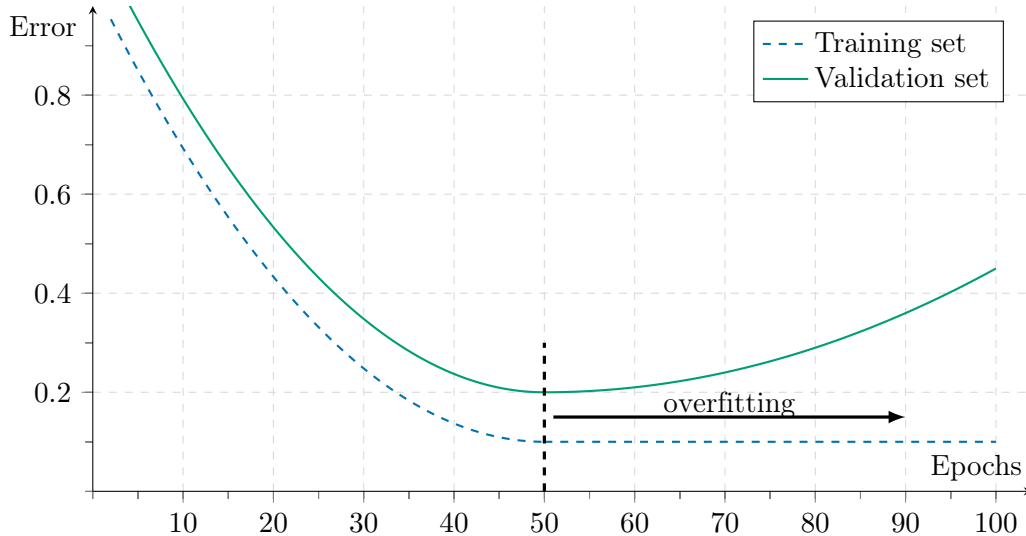
Figure 2.7.: A typical validation curve: In this case, the hyperparameter is the number of epochs and the quality metric is the error $(1 - \text{accuracy})$. The longer the network is trained, the better it gets on the training set. At some point the network is fit too well to the training data and loses its capability to generalize. At this point the quality curve of the training set and the validation set diverge. While the classifier is still improving on the training set, it gets worse on the validation and the test set.

When the epoch-loss validation curve has plateaus as in Figure 2.8, this means the optimization process did not improve for several epochs. Three possible ways to reduce the problem of plateaus are (i) to change weight initialization if the plateau was at the beginning, (ii) regularizing the model or (iii) changing the optimization algorithm.

Loss functions

The loss function (also called *error function* or *cost function*) is a function which assigns a real value to a complex event like the predicted class of a feature vector. It is used to define the *objective function*. For classification problems the loss function is typically cross-entropy with ℓ_1 or ℓ_2 regularization, as it was described in [NH92]:

$$E_{CE}(W) = \underbrace{- \sum_{x \in X} \sum_{k=1}^{K} [t_k^x \log(o_k^x) + (1 - t_k^x) \log(1 - o_k^x)]}_{\text{cross-entropy data loss}} + \underbrace{\lambda_1 \cdot \overbrace{\sum_{w \in W} |w|}^{\ell_1} + \lambda_2 \cdot \overbrace{\sum_{w \in W} w^2}^{\ell_2}}_{\text{model complexity loss}}$$

where W are the weights, X is the training data set, $K \in \mathbb{N}_{\geq}0$ is the number of classes and t_k^x indicates if the training example x is of class k. o_k^x is the output of the classification algorithm which depends on the weights. $\lambda_1, \lambda_2 \in [0, \infty)$ weights the regularization and is typically smaller than 0.1.
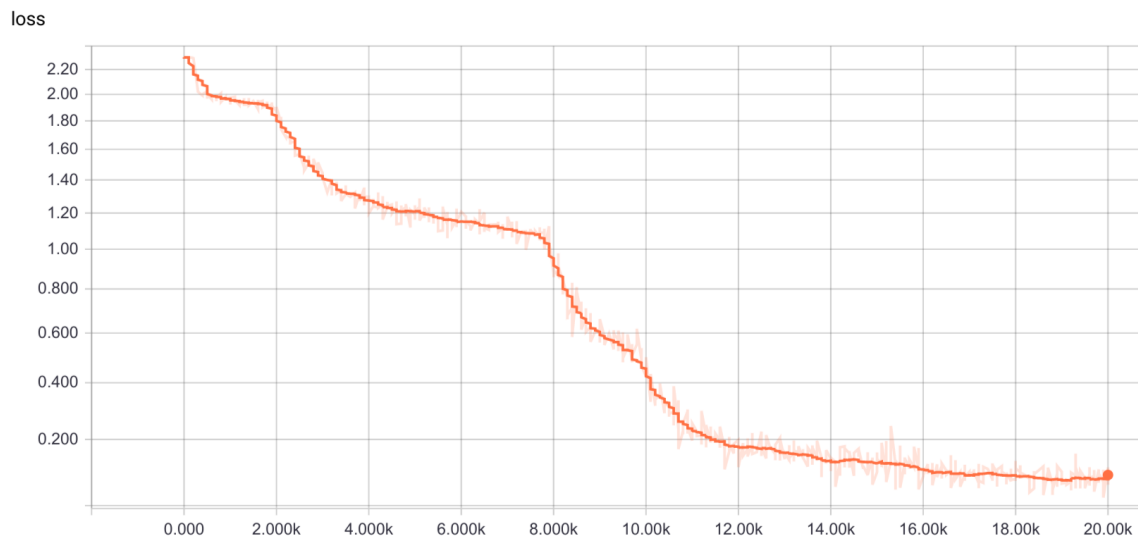
loss

Figure 2.8.: Example for a validation curve (plotted loss function) with plateaus. The dark orange curve is smoothed, but the non-smoothed curve is also plotted in light orange.

The data loss is positive whenever the classification is not correct, whereas the model complexity loss is higher for more complex models. The model complexity loss exists due to the intuition of *Occam's razor*: If two models explain the same data with an accuracy of 100 %, the simpler model is to be preferred.

A reason to show the loss for the validation curve technique instead of other quality metrics is that it contains more information about the quality of the model. A reason against the loss is that it has no upper bound like the accuracy and can be hard to interpret. The loss only shows relative learning progress whereas the accuracy shows absolute progress to human readers.

There are three observations in the loss validation curve which can help to improve the network:

- If the loss does not decrease for several epochs, the learning rate might be too low. The optimization process might also be stuck in a local minimum.

- Loss being NAN might be due to too high learning rates. Another reason is division by zero or taking the logarithm of zero. In both cases, adding a small constant like 10^{-7} fixes the problem.

- If the loss-epoch validation curve has a plateau at the beginning, the weight initialization might be bad.

Quality criteria

There are several quality criteria for classification models. Most quality criteria are based the confusion matrix c which denotes at c_{ij} the number of times the real class was i and j was predicted. This means the diagonal contains the number of correct predictions. For the following, let $t_i = \sum_{j=1}^{k} c_{ij}$ be the number of training samples for class i. The most common quality criterion is accuracy:

$$\text{accuracy}(c) = \frac{\sum_{i=1}^{k} c_{ii}}{\sum_{i=1}^{k} t_i} \in [0, 1]$$

One problem of accuracy as a quality criterion are skewed classes. If one class is by far more common than all other classes, then the simplest way to achieve a high score is to always classify everything as the most common class.

In order to fix this problem, one can use the mean accuracy:

$$\text{mean-accuracy}(c) = \frac{1}{k} \cdot \sum_{i=1}^{k} \frac{c_{ii}}{t_i} \in [0, 1]$$

For two-class problems there are many other metrics like precision, recall and F_β-score. Quality criteria for semantic segmentation are explained in [Tho16].

Besides the quality of the classification result, several other quality criteria are important in practice:

- Speed of evaluation for new images,

- latency,

- power consumption,

- robustness against (non)random perturbations in the training data (see [SZS+13, PMW+15]),

- robustness against (non)random perturbations in the training labels (see [NDRT13, XXE12]),

- model size

As reducing the floating point accuracy allows to process more data on a given device [Har15], analysis under this aspect is also highly relevant in some scenarios.

However, the following focuses on the quality of the classification result.

2.5.4. Learning Curves

A learning curve is a plot where the horizontal axis displays the number of training samples given to the network and the vertical axis displays the error. Two curves are plotted: The error on the training set (of which the size is given by the horizontal axis) and the error on the test set (which is of fixed size). See Figure 2.9 for an example. The learning curve for the validation set is an indicator if more training data without any other changes will improve the networks performance. Having the training set's learning curve, it is possible to estimate if the capacity of the model to fit the data is high enough for the desired classification error. The error on the validation set should never be expected to be significantly lower than the error on the training set. If the error on the training set is too high, then more data will *not* help. Instead, the model or the training algorithm need to be adjusted.

If the training set's learning curve is significantly higher than the validation set's learning curve, then removing features (e.g., by decreasing the images resolution), more training samples or more regularization will help.
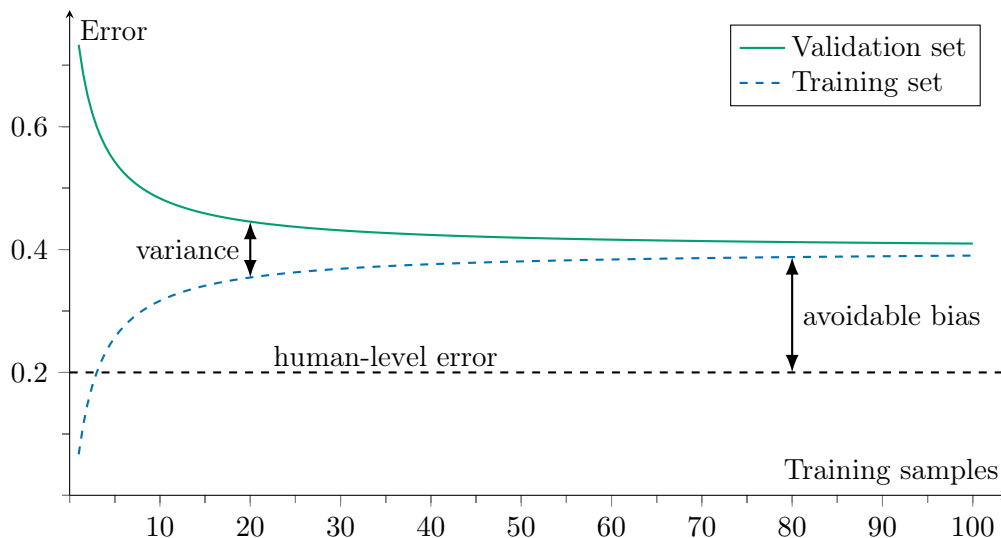
Figure 2.9.: A typical learning curve: The more data is used for training, the more errors a given architecture will make to fit the given training data. At the same time, it is expected that the training data gets more similar to the true distribution of the data which should be captured by the test data. At some point, the error on the training and test set should be about the same. The term "avoidable bias" was coined by Andrew Ng [Ng16]. In some cases it is not possible to classify data correctly by the given features. If humans can classify the data given the features correctly, however, then the bias is avoidable by building a better classifier.

The major drawback of this analysis technique is its computational intensity. In order to get one point on the training curve and one point on the testing curve, a complete training has to be executed. On the full data set, this can be several days on high-end computers.

2.5.5. Input-feature based model explanations

Understanding which clues the model took to come to its prediction is crucial to check if the model actually learns what the developer thinks it learns. For example, a model which has to distinguish sled dogs from Chihuahuas might simply look at the background and check if there is snow. Depending on the training and test data, this works exceptionally well. However, it is not the desired solution.

For classification problems in computer vision, there are two types of visualizations which help to diagnose such problems. Both color superpixels of the original image to convey information how the model used those superpixels:

- **Correct class heatmap**: The probability of the correct class is encoded to give a heat map which superpixels are important for the correct class. This can also be done by setting the opacity accordingly.
- **Most-likely class image**: Each of the most likely classes for all superpixels is represented by a color. The colored image thus gives clues why different predictions were assigned a high probability.

Two methods to generate such images are explained in the following.

Occlusion Sensitivity Analysis

Occlusion sensitivity analysis is described in [ZF14]. The idea is to occlude a part of the image by something. This could be a gray square as in [ZF14] or a black superpixel as in [RSG16]. Then the classifier is run on the image again. This is done for each region (e.g., superpixel or position of the square) and the regions are then colored to generate either a correct class heatmap of the most-likely class image. It is important to note that the color at region r_i denotes the result if r_i is occluded.

Both visualizations are shown in Figure 2.10. One can see that the network makes sensible predictions for this image of the class "Pomeranian". However, the image of the class "Afghan Hound" gets confused with "Ice lolly", which is a sign that this needs further investigation.

Gradient-based approaches

In [SVZ13], a gradient-based approach was used to generate *image-specific class saliency maps*. The authors describe the problem as a ranking problem, where each pixel of the image I_0 is assigned a score $S_c(I_0)$ for a class c of interest. CNNs are non-linear functions, but they can be approximated by the first order Taylor expansion $S_c(I) \approx w^T I + b$ where w is the derivative of S_c at I_0.

2.5.6. Argmax Method

The *argmax method* has two variants:

- **Fixed class argmax**: Propagate all elements of a given class through the network and analyze which neurons are activated most often / have the highest activation.

- **Fixed neuron argmax**: Propagate the data through the network and find the n data elements which cause the highest activation for a given neuron.

Note that a "neuron" is a filter in a CNN. The amount of activation of a filter F by an image I is calculated by applying F to I and calculating the element-wise sum of the result.

Fixed-neuron argmax was applied in [ZF14]. However, they did not stop with that. Besides showing the 9 images which caused the highest activation, they also trained a deconvolutional neural network to project the activation of the filter back into pixel space.

The fixed neuron argmax can be used qualitatively to get an impression of the kind of features which are learned. This is useful to diagnose problems, for example in [AM15] it is described that the network recognized the class "dumbbell" only if a hand was present, too.

Fixed neuron argmax can also be used quantitatively to estimate the amount of parameters being shared between classes or how many parameters are mainly assigned to which classes.

Going one step further from the fixed neuron argmax method is using an optimization algorithm to change an initial image minimally in such a way that any desired class gets predicted. This is called *caricaturization* in [MV16].

2.5.7. Feature Map Reconstructions

Feature map visualizations such as the ones made in [ZF14] (see Figure 2.11) give insights into the learned features. This shows what the network emphasizes. However, it is not necessarily the case that the feature maps allow direct and easy conclusions about the learned features. This technique is called *inversion* in [MV16].

A key idea of feature map visualizations is to reconstruct a layers input, given its activation. This makes it possible find which inputs would cause neurons to activate with extremely high or low values.

More recent work like [NYC16] tries to make the reconstructions appearance look more natural.

2.5.8. Filter comparison

One question which might lead to some insight is how robust the features are which are learned. If the same network is trained with the same data, but different weight initializations, the learned weights should still be comparable.

If the set of learned filters changes with initialization, this might be an indicator for too little capacity of that layer. Hence adding more filters to that layer could improve the performance.

Filters can be compared with the k-translation correlation as introduced in [ZCZL16]:

$$\rho_k(\mathbf{W_i}, \mathbf{W_j}) = \max_{(x,y) \in \{-k,...,k\}^2 \setminus (0,0)} \frac{\langle \mathbf{W_i}, T(\mathbf{W_j}, x, y) \rangle_f}{\|\mathbf{W_i}\|_2 \|\mathbf{W_j}\|_2} \in [-1, 1],$$

where $T(\cdot, x, y)$ denotes the translation of the first operand by (x, y), with zero padding at the borders to keep the shape. $\langle \cdot, \cdot \rangle_f$ denotes the flattened inner product, where the two operands are flattened into column vectors before applying the standard inner product. The closer the absolute value of the k-translation correlation to one, the more similar two filters W_i, W_j are. According to [ZCZL16], standard CNNs like AlexNet (see Appendix D.2) and VGG-16 (see Appendix D.3) have many filters which are highly correlated. They found this by comparing the *averaged maximum k-translational correlation* of the networks with Gaussian-distributed initialized filters. The averaged maximum k-translational correlation is defined as

$$\bar{\rho}_k(\mathbf{W}) = \frac{1}{N} \sum_{i=1}^{N} \max_{j=1, j \neq i}^{N} \rho_k(\mathbf{W}_i, \mathbf{W}_j)$$

where N is the number of filters in the layer $\mathbf{W}$ and $\mathbf{W}_i$ denotes the ith filter.

2.5.9. Weight update tracking

Andrej Karpathy proposed in the 5th lecture of CS231n to track weight updates to check if the learning rate is well-chosen. He suggests that the weight update should be in the order of 10^{-3}. If the weight update is too high, then the learning rate has to be decreased. If the weight update is too low, then the learning rate has to be increased.

The order of the weight updates as well as possible implications highly depend on the model and the training algorithm. See Appendix B.5 for a short overview of training algorithms for neural networks.

2.6. Accuracy boosting techniques

There are techniques which can almost always be applied to improve accuracy of CNN classifiers:

- Ensembles [CMS12]

- Training-time augmentation (see Appendix B.2)

- Test-time transformations [DDFK16, How13, HZRS15b]

- Pre-training and fine-tuning [ZDGD14, GDDM14]

One of the most simple ensemble techniques which was introduced in [CMS12] is averaging the prediction of n classifiers. This improves the accuracy even if the classifiers use exactly the same training setup by reducing variance.

Data augmentation techniques give the optimizer the possibility to take invariances like rotation into account by generating artificial training samples from real training samples. Data augmentation hence reduces bias and variance with no cost at inference time.

Data augmentation at inference time reduces the variance of the classifier. Similar to using an ensemble, it increases the computational cost of inference.

Pretraining the classifier on another dataset to obtain start from a good position or finetuning a model which was originally created for another task is also a common technique.
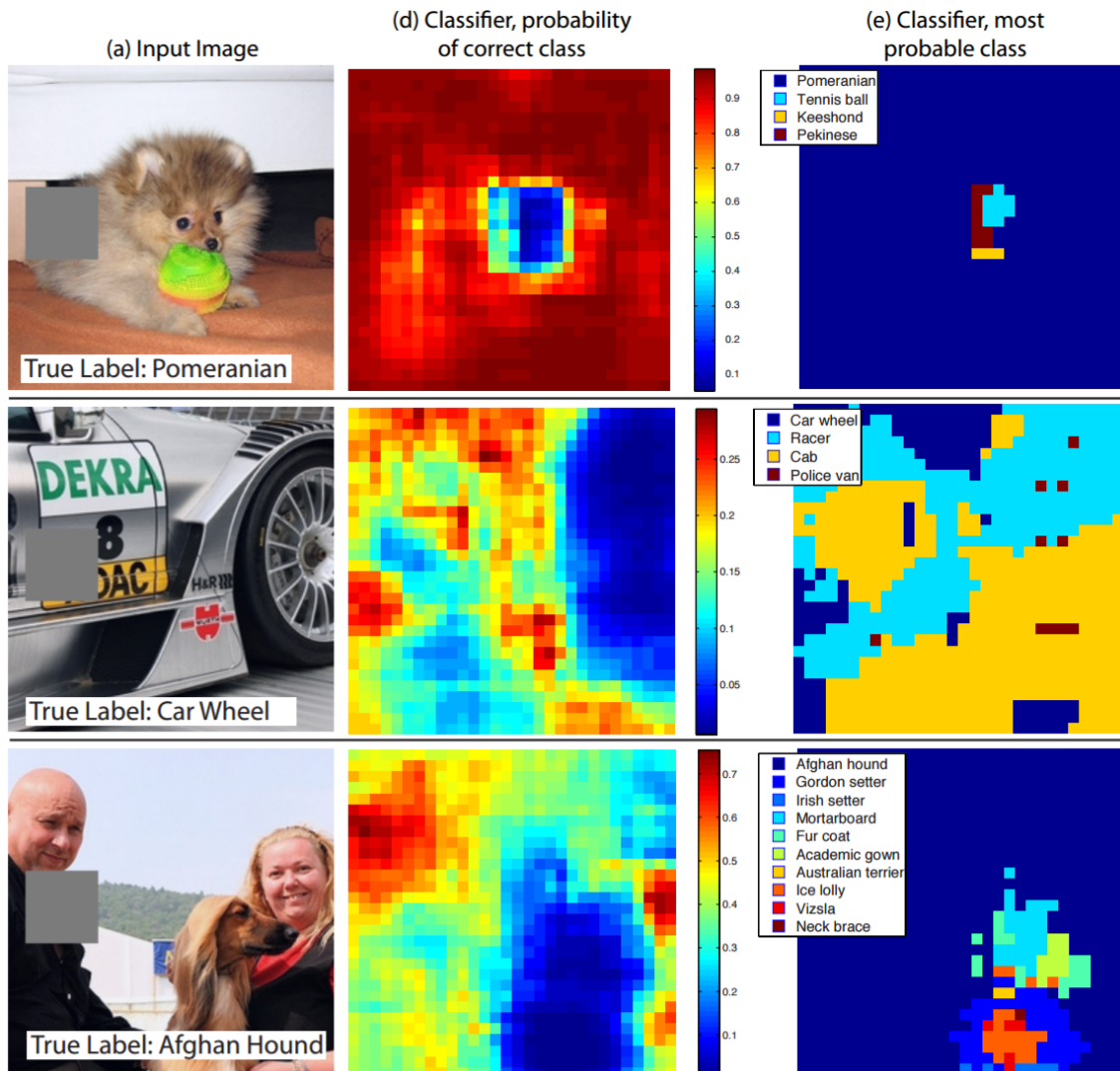
Figure 2.10.: Occlusion sensitivity analysis by [ZF14]: The left column shows three example images, where a gray square occluded a part of the image. This gray squares center (x, y) was moved over the complete image and the classifier was run on each of the occluded images. The probability of the correct class, depending on the gray squares position, is showed in the middle column. One can see that the predicted probability of the correct class "Pomeranian" drops if the face of the dog is occluded. The last image gives the class with the highest predicted probability. In the case of the Pomeranian, it always predicts the correct class if the head is visible. However, if the head of the dog is occluded, it predicts other classes.
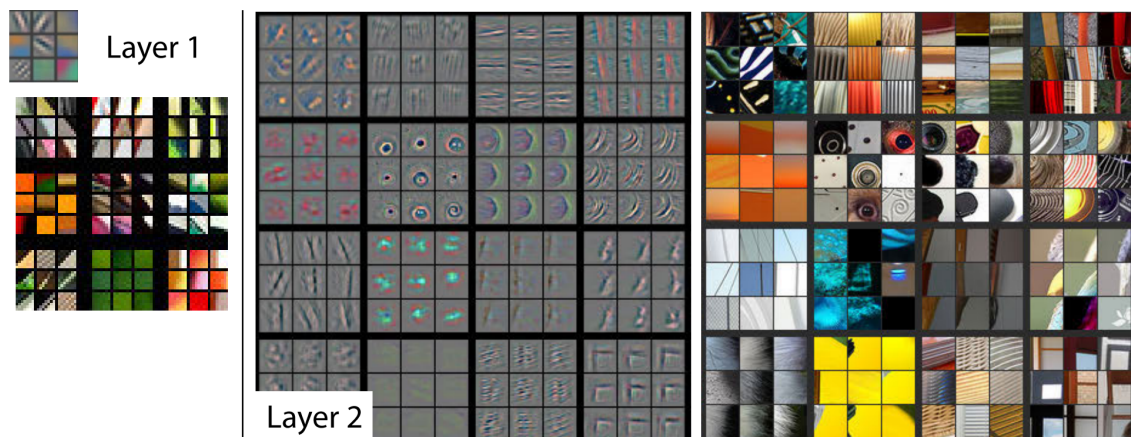
Figure 2.11.: Filter visualization from [ZF14]: The filters themselves as well as the input feature maps which caused the highest activation are displayed.

3. Topology Learning

The topology of a neural network is crucial for the number of parameters, the number of floating point operations (FLOPs), the required memory, as well as the features being learned. The choice of the topology, however, is still mainly done by trial-and-error.

This chapter introduces three general approaches to automatic topology learning: Growing a networks from a minimal network in Section 3.1, pruning in Section 3.2, genetic approaches in Section 3.3 and reinforcement learning approaches in Section 3.4.

3.1. Growing approaches

Growing approaches for topology learning start with a minimal network, which only has the necessary number of input nodes and the number of output nodes which are determined by the application and the features of the input. They then apply a criterion to insert new layers / neurons into the network.

In the following, Cascade-Correlation, Meiosis Networks and Automatic Structure Optimization are introduced.

3.1.1. Cascade-Correlation

Cascade-Correlation was introduced in [FL89]. It generates a cascading architecture which is similar to dense block described in Section 2.3.3.

Cascade-Correlation works as follows:

1. **Initialization**: The number of input nodes and the number of output nodes are defined by the problem. Create a minimal, fully connected network for those.

2. **Training**: Train the network until the error no longer decreases.

3. **Candidate Generation**: Generate candidate nodes. Each candidate node is connected to all inputs. They are not connected to other candidate nodes and not connected to the output nodes.

4. **Correlation Maximization**: Train the weights of the candidates by maximizing S, the correlation between candidates output value V with the networks residual error:

$$S = \sum_{o \in O} \left| \sum_{p \in T} \left(V_p - \bar{V} \right) \left(E_{p,o} - \bar{E}_o \right) \right|$$

where O is the set of output nodes, T is the training set, V_p is the candidate neurons activation for a training pattern p. $E_{p,o}$ is the residual output error at node o for pattern p. $\bar{V}$ and $\bar{E}_o$ are averaged values over all elements of T. This step is finished when the correlation no longer increases.

5. **Candidate selection**: Keep the candidate node with the highest correlation, freeze its incoming weights and add connections to the output nodes.

6. **Continue**: If the error is higher than desired, continue with step 2.

One network with three hidden nodes trained by Cascade-Correlation is shown in Figure 3.1.
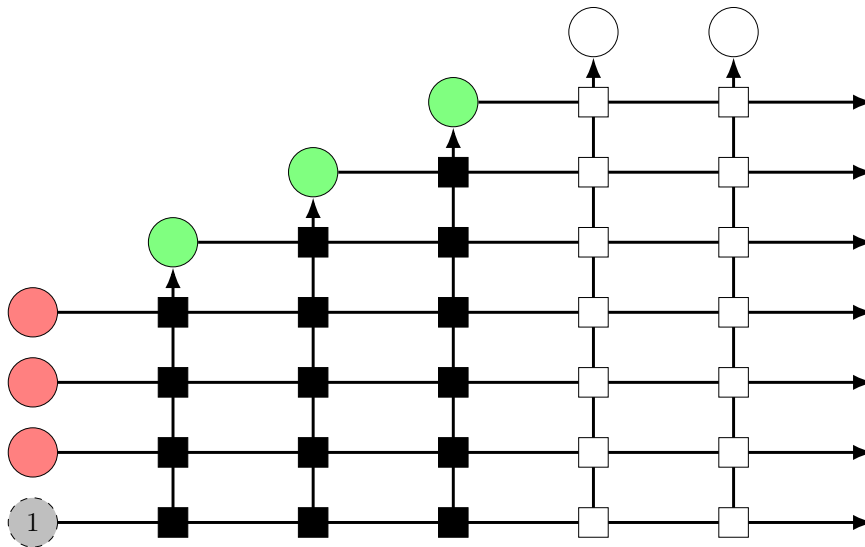
Figure 3.1.: A Cascade-Correlation network with three input nodes (red) and one bias node (gray) to the left, three hidden nodes (green) in the middle and two output nodes in the upper right corner. The black squares represent frozen weights which are found by correlation maximization whereas the white squares are trainable weights.

3.1.2. Meiosis Networks

Meiosis Networks are introduced in [Han89]. In contrast to most MLPs and CNNs, where weights are deterministic and fixed at prediction time, each weight w_{ij} in Meiosis networks follows a normal distribution:

$$w_{ij} \sim \mathcal{N}(\mu_{ij}, \sigma_{ij}^2)$$

Hence every connection has two learned parameters: μ_{ij} and σ_{ij}^2.

The key idea of Meiosis networks is to allow neurons to perform Meiosis, which is cell division. A node j is splitted, when the random part dominates the value of the sampled weights:

$$\frac{\sum_i \sigma_{ij}}{\sum_i \mu_{ij}} > 1 \text{ and } \frac{\sum_k \sigma_{jk}}{\sum_k \mu_{jk}} > 1$$

The mean of the new nodes is sampled around the old mean, half the variance is assigned to the new connections.

Hence Meiosis networks only change the number of neurons per layer. They do not add layers or add skip connections.

3.1.3. Automatic Structure Optimization

Automatic Structure Optimization (ASO) was introduced in [BM93] for the task of on-line handwriting recognition. It makes use of the confusion matrix $C = (c_{ij}) \in \mathbb{N}_{\geq 0}^{k \times k}$ (see Section 2.5.2) to guide the topology learning. They define a confusion-symmetry matrix S with $s_i j = s_j i = c_{ij} \cdot c_{ji}$. The maximum of S defines where the ASO algorithm adds more parameters. The details how the resources are added are not transferable to CNNs.

3.2. Pruning approaches

Pruning approaches start with a network which is bigger than necessary and prune it. The motivation to prune a network which has the desired accuracy is to save storage for easier model sharing, memory for easier deployment and FLOPs to reduce inference time and energy consumption. Especially for embedded systems, deployment is a challenge and low energy consumption is important.

Pruning generally works as follows:

1. Train a given network until a reasonable solution is obtained,

2. prune weights according to a pruning criterion and

3. retrain the pruned network.

This procedure can be repeated.

One family of pruning criterions uses the *Hessian matrix*. For example, Optimal Brain Damage (OBD) as introduced in [LDS+89]. For every single parameter k, OBD calculates the effect on the objective function of deleting k. The authors call the effect of the deletion

of parameter k the saliency s_k. The parameters with the lowest saliency are deleted, which means they are set to 0 and are not updated anymore.

A follow-up method called *Optimal Brain Surgeon* [HSW93] claims to choose the weights in a much better way. This requires, however, to calculate the inverse Hessian matrix $H^{-1} \in \mathbb{R}^{n \times n}$ where $n \in \mathbb{N}$ is typically $n > 10^6$.

A much simpler and computationally cheaper pruning criterion is the *weight magnitude*. [HPTD15] prunes all weights w which are below a threshold θ:

$$w \leftarrow \begin{cases} w & \text{if } w \geq \theta \\ 0 & \text{otherwise} \end{cases}$$

3.3. Genetic approaches

The general idea of genetic algorithms (GAs) is to encode the solution space as genes, which can recombine themselves via crossover and inversion. An introduction to such algorithms is given in [ES03].

Commonly used techniques to generate neural networks by GAs are NEAT [SM02] and its successors HyperNEAT [SDG09] and ES-HyperNEAT [RLS10].

The results, however, are of unacceptable quality: On MNIST (see Appendix E), where random chance gives 10% accuracy, even simple topologies trained with SGD achieve about 92% accuracy [TF-16a] and state of the art is 99.79% [WZZ$^+$13], the HyperNEAT algorithm achieves only 23.9% accuracy [VH13].

Kocmánek shows in [Koc15] that HyperNEAT approaches can achieve 96.47% accuracy on MNIST. Kocmánek mentions that HyperNEAT becomes slower with each hidden layer so that not more than three hidden layers could be trained. At the same time, VGG-19 [SZ14] already has 19 hidden layers and ResNets are successfully trained with 1202 layers in [HZRS15a].

[LX17] shows that Genetic algorithms can achieve competitive results on MNIST and SVHN, but the best results on CIFAR-10 were 7.10% error whereas the state of the art is at 3.74% [HLW16]. Similarly, the Genetic algorithm achieves 29.03% error on CIFAR-100, but the state of the art is 17.18% [HLW16].

3.4. Reinforcement Learning

Reinforcement learning is a sub-field of machine learning, which focuses on the question how to choose actions that lead to high rewards.

One can think of the search for good neural network topologies as a reinforcement learning problem. The agent is a recurrent neural network which can generate bitstrings. Those variable-length bitstrings encode neural network topologies.

In 2016, this approach was applied to construct neural networks for computer vision. In [BGNR16], Q-learning with an ε-greedy exploration was applied.

In [ZL16], the `REINFORCE` algorithm from [Wil92] was used to train state of the art models for CIFAR-10 and the Penn Treebank dataset. A drawback of this method is that enormous amounts of computational resources were used to obtain those results.

3.5. Convolutional Neural Fabrics

Convolutional Neural Fabrics are introduced in [SV16]. They side-step hard decisions about topologies by learning an ensemble of different CNN architectures. The idea is to define a single architecture as a trellis through a 3D grid of nodes. Each node represents a convolutional layer. One dimension is the index of the layer, the other two dimensions are the amount of filters and the feature size. Each node is connected to nine other nodes and thus represents nine possible choices of convolutional layers:

- **Resolution**: (i) convolution with `stride=1` or (ii) convolution with `stride=2` or (iii) deconvolution (doubling the resolution)

- **Channels**: (i) half the number of filters than the layer before (ii) the same number of filters as the layer before (iii) double the number of filters than the layer before

They always use ReLU as an activation function and they always use filters of size 3×3. They don't use pooling at all.

4. Hierarchical Classification

Designing a classifier for a new dataset is hard for two main reasons: Many design choices are not clearly superior to others and evaluating one design choice takes much time. Especially CNNs are known to take several days [KSH12, SLJ+15] or even weeks [SZ14] to train. Additionally, some methods for analyzing a dataset become harder to use with more classes and more training samples. Examples are t-SNE, the manual inspection of errors and confusion matrices, and the argmax method.

One idea to approach this problem is by building a hierarchy of classifiers. The root classifier distinguishes clusters of classes, whereas the leaf classifiers distinguish single classes. Figure 4.1 gives an example for an hierarchy of classifiers.
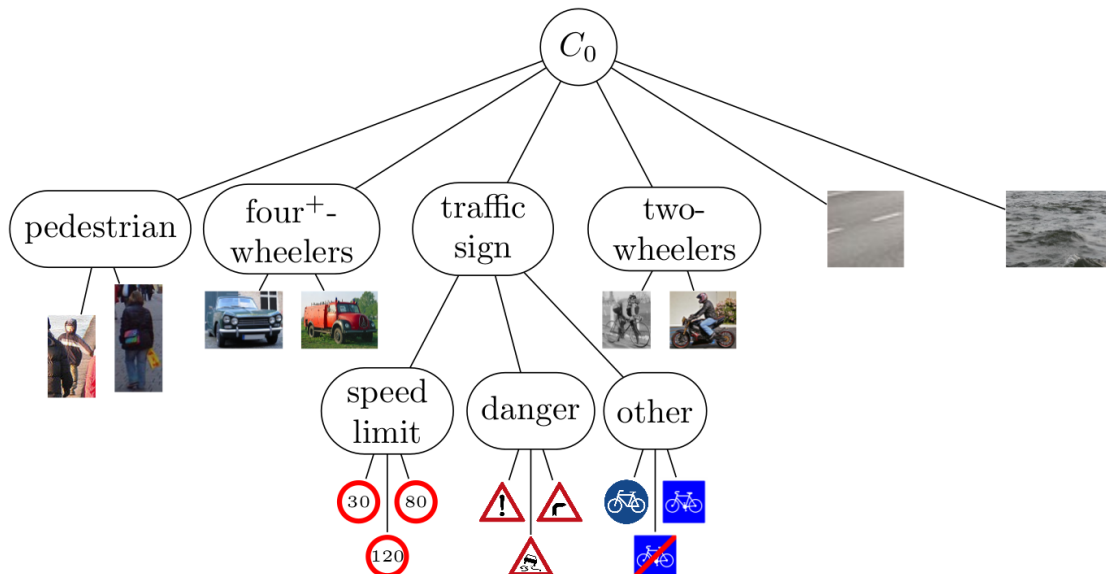
Figure 4.1.: Example for a hierarchy of classifiers. Each classifier is visualized by a rounded rectangle. The root classifier C_0 has to distinguish six coarse classes (pedestrian, four+-wheelers, traffic signs, two-wheelers, street, other) or 17 fine-grained classes. If C_0 predicts a `pedestrian`, another classifier has to predict if it is an adult or a child. Similar, if C_0 predicts `traffic sign`, then another classifier has to predict if it is a speed limit, a sign indicating danger or something else. If C_0, however, predicts `road`, then no other classifier will become active.
In this example, the problem has 17 classes. The hierarchical approach introduces 7 clusters of classes and thus uses 8 classifiers.

Such a hierarchy of classifiers needs clusters of classes.

4.1. Advantages of classifier hierarchies

Having a classifier hierarchy has five advantages:

- **Division of labor**: Different teams can work together. Instead of having a monolithic task, the solutions can be combined.

- **Guarantees**: Changing a classifier will only change the prediction of itself and its children. Siblings are not affected. In the example from Figure 4.1, the classifier which distinguishes traffic signs can be changed while the classification as `pedestrian`, `four`$^+$`-wheelers`, `traffic sign`, `street`, `other` will not be affected. Also, the classification between speed limits, danger signs and other signs will not change.

- **Faster training**: Except for the root classifier C_0, each other classifier will have less than the total amount of training data. Depending on the combined classes, the models could also be simpler. Hence the training time is reduced.

- **Weighting of errors**: In practice, some errors are more severe than others. For example, it could be acceptable if the `two-wheelers` classifier has an error rate of 40%. But it is not acceptable if the `speed limit` classifier has such a high error rate.

- **Post-hoc explanations**: The simpler a model is, the easier it is to explain why a classification is made the way it is made.

4.2. Clustering classes

There are two ways to cluster classes: By similarity or by semantics. While semantic clustering needs either additional information or manual work, the similarity can be automatically inferred from the data. As pointed out in [XZY$^+$14], semantically similar classes are often also visually similar. For example, in the ImageNet dataset most dogs are semantically and visually more similar to each other than to non-dogs. An example where this is obviously not the case are symbols: The summation symbol `\sum` is identical in appearance to the Greek letter `\Sigma`, but semantically much closer to the addition operator `+`.

One approach to cluster classes by similarity is to train a classifier and examine its predictions. Each class is represented in the confusion matrix by one row. Those rows can be directly with standard clustering algorithms such as k-means, DBSCAN [EKS$^+$96], OPTICS [ABKS99], CLARANS [NH02], DIANA [KR09], AHC (see [HPK11]) or spectral clustering as in [XZY$^+$14]. Those clusterings, however, are hard to interpret and most of them do not allow a human to improve the found clustering manually.

The confusion matrix $(c)_{ij} \in \mathbb{N}^{k \times k}$ states how often class i was present and class j was

predicted. The more often this confusion happens, the more similar those two classes are to the classifier. Based on the confusion matrix, the classes can be clustered as explained in the following.

[HAE16] indicates that more classes make it easier to generalize, but the accuracy gains diminish after a critical point of classes is reached. Hence a binary tree might not be a good choice. As an alternative, an approach which allows building arbitrary many clusters, is proposed.

The proposed algorithm has two main ideas:

- The order of columns and rows in the confusion matrix is arbitrary. This means one can swap rows and columns. If row i and j are swapped, then the columns i and j have to be swapped to in order to keep the same confusion matrix.

- If two classes are confused often, then they are similar to the classifier.

Hence the order of the classes is permutated in such a way that the highest errors are close to the diagonal. One possible objective function to be minimized is

$$f(C) = \sum_{i=1}^{n} \sum_{j=1}^{n} C_{ij} \cdot |i - j| \qquad [4.1]$$

which punishes errors linearly with the distance to the diagonal. This method is called CMO in the following.

As pointed out by Tobias Ribizel (personal communication), this optimization problem is a weighted version of *Optimal Linear Arrangement problem*. That problem is NP-complete [GJ02, GJS76]. Simulated Annealing as described in Algorithm 1, however, produces reasonable clusterings as well as visually appealing confusion matrices. The algorithm works as follows: First, decide with probability 0.5 if only two random rows are swapped or a block is swapped. If two rows are swapped, choose both of them randomly. If a block is swapped, then choose the start randomly and the end of the block randomly after the start. The insert position has to be a valid position considering the block length, but besides that it is also chosen uniformly random.

Simple row-swapping can exploit local improvements. For example, in the context of ImageNet, it can swap the dog-class `Silky Terrier` to the dog-class `Yorkshire terrier` and both dog classes `Dalmatian` and `Greyhound` next to each other. Both the two clusters of dog breeds could be separated by `car` and `bus` due to random chance. Moving any single class increases the score, but moving either one of the dog breed clusters or the vehicle cluster decreases the score. Hence it is beneficial to implement block moving.

One advantage of permutating the classes in order to minimize Equation (4.1) in comparison to spectral clustering as used in [XZY$^+$14] is that the adjusted confusion matrix can be

split into many much smaller matrices along the diagonal. In the case of many classes (e.g., 1000 classes of ImageNet or 369 classes of HASYv2) this permutation makes it possible to visualize the types of errors made. If the errors are systematic due to visual similarity, many confusions are not made and thus many elements of the confusion matrix are close to 0. Those will be moved to the corners of the confusion matrix by optimizing Equation (4.1).

Once a permutation of the classes is found which has a low score Equation (4.1), the clusters can either be made by hand by deciding why classes should not be in one clusters. With such a permutation, only $n - 1$ binary decisions have to be made and hence only the list of classes has to be read. Alternatively, one can calculate the confusions $C'_{i,i+1} + C'_{i+1,i}$ for each pair of classes which are neighbors in the confusion matrix. The higher this value, the more similar are the classes according to the classifier. Hence a threshold θ can be applied. θ can either be set automatically (e.g., such that 10% of all pairs are above the threshold) or semi-automatically by asking the user for information if two classes belong to the same cluster. Such an approach only needs $\log(n)$ binary decisions from the user where n is the number of classes.

Please note that CMO only works if the classifier is neither too bad nor too good. A classifier which does not solve the task at all might just give almost uniform predictions whereas the confusion matrix of an extremely good classifier is almost diagonal and thus contains no information about the similarity of classes. One possible solution to this problem is to take the prediction of the class in contrast to using only the argmax in order to find a useful permutation.

5. Experimental Evaluation

All experiments are implemented using Keras 2.0 [Cho15] with Tensorflow 1.0 [AAB$^+$16] and cuDNN 5.1 [CWV$^+$14] as the backend. The experiments were run on different machines with different Nvidia graphics processing units (GPUs), including the Titan Black, GeForce GTX 970 and GeForce 940MX.

The GTSRB [SSSI12], SVHN [NWC$^+$11b], CIFAR-10 and CIFAR-100 [Kri], MNIST [YL98], HASYv2 [Tho17a], STL-10 [CLN10] dataset are used for the evaluation. Those datasets are used as their size is small enough to be trained within a day. Other classification datasets which were considered are listed in Appendix E.

CIFAR-10 (Canadian Institute for Advanced Research 10) is a 10-class dataset of color images of the size $32\,\mathrm{px} \times 32\,\mathrm{px}$. Its ten classes are airplane, automobile, bird, cat, deer, dog, frog, horse, ship, truck. The state of the art achieves an accuracy of 96.54 % [HLW16]. According to [Kar11], human accuracy is at about 94 %.

CIFAR-100 is a 100-class dataset of color images of the size $32\,\mathrm{px} \times 32\,\mathrm{px}$. Its 100 classes are grouped to 20 superclasses. It includes animals, people, plants, outdoor scenes, vehicles and other items. CIFAR-100 is not a superset of CIFAR-10, as CIFAR-100 does not contain the class `airplane`. The state of the art achieves an accuracy of 82.82 % [HLW16].

GTSRB (German Traffic Sign Recognition Benchmark) is a 43-class dataset of traffic signs. The 51 839 images are in color and of a minimum size of $25\,\mathrm{px} \times 25\,\mathrm{px}$ up to $266\,\mathrm{px} \times 232\,\mathrm{px}$. The state of the art achieves 99.46 % accuracy with an ensemble of 25 CNNs [SL11]. According to [SSSI], human performance is at 98.84 %.

HASYv2 (Handwritten Symbols version 2) is a 369 class dataset of black-and-white images of the size $32\,\mathrm{px} \times 32\,\mathrm{px}$. The 369 classes contain the Latin and Greek letters, arrows, mathematical symbols. The state of the art achieves an accuracy of 82.00 % [Tho17a].

STL-10 (self-taught learning 10) is a 10-class dataset of color images of the size $96\,\mathrm{px} \times 96\,\mathrm{px}$. Its ten classes are airplane, bird, car, cat, deer, dog, horse, monkey, ship, truck. The state of the art achieves an accuracy of 74.80 % [ZMGL15]. It contains 100 000 unlabeled images for unsupervised training and 500 images per class for supervised training.

SVHN (Street View House Numbers) exists in two formats. For the following experiments, the cropped digit format was used. It contains the 10 digits cropped from photos of Google Street View. The images are in color and of size $32\,\mathrm{px} \times 32\,\mathrm{px}$. The state of the art

achieves an accuracy of 98.41 % [HLW16]. According to [NWC$^+$11a], human performance is at 98.0 %.

As a preprocessing step, the pixel-features were divided by 255 to obtain values in $[0, 1]$. For GTSRB, the training and test data was scaled to 32 px $\times$ 32 px.

5.1. Baseline Model and Training setup

The baseline model is trained with Adam [KB14], an initial learning rate of 10^{-4}, a batch size of 64 for at most 1000 epochs with data augmentation. The kind of data augmentation depends on the dataset:

- **CIFAR-10**, **CIFAR-100** and STL-10: Random width and height shift by at most ± 3 pixels in either direction; Random horizontal flip.

- **GTSRB**, **MNIST**: Random width and height shift by at most ± 5 pixels in either direction; random rotation by at most ± 15 degrees; random channel shift; random zoom in $[0.5, 1.5]$; random shear by at most 6 degrees.

- **HASYv2**: Random width and height shift by at most ± 5 pixels in either direction; random rotation by at most ± 5 degree.

- **SVHN**: No data augmentation.

If the dataset does not define a training/test set, a stratified 67 % / 33 % split is applied. If the dataset does not define a validation set, the training set is split in a stratified manner into 90 % training set / 10 % test set.

Early stopping [Pre98] with the validation accuracy as a stopping criterion and a patience of 10 epochs is applied. After this, the model is trained without data augmentation for at most 1000 epochs with early stopping and the validation accuracy as a stopping criterion and a patience of 10 epochs. Kernel weights are initialized according to the uniform initialization scheme of He [HZRS15b] (see Appendix B.3).

The architecture of the baseline model uses a pattern of

$$\text{Conv-Block}(n) = (\text{Convolution} - \text{Batch Normalization} - \text{Activation})^n - \text{Pooling}$$

The activation function is the Exponential Linear Unit (ELU) (see Table B.3), except for the last layer where softmax is used. Before the last two convolutional layer, a dropout layer with dropout probability 0.5 is applied. The architecture is given in detail in Table 5.1. Please note that the number of input- and output channels of the network depends on the dataset. If the input image is larger than 32 px $\times$ 32 px, for each power of two a Conv-Block(2) is added at the input. For MNIST, the images are bilinearly upsampled to 32 px $\times$ 32 px.

#	Type	Filters @ Patch size / stride		Parameters	FLOPs	Output size		
	Input			0	0	3 @ 32 ×	32
1	Convolution	32 @ 3 × 3 × 3	/ 1	896	1 736 704	**32 @ 32 ×**	**32**
2	BN + ELU			64	163 904	**32 @ 32 ×**	**32**
3	Convolution	32 @ 3 × 3 × 32	/ 1	9 248	18 841 600	**32 @ 32 ×**	**32**
4	BN + ELU			64	163 904	**32 @ 32 ×**	**32**
	Max pooling	2 × 2	/ 2	0	40 960	32 @ 16 ×	16
5	Convolution	64 @ 3 × 3 × 32	/ 1	18 496	9 420 800	64 @ 16 ×	16
6	BN + ELU			128	82 048	64 @ 16 ×	16
7	Convolution	64 @ 3 × 3 × 64	/ 1	36 928	**18 857 984**	64 @ 16 ×	16
8	BN + ELU			128	82 048	64 @ 16 ×	16
	Max pooling	2 × 2	/ 2		20 480	64 @ 8 ×	8
9	Convolution	64 @ 3 × 3 × 64	/ 1	36 928	4 714 496	64 @ 8 ×	8
10	BN + ELU			128	20 608	64 @ 8 ×	8
	Max pooling	2 × 2	/ 2		5 120	64 @ 4 ×	4
11	Convolution (v)	512 @ 4 × 4 × 64	/ 1	**524 800**	1 048 064	512 @ 1 ×	1
12	BN + ELU			1 024	3 584	512 @ 1 ×	1
	Dropout 0.5			0	0	512 @ 1 ×	1
13	Convolution	512 @ 1 × 1 × 512	/ 1	262 656	523 776	512 @ 1 ×	1
14	BN + ELU			1 024	3 584	512 @ 1 ×	1
	Dropout 0.5			0	0	512 @ 1 ×	1
15	Convolution	k @ 1 × 1 × 512	/ 1	$k \cdot (512 + 1)$	$1024 \cdot k$	k @ 1 ×	1
	Global avg Pooling	1 × 1		0	k	k @ 1 ×	1
16	BN + Softmax			$2k$	$7k$	k @ 1 ×	1
	$\sum$			$515k$ +892 512	$1032k$ +55 729 664	103 424 + 2k	

Table 5.1.: Baseline architecture with 3 input channels of size 32×32. All convolutional layers use `SAME` padding, except for layer 11 which used `VALID` padding in order to decrease the feature map size to 1×1. If the input feature map is bigger than 32×32, for each power of two there are two `Convolution + BN + ELU` blocks and one `Max pooling` block added. This is the framed part in the table.
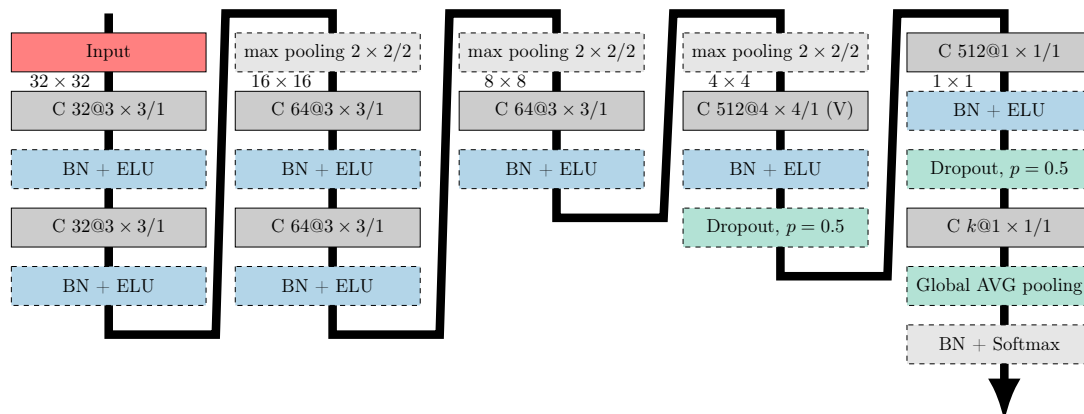

Figure 5.1.: Architecture of the baseline model. `C` $32@3 \times 3/1$ is a convolutional layer with 32 filters of kernel size 3×3 with stride 1.

5.1.1. Baseline Evaluation

The results for the baseline model evaluated on eight datasets are given in Table 5.2. The speed for inference for different GPUs is given in Table 5.3.

Dataset	Single Model Accuracy				Ensemble of 10	
	Training Set		Test Set		Training Set	Test Set
Asirra	94.22 %	$\sigma = 3.49$	94.37 %	$\sigma = 3.47$	97.07 %	97.37 %
CIFAR-10	91.23 %	$\sigma = 1.10$	85.84 %	$\sigma = 0.87$	92.36 %	86.75 %
CIFAR-100	76.64 %	$\sigma = 1.48$	63.38 %	$\sigma = 0.55$	78.30 %	64.70 %
GTSRB	100.00 %	$\sigma = 0.00$	99.18 %	$\sigma = 0.11$	100.00 %	99.46 %
HASYv2	89.49 %	$\sigma = 0.42$	85.35 %	$\sigma = 0.10$	89.94 %	86.03 %
MNIST	99.93 %	$\sigma = 0.07$	99.53 %	$\sigma = 0.06$	99.99 %	99.58 %
STL-10	94.12 %	$\sigma = 0.87$	75.67 %	$\sigma = 0.34$	96.35 %	77.62 %
SVHN	99.02 %	$\sigma = 0.07$	96.28 %	$\sigma = 0.10$	99.42 %	97.20 %

Table 5.2.: Baseline model accuracy on eight datasets. The single model actuary is the 10 models used in the ensemble. The empirical standard deviation σ of the accuracy is also given. CIFAR-10, CIFAR-100 and STL-10 models use test-time transformations. None of the models uses unlabeled data or data from other datasets. For HASYv2 no test time transformations are used.

Network	GPU	Tensorflow	Inference per		Training
			1 Image	128 images	time / epoch
Baseline	Default	Intel i7-4930K	3 ms	244 ms	231.0 s
Baseline	Optimized	Intel i7-4930K	2 ms	143 ms	149.0 s
Baseline	Default	GeForce 940MX	4 ms	120 ms	145.6 s
Baseline	Default	GTX 970	6 ms	32 ms	25.0 s-26.3 s
Baseline	Default	GTX 980	3 ms	24 ms	20.5 s-21.1 s
Baseline	Default	GTX 980 Ti	5 ms	27 ms	22.0 s-22.1 s
Baseline	Default	GTX 1070	**2 ms**	**15 ms**	**14.4 s-14.5 s**
Baseline	Default	Titan Black	4 ms	25 ms	28.1 s-28.1 s
Baseline	Optimized	Titan Black	3 ms	22 ms	24.4 s-24.4 s
DenseNet-40-12	Default	GeForce 940MX	27 ms	2403 ms	—

Table 5.3.: Speed comparison of the baseline model on CIFAR-10. The baseline model is evaluated on six Nvidia GPUs and one CPU. The weights for DenseNet-40-12 are taken from [Maj17]. Weights the baseline model can be found at [Tho17b]. The optimized Tensorflow build makes use of SSE4.X, AVX, AVX2 and FMA instructions.

5.1.2. Weight distribution

The distribution of filter weights by layer is visualized in Figure 5.2 and the distribution of bias weights by layer is shown in Figure 5.3. Although both figures only show the distribution for one specific model trained on CIFAR-100, the following observed patterns are consistent for 70 models (7 datasets and 10 models per dataset):

- The empiric $[0.5 - \text{percentile}, 99.5 - \text{percentile}]$ interval which contains 99% of the filter weights is almost symmetric around zero. The same is true for the bias weights.

- The farther a layer is from the input away, the smaller the 99-percentile interval is, except for the last layer (see Table A.1).

- The 99-percentile interval of the first layers filter weights is about $[-0.5, +0.5]$, except for MNIST and HASYv2 where it is in $[-0.8, 0.8]$.

- The 99-percentile interval of the first layers bias weights is always in $[-0.2, 0.2]$.

- The distribution of filter weights of the last convolutional layer is not symmetric. In some cases the distribution is also not unimodal.

- The bias weights of the last three layers are very close to zero. The absolute value of most of them is smaller than 10^{-2}.

Similarly, Figure 5.4 and Figure 5.5 show the distribution of the γ and the β parameter of Batch Normalization. It is expected that γ is close to 1 and β is close to 0. In those cases, the Batch Normalization layer equals the identity and thus is only relevant for the training. While γ and β do not show as clear patterns as the filter and bias weights of convolutional layers, some observations are also consistent through all models even for different datasets:

- γ of the last layer (layer 16) is bigger than 1.3.

- The 99-percentile interval for β of the last layer is longer than the other 99-percentile intervals.

- The 99-percentile interval for β of the fourth-last (layer 14 for STL-10, layer 10 for all other models) is more negative then all other layers.

Finally, the distribution of filter weight ranges is plotted in Figure 5.6 for each convolutional layer. The ranges are calculated for each channel and filter separately. The smaller the values are, the less information is lost if the filters are replaced by smaller filters.
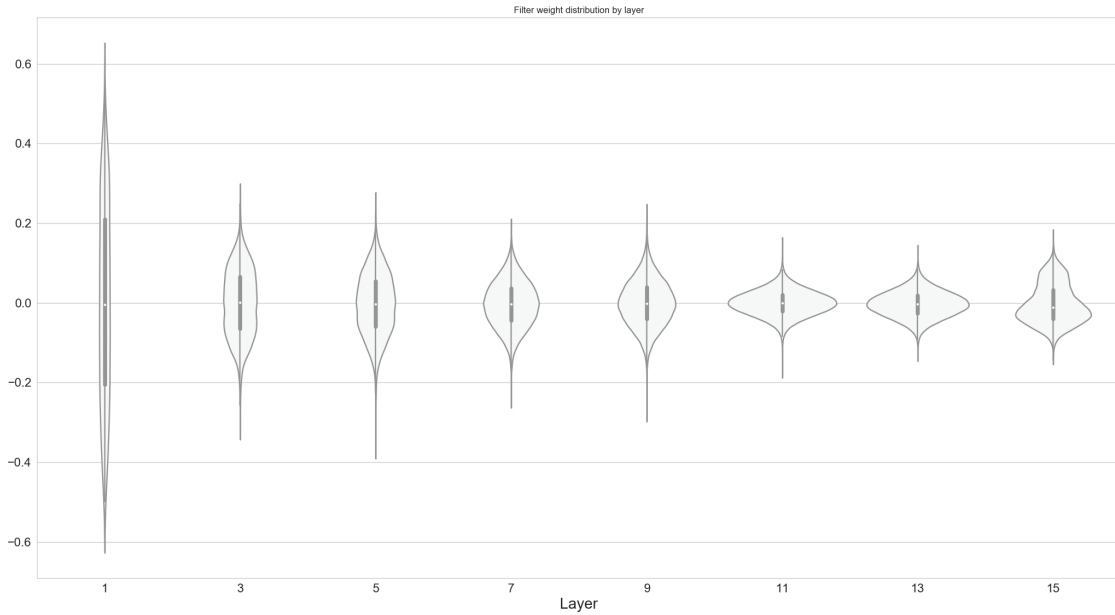
Figure 5.2.: Violin plots of the distribution of filter weights of a baseline model trained on CIFAR-100. The weights of the first layer are relatively evenly spread in the interval $[-0.4, +0.4]$. With every layer the interval which contains 95 % of the weights and is centered around the mean becomes smaller, especially with layer 11 where the feature maps are of size 1×1. In contrast to the other layers, the last convolutional layer has a bimodal distribution.

This plot indicates that the network might benefit from bigger filters in the first layer, whereas the filters in layers $7 - 11$ could potentially be smaller.
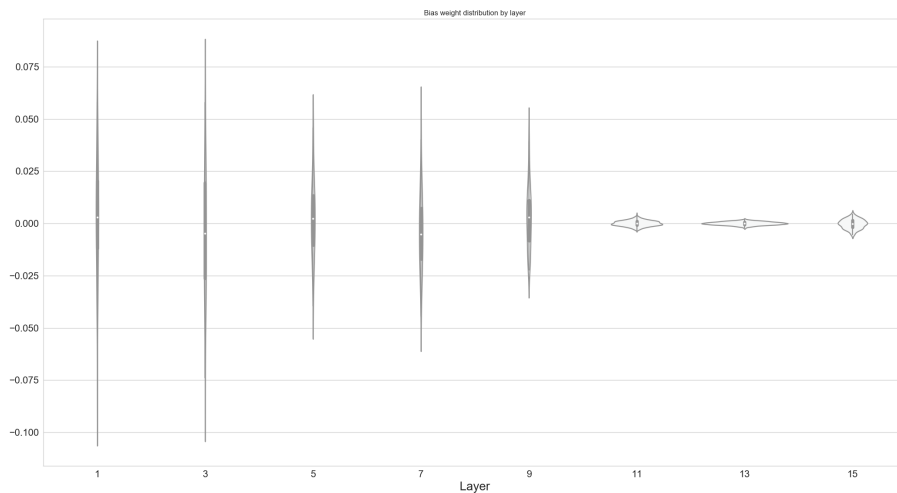
Figure 5.3.: Violin plots of the distribution of bias weights of a baseline model trained on CIFAR-100. While the first layers biases are in $[-0.1, +0.1]$, after each max-pooling layer the interval which contains 95 % of the weights and is centered around the mean becomes smaller. In the last three convolutional layer, most bias weights are in $[-0.005, +0.005]$.
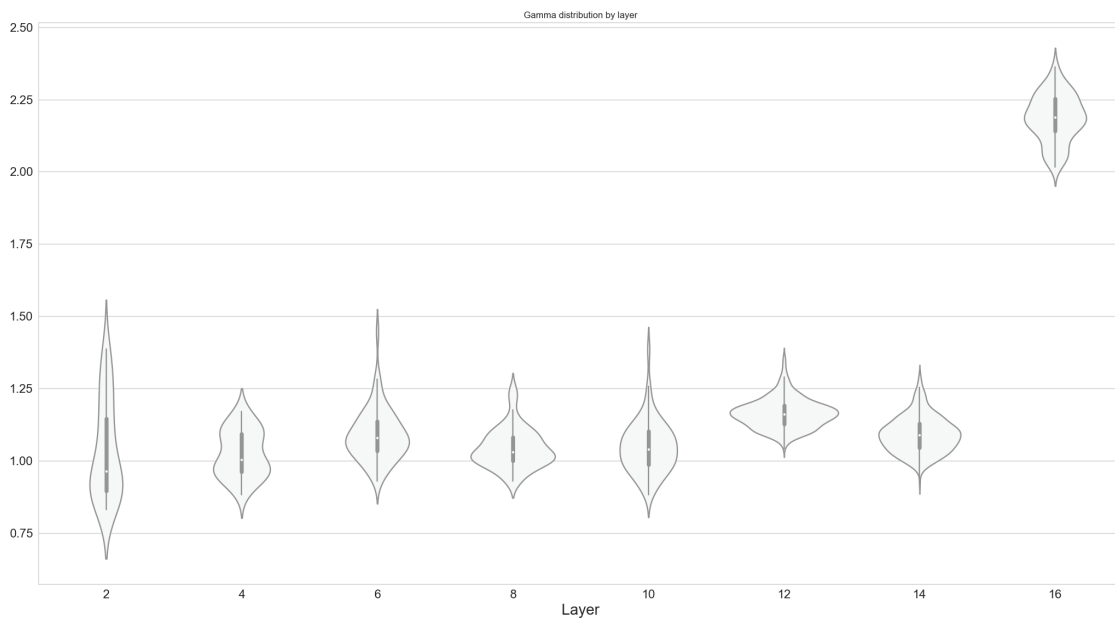
Figure 5.4.: Violin plots of the distribution of the γ parameter of Batch Normalization layers of a baseline model trained on CIFAR-100.
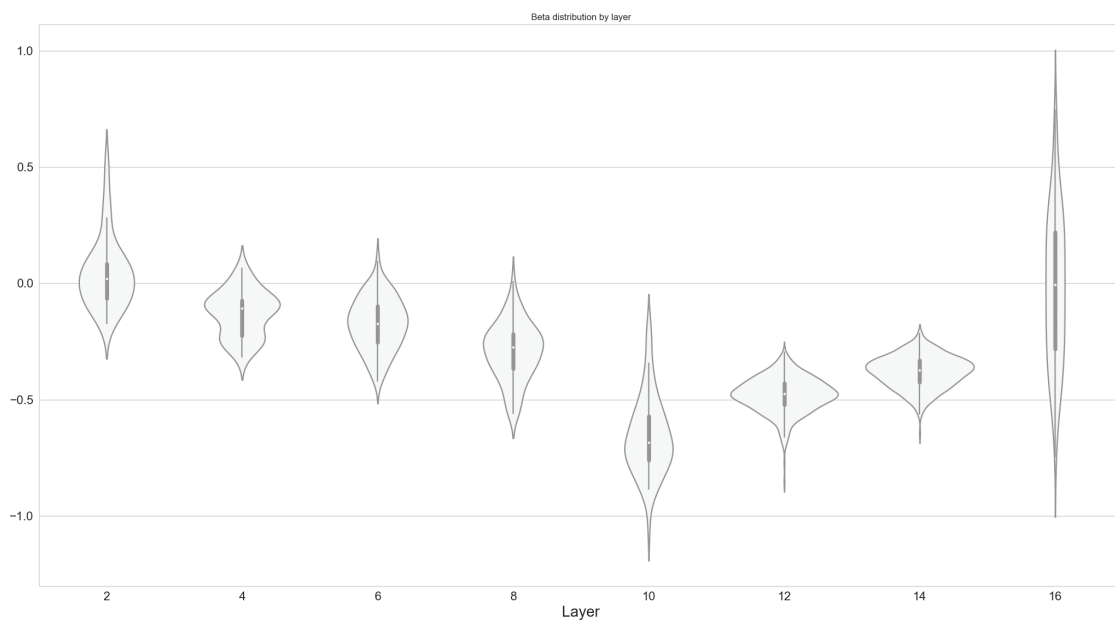
Figure 5.5.: The distribution of the β parameter of Batch Normalization layers of a baseline model trained on CIFAR-100.
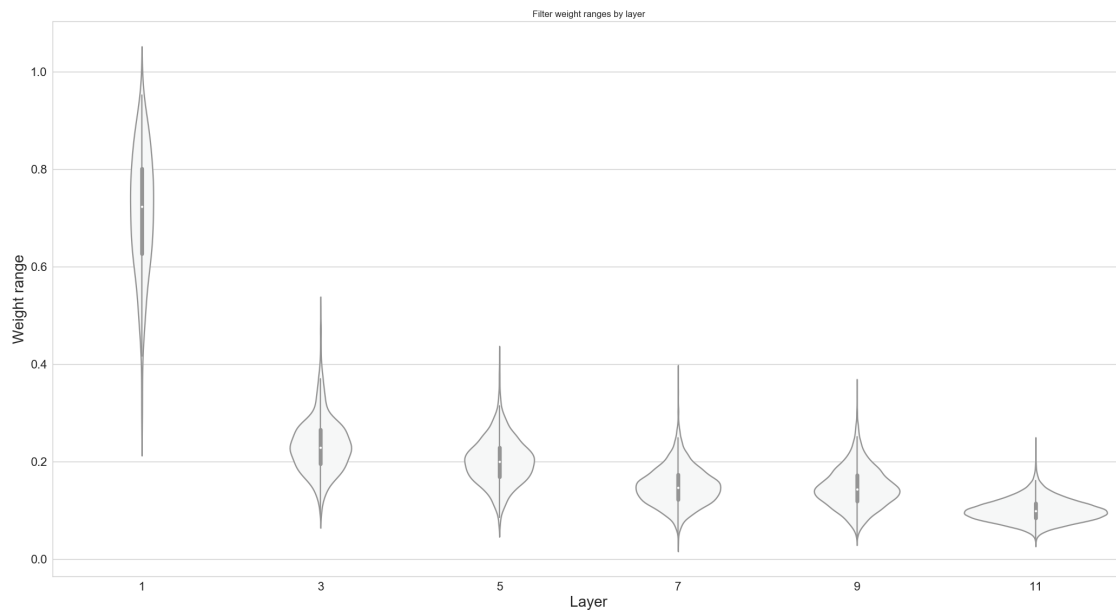
Figure 5.6.: The distribution of the range of values (max - min) of filters by channel and layer. For each filter, the range of values is recorded by channel. The smaller this range is, the less information is lost if a $n \times n$ filter is replaced by a $(n-1) \times (n-1)$ filter.

5.1.3. Training behavior

Due to early stopping, the number of epochs which a model was trained differ. The number of epochs trained with augmentation ranged from 133 epochs to 182 epochs with a standard deviation of 17.3 epochs for CIFAR-100.

Figure 5.7 shows the worst and the best validation accuracy during the training with augmented data. Different initializations lead to very similar validation accuracies during training. The image might lead to the wrong conclusion that models which are better at the start are also better at the end. In order to check this hypothesis, the relative order of validation accuracies for the 10 CIFAR-100 models was examined. If the relative ordering stays approximately the same, then it can be considered to run the first few epochs many times and only train the best models to the end. For 10 models, there can be $\frac{10^2-10}{2} = 45$ pair-wise changes in the ordering at maximum if the relative order of validation accuracies is reversed. For the baseline model, 21.8 changes in the relative order of accuracies occurred in average for each pair of epochs $(i, i+1)$. This means if one knows only the relative order of the validation accuracy of two models m and m' in epoch i, it is doubtful if one can make any statement about the ordering of m and m' in epoch $i+1$.
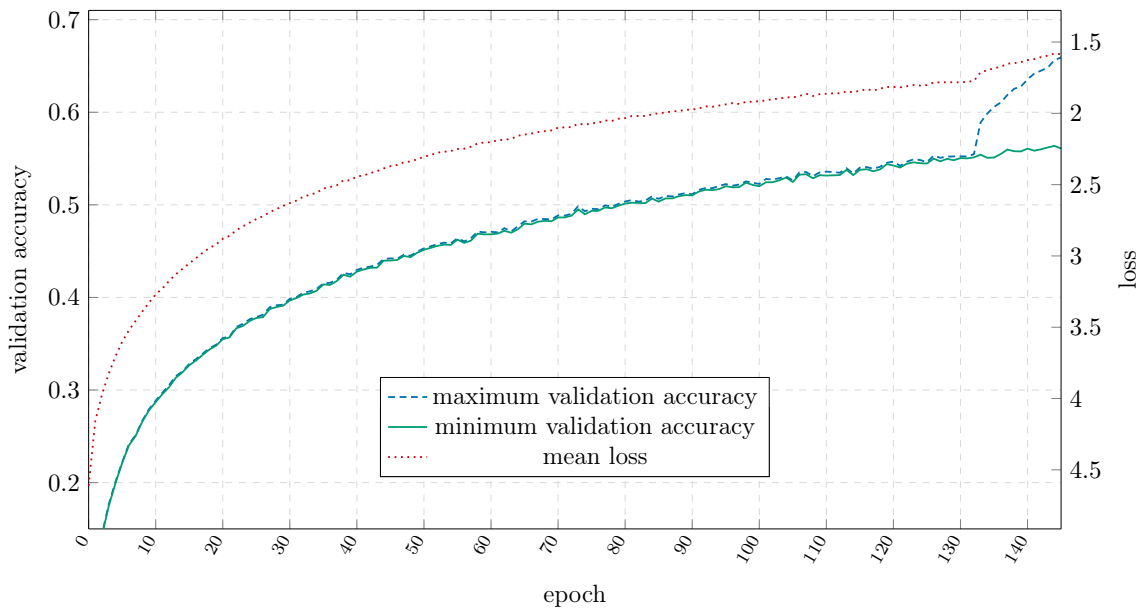
Figure 5.7.: Minimum and maximum validation accuracy of the 10 trained models by epoch. The differences do not exceed 1 % and does not increase by training epoch. Four models stopped the first training stage at epoch 133 which causes the shift in the loss and the maximum validation accuracy.

Figures 5.8 to 5.10 show how the weights changed while training on CIFAR-100. It was expected that the absolute value of weight updates during epochs (sum, max, and mean) decrease in later training stages. The intuition was that weights need to be adjusted in a coarse way first. After that, the intuition was that only slight modifications are applied by

the SGD based training algorithm (ADAM). The mean, max and sum of weight updates as displayed in Figures 5.8 to 5.10, however, do not show such a clear pattern. The biggest change happens as expected in the first epoch after the weights are initialized. The change from augmented training to non-augmented training was at epoch 156 to epoch 157

It can be observed, that layers which receive more input feature maps get larger weight updates in mean. As layers which are closer to the output take more input feature maps, their weight updates are larger. This pattern does not occur when SGD is used as the optimizer.
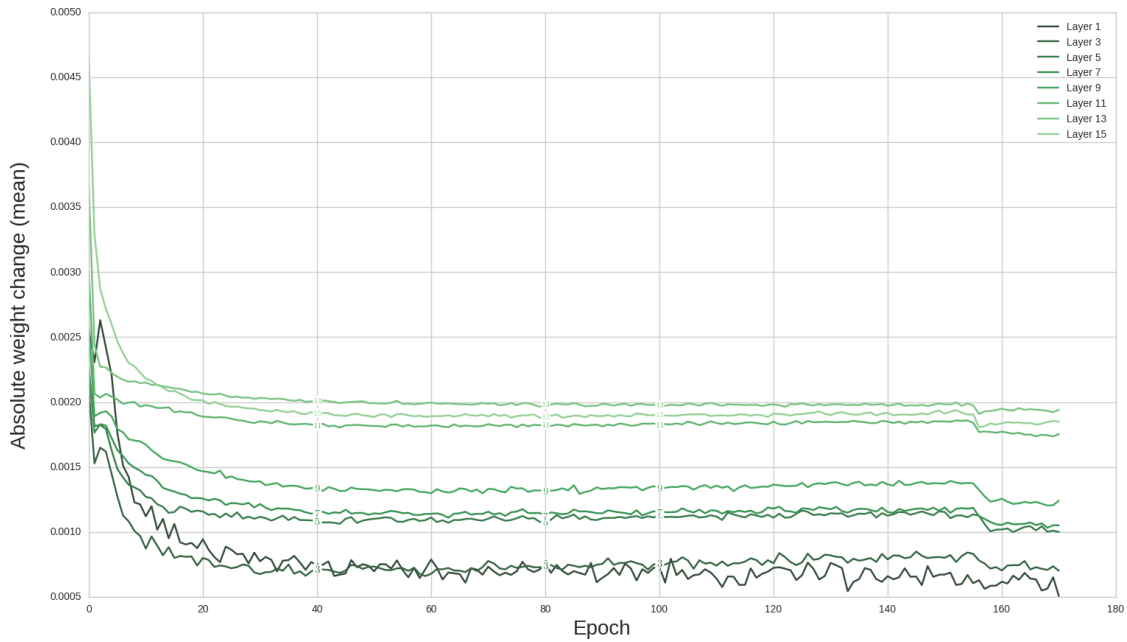
Figure 5.8.: Mean weight updates of the baseline model between epochs by layer.
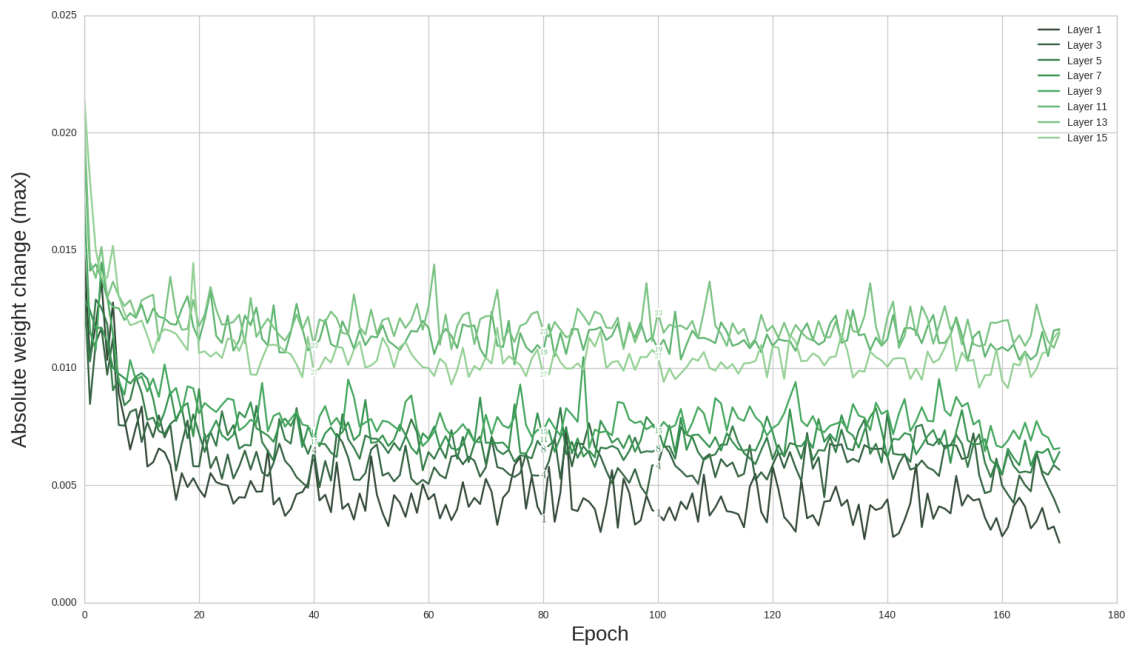
Figure 5.9.: Maximum weight updates of the baseline model between epochs by layer.
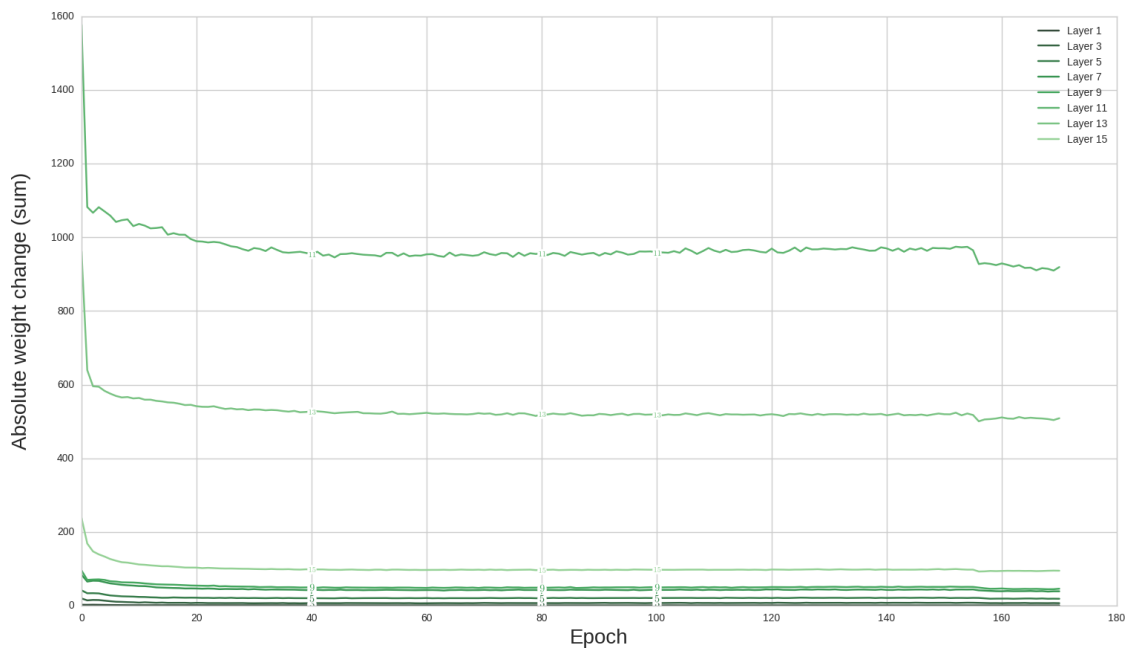
Figure 5.10.: Sum of weight updates of the baseline model between epochs by layer.

5.2. Confusion Matrix Ordering

The visualization of the confusion matrix can give valuable information about which part of the task is hard. For more than about 10 classes, however, it becomes hard to visualize and read.

For CIFAR-10, the proposed method groups the four object classes and the six animal classes together (see Figure 5.11a).

(a) CIFAR-10 Test set
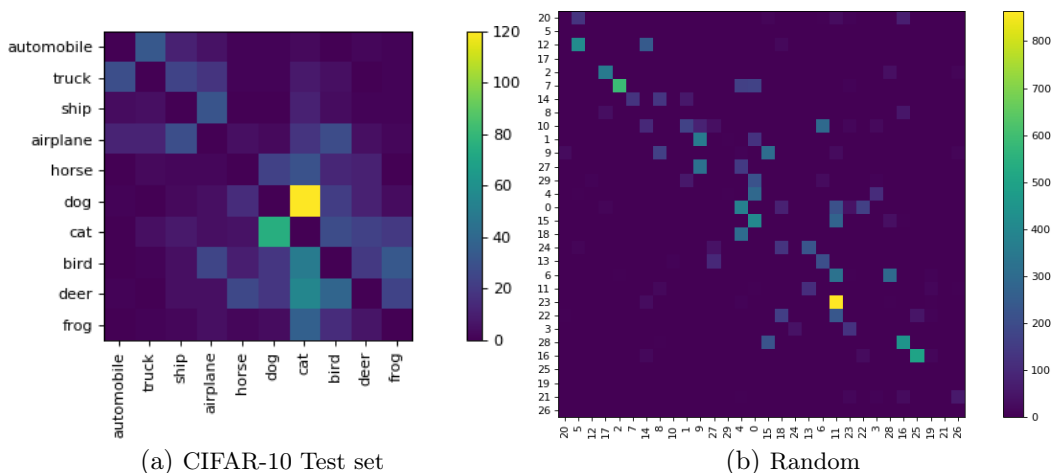
(b) Random

Figure 5.11.: Figure 5.11a shows an ordered confusion matrix of the CIFAR-10 dataset. The diagonal elements are set to 0 in order to make other elements easier to see.
Figure 5.11b shows a confusion matrix with random mistakes.

The first image of Figure 5.12 shows one example of a classifier with only 97.13 % test accuracy where a good permutation was found. Please note that this is not the best classifier. The confusion matrix which resulted from a baseline classifier with 99.32 % test accuracy is displayed in as the second image.

Those results suggest that the ordering of classes is a valuable tool to make patterns easier to see. Humans, however, are good at finding patterns even if they come from random noise. Hence, for comparison, a confusion matrix of a classifier with 30 classes, 60 % accuracy and 40 % uniformly random errors of a balanced dataset is created, optimized according to Equation (4.1) and shown in Figure 5.11b. It clearly looks different than Figure 5.11a.

On the HASYv2 dataset the class-ordering is necessary to see anything as most possible confusions do not happen. See Figure 5.13 for comparison of the first 50 classes of the unsorted confusion matrix and the sorted confusion matrix. If confusion matrices of a maximum size of 50 × 50 are displayed, the ordered method can show only 8 matrices because the off-diagonal matrices are almost 0. Without sorting, 64 matrices have to be displayed.
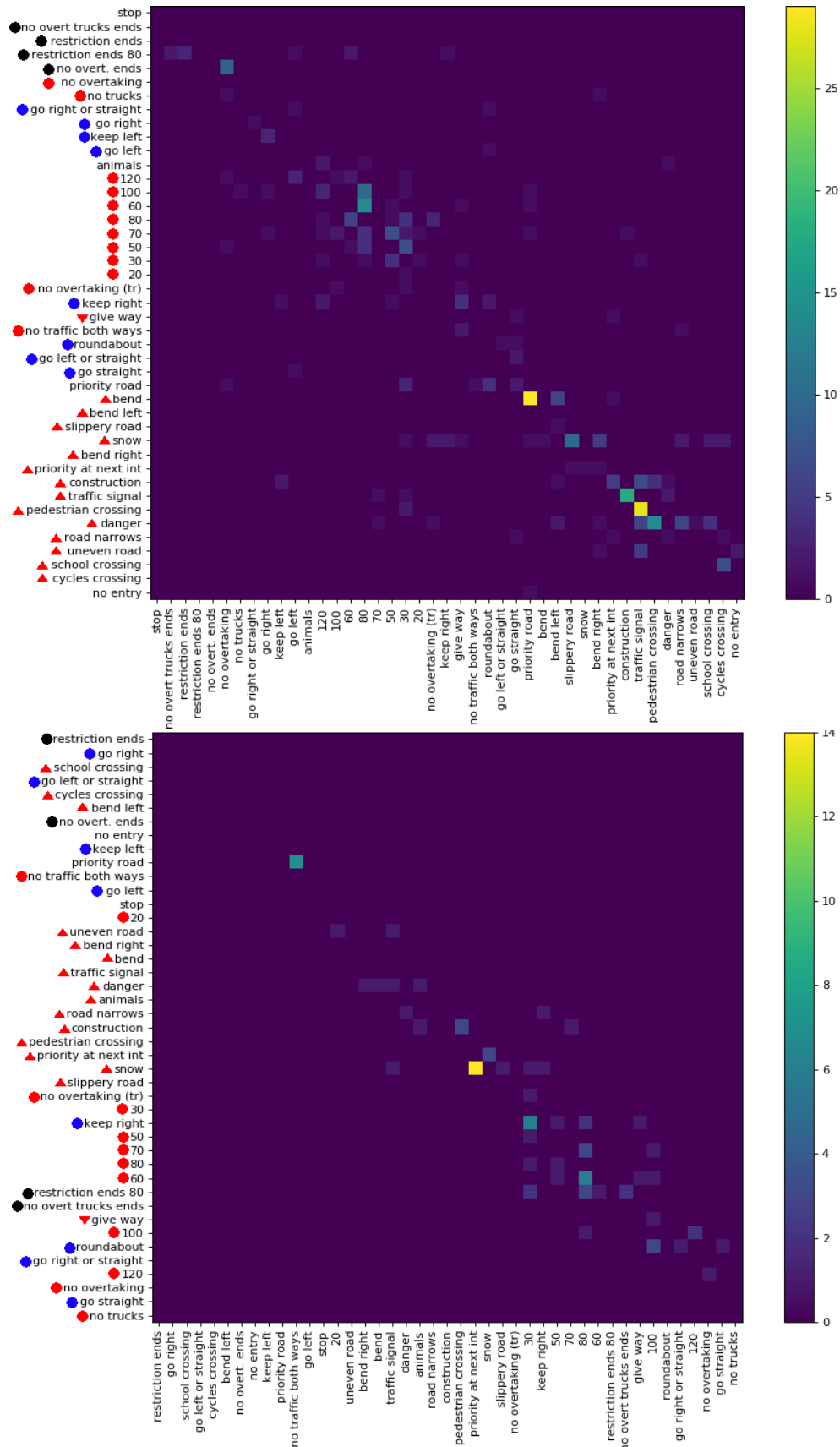
Figure 5.12.: The first image shows the confusion matrix for the test of GTSRB set after optimization to Equation (4.1). The diagonal elements are set to 0 in order to make other elements easier to see. The symbols next to the label on the vertical axis indicate the shape and the color of the signs.
The second image shows the same, but with baseline model.
Best viewed in electronic form.

49
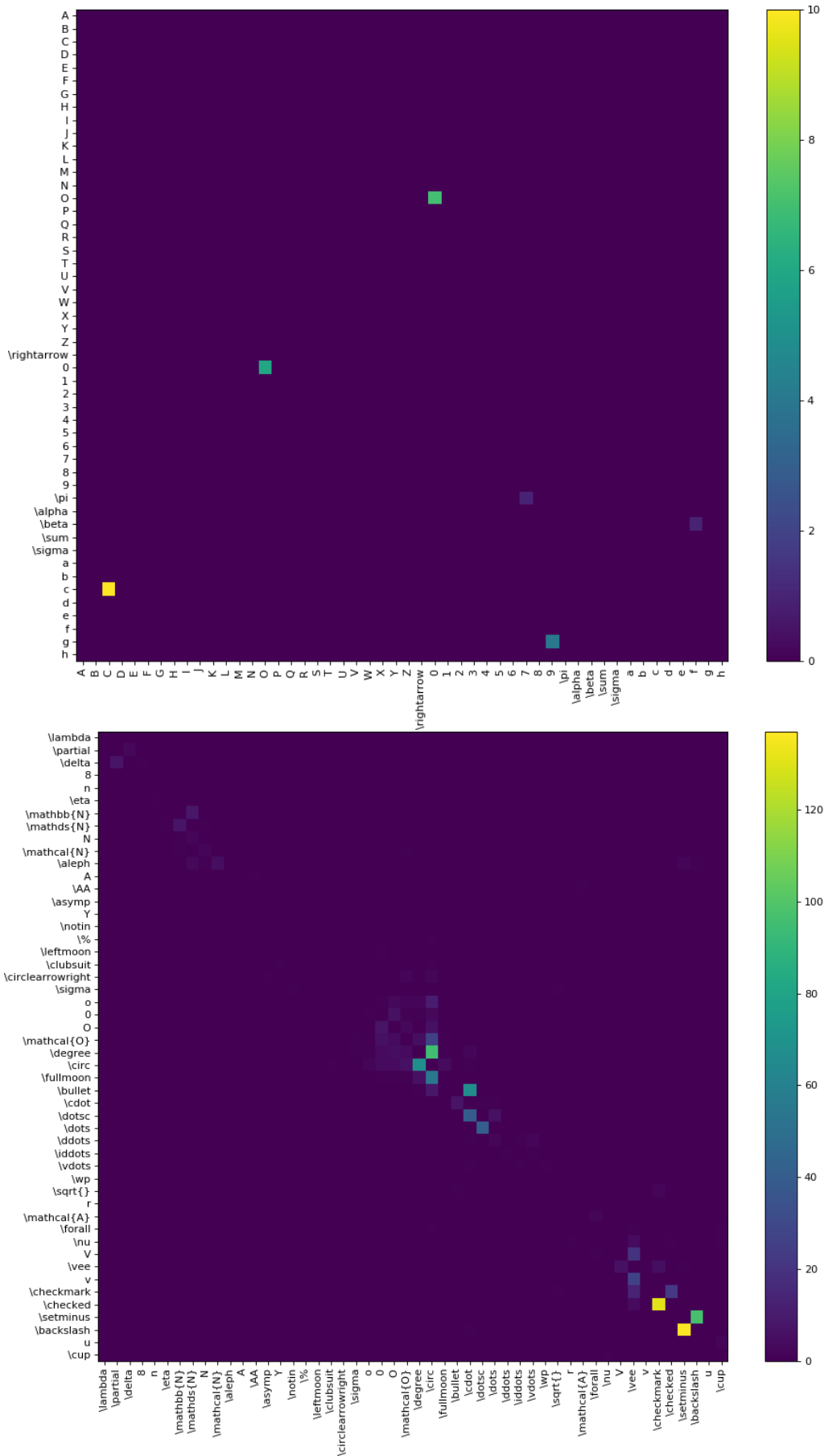
Figure 5.13.: The first 50 entries of the confusion matrix of the HASYv2 dataset. The diagonal elements are set to 0 in order to make other elements easier to see. The top image shows arbitrary class ordering, the bottom image shows the optimized ordering.

5.3. Spectral Clustering vs CMO

This section evaluates the clustering quality of CMO in comparison to the clustering quality of spectral clustering.

The evaluated model achieves 70.50% training accuracy and 53.16% test accuracy on CIFAR-100. Figure 5.14 shows the sorted confusion matrix.
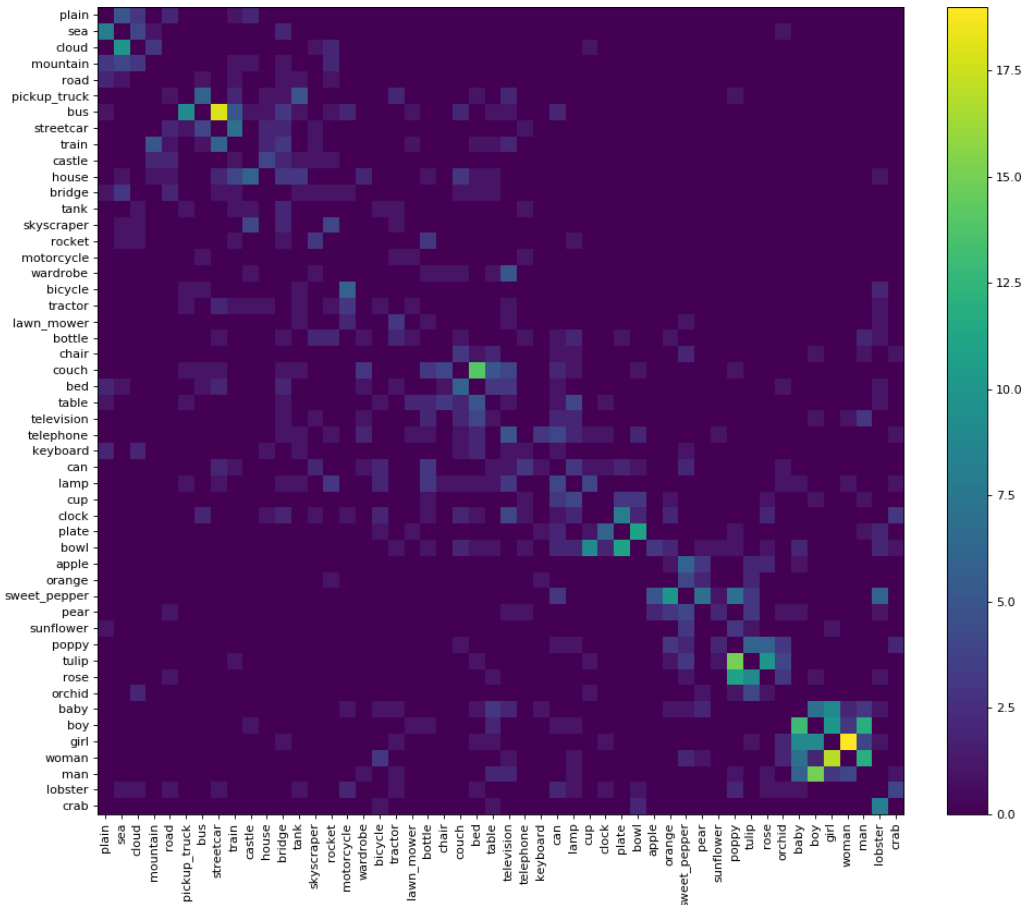
Figure 5.14.: The first 50 entries of the ordered confusion matrix of the CIFAR-100 dataset. The diagonal elements are set to 0 in order to make other elements easier to see. Best viewed in electronic form.

CIFAR-100 has pre-defined coarse classes. Those are used as a ground truth for the clusters which are to be found. The number of errors is determined by (i) Join all n clusters which contain the classes of the coarse class C to a set M. The error is n. (ii) Within M, find the set of classes M^- which do not belong to C. (iii) The final error is $n + |M^-|$. As can be seen in Table 5.4, both clustering methods find reasonable clusters. CMO, however, has only half the error of spectral clustering.

The results for the HASYv2 dataset are qualitatively similar (see Table 5.5). It should be noted that the number of clusters was determined by using the semi-automatic method based on CMO as described in Section 4.2.

Cluster	Spectral clustering	Errors	CMO	Errors
fish	aquarium fish, orchid + flatfish + ray, shark + trout, lion	5	aquarium fish, orchid + flatfish + ray + shark, trout	4
flowers	orchid, aquarium fish + sunflower + poppy, tulip + rose, train	5	orchid, aquarium fish + sunflower, poppy, tulip, rose	2
people	baby, boy, man + girl + woman	2	baby, boy, girl, woman, man	0
reptiles	crocodile, plain, road, table, wardrobe + dinosaur + lizard + snake, worm + turtle	9	crocodile, lizard, lobster, caterpillar + dinosaur + snake + turtle, crab	6
trees	maple, oak, pine + willow, forest + palm	3	palm, willow, pine, maple, oak	0
Total		24		12

Table 5.4.: Differences in spectral clustering and CMO. Classes in a cluster are separated by ,, whereas clusters are separated by +.

Cluster	Spectral clustering	Errors	CMO	Errors
A	A, $\mathcal{A}$, $\mathscr{A}$	0	A, $\mathcal{A}$, $\mathscr{A}$, Å	1
B	B, $\mathcal{B}$	0	B, $\mathcal{B}$	0
C	C, c, $\subset$ and $\mathscr{C}$, ξ, $\mathscr{E}$ and $\mathcal{C}$	4	C, c, $\subset$, $\mathcal{C}$ and $\mathscr{C}$	1
D	D, $\mathcal{D}$, $\mathscr{D}$, $\triangleright$	1	D, $\mathcal{D}$, $\mathscr{D}$	0
E	E and $\mathcal{E}$, ε	2	E and $\mathcal{E}$, ε, ϵ, $\in$	4
F	F and $\mathcal{F}$, $\mathscr{F}$	1	F and $\mathcal{F}$, $\mathscr{F}$	1
H	H and $\mathscr{H}$, $\varkappa$ and $\mathcal{H}$	3	H and $\mathcal{H}$, $\mathscr{H}$	1
K	K, κ	0	K, κ	0
L	L, $\lfloor$ and $\mathcal{L}$, $\mathscr{L}$	1	L, $\lfloor$ and $\mathcal{L}$, $\mathscr{L}$	1
M	M and $\mathcal{M}$ and $\mathfrak{M}$	2	M and μ, $\mathcal{M}$ and $\mathfrak{M}$	3
N	N and $\mathbb{N}$, $\mathbb{N}$ and $\mathcal{N}$	2	N and $\mathbb{N}$, $\mathbb{N}$ and $\mathcal{N}$, $\aleph$	3
O	O, $\mathcal{O}$, 0, $\circ$, $^\circ$, $\bigcirc$ and o	1	O, $\mathcal{O}$, 0, $\circ$, $^\circ$ and $\bigcirc$ and o	2
P	P, $\mathcal{P}$ and p, ρ and $\mathscr{P}$ and $\wp$	3	P and $\mathcal{P}$, $\mathscr{P}$, $\wp$ and p, ρ	2
Q	Q, $\mathbb{Q}$, $\mathbb{Q}$, ι, $\sqcup$, $\gtrsim$, ℓ, $\Im$, Æ, 1	7	Q and $\mathbb{Q}$, $\mathbb{Q}$	1
R	R, $\mathcal{R}$ and $\mathbb{R}$, $\mathbb{R}$, k and $\Re$	3	R and $\Re$, $\mathcal{R}$, $\mathbb{R}$, $\mathbb{R}$	1
S	S, s, $\mathcal{S}$	0	S, s, $\mathcal{S}$	0
T	T, $\top$ and $\mathcal{T}$, τ	1	T, $\top$ and $\mathcal{T}$, τ	1
U	U, $\cup$ and u, $\mathcal{U}$, $\mathfrak{A}$	1	U, u, $\mathcal{U}$, $\mathfrak{A}$ and $\cup$	2
V	V, v, $\vee$	0	V, v, $\vee$	0
W	W, w, ω	0	W, w and ω	1
X	X, x, $\mathcal{X}$, χ, $\times$	0	X, x, $\mathcal{X}$, χ, $\times$	0
Y	Y and y	1	Y, y	0
Z	Z, z, $\mathcal{Z}$ and $\mathbb{Z}$, $\mathbb{Z}$	1	Z, z, $\mathbb{Z}$, $\mathcal{Z}$, $\mathbb{Z}$	0
Total		34		25

Table 5.5.: Differences in spectral clustering and CMO.

5.4. Hierarchy of Classifiers

In a first step, a classifier is trained on the 100 classes of CIFAR-100. The fine-grained root classifier achieves an accuracy of 65.29 % with test-time transformations. The accuracy on the found sub-classes are listed in Table 5.6. The fact that the root classifier achieves better results within a cluster than the specialized leaf classifiers in 13 of 14 cases could either be due to limited training data, overfitting or the small size of $32\,px \times 32\,px$ of the data. The experiment also shows that most of the errors are due to not identifying the correct cluster. Hence, in this case, more work in improving the root classifier is necessary rather than improving the discrimination of classes within a cluster.

Although the classes within a cluster capture most of the classifications, many misclassifications happen outside of the clusters. For example, in cluster 3, a perfect leaf classifier would push the accuracy in the *full* column only to 63.50 % due to errors of the root classifier where the root classifier does not predict the correct cluster.

The leaf classifiers use the same topology as the root classifier. By initializing them with the root classifiers weights their performance can be pushed at about the *inner* accuracy. They are, however, only useful if their accuracy is well above the *inner* accuracy of the root classifier. Hence, for CIFAR-100, building hierarchies of classifiers is not useful.

| | | accuracy | | |
| | | root classifier | | leaf classifier |
Cluster	Classes	cluster identified	class identified | cluster	class identified | cluster
1	3	69.67 %	84.27 %	72.98 %
2	5	46.60 %	58.54 %	43.47 %
3	2	58.50 %	92.13 %	83.46 %
4	2	50.50 %	87.83 %	81.74 %
5	3	44.67 %	79.29 %	71.01 %
6	2	29.50 %	78.67 %	72.00 %
7	2	52.50 %	92.11 %	87.72 %
8	2	59.50 %	86.23 %	81.88 %
9	2	59.00 %	90.08 %	87.79 %
10	2	62.00 %	85.52 %	73.10 %
11	2	67.00 %	87.01 %	75.32 %
12	2	72.50 %	94.77 %	76.77 %
13	2	64.00 %	82.58 %	86.27 %
14	2	79.67 %	89.85 %	89.10 %

Table 5.6.: Accuracies of the root classifier trained on the full set of 100 classes evaluated on 14 clusters of classes. Each class has 100 elements to test. The column *cluster identified* gives the percentage that the root classifiers argmax prediction is within the correct cluster, but not necessarily the correct class. The columns *class identified / cluster* only consider data points where the root classifier correctly identified the cluster.

5.5. Increased width for faster learning

More filters in one layer could simplify the optimization problem as each filter needs smaller updates. Hence a CNN N with n_i filters in layer i is expected to take more epochs than a CNN N' with $2 \cdot n_i$ filters in layer i to achieve the same validation accuracy.

This hypothesis can be falsified by training a CNN N and a CNN N' and comparing the trained number of epochs. As more filters can lead to different results depending on the layer where they are added, five models are trained. The details about those models are given in Table 5.7

Name	Layer	Filter count Baseline	New	Total parameters
m_9	9	64	638	5 978 566
m_9'	9	64	974	8 925 622
m_{11}	11	512	3786	5 982 698
m_{11}'	11	512	1024	1 731 980
m_{13}	13	512	8704	5 982 092

Table 5.7.: Models which are identical to the baseline, except that the number of filters of one layer was increased.

The detailed results are given in Table 5.8. As expected, the number of training epochs of the models with increased numbers of parameters is lower. The wall-clock time, however, is higher due to the increase in computation per forward- and backward-pass.

For m_9, m_{11} and m_{13}, the filter weight range of the layer with increased capacity decreases compared to Figure 5.6, the filter weights of the layer with increased capacity are more concentrated around zero compared to Figure 5.2. For model m_{13}, the distribution of weight of the output layer changed to a more bell-shaped distribution. Except for this, the distribution of filter weights in other layers did not change for all three models compared to the baseline.

Model	Parameters	Accuracy Single Model Mean	std	Ensemble	Training Mean Epochs	Mean Time
baseline	944 012	63.38 %	0.55	64.70 %	154.7	3856 s
m_9	5 978 566	65.53 %	**0.37**	66.72 %	105.7	4472 s
m_9'	8 925 622	65.10 %	1.09	66.54 %	**95.6**	5261 s
m_{11}	5 982 698	**65.73 %**	0.77	**67.38 %**	149.2	5450 s
m_{11}'	1 731 980	62.12 %	0.48	62.89 %	143.6	**3665 s**
m_{13}	5 982 092	62.39 %	0.66	63.77 %	147.8	4485 s

Table 5.8.: Training time in epochs and wall-clock time for the baseline and models m_9, m_{11}, m_{13} as well as their accuracies.

5.6. Weight updates

Section 5.5 shows that wider networks learn faster. One hypothesis why this happens is that every single weight updates can be smaller to learn the same function. Thus the loss function is smoother and thus gradient descent based optimization algorithms lead to more consistent weight updates.

Consequently, it is expected that layers with fewer filters have more erratic updates. If there are many filters, the weights of a filter which does not contribute much to the end results or is even harmful filter can gradually be set to zero, essentially removing one path in the network.

In order to test the hypothesis, the baseline model was adjusted. The number of filters in layer 5 was reduced from 64 filters to 3 filters. As one can see in Figure 5.15, the mean weight update of the layers 1, 3, 5, 7 and 9 have a far bigger range than the layers 11, 13 and 15 after epoch 50. Compared to the baseline models mean updates (Figure 5.8, Page 46), the mean weight updates of layers 1 and 3 are higher, the range of the mean weight update from epoch 50 is higher for layer 5 and the range of mean updates of layer 7 is higher.

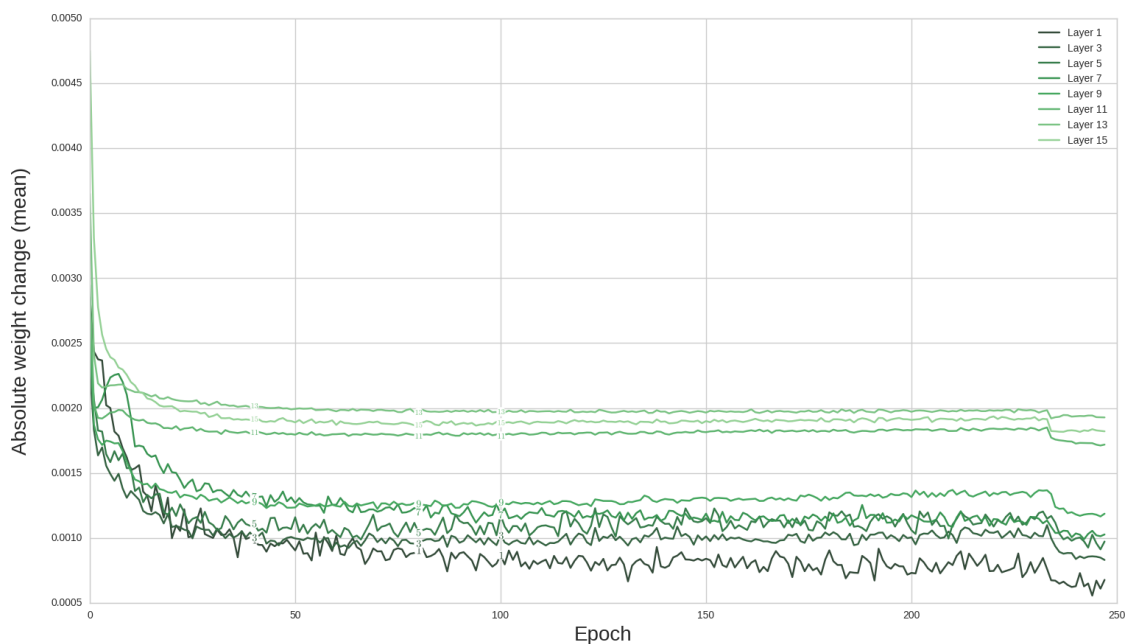For the maximum and the sum, no similar pattern could be observed (see Figures A.3 and A.4).

Figure 5.15.: Mean weight updates between epochs by layer. The model is the baseline model, but with layer 5 reduced to 3 filters.

5.7. Multiple narrow layers vs One wide layer

On a given feature map size one can have an arbitrary number of convolutional layers with `SAME` padding and each layer can have an arbitrary number of filters. A convolutional layer with more filters is called *wider* [ZK16], a convolutional layer with fewer filters is thus called narrower and the number of filters in a convolutional layer is the layers *width*.

If the number of parameters which may be used for the feature map scale is fixed and high enough, there are still many combinations. If n_i with $i = 0, \ldots, k$ is the number of output feature maps of layer i where $i = 0$ is the input layer and all filters are 3×3 filters without a bias, then the number of parameters is

$$\text{Parameters} = \sum_{i=1}^{k} \left((n_{i-1} \cdot 3^2 + 1) \cdot n_i \right)$$

Hence the width of one layer does not only influence the parameters in this layer, but also in the next layer.

The number of possible subsequent layers of one feature map size is enormous, even if constraints are placed on the number of parameters. For example, the first convolutional layer of the baseline model has 896 parameters. If one assumes that less than 3 filters per layer are not desirable, one keeps all layers having a bias and all layers only use 3×3 filters, then the maximum depth is 10. If one furthermore assumes that at least 800 parameters should be used, there are still 120 possible layer combinations. As experimentally evaluating one layer combination takes about 10 hours on a GTX 970 for CIFAR-100 it is not possible to evaluate all layer combinations. In the following, a couple of changes to the network width / depth will be evaluated.

Each layer expands the perceptive field. Hence deeper layer can use more of the input for every single output value. But deeper networks need more time for inference as the output of layer i has to be computed before the output of $i + 1$ can be computed. Hence there is less potential to parallelize computations. Each filter can be seen as a concept which can be learned. The deeper the filter is in the network, the higher is the abstraction level of the concept. In most cases, both is necessary: Many different concepts (width) and high-level concepts (depth).

Reducing the two first convolutional layers of the baseline model (see Page 39) to one convolutional layer of 48 filters (944 396 parameters in total, whereas the baseline model has 944 012 parameters) resulted in a mean accuracy of 61.64 % (-1.74 %) and a standard deviation of $\sigma = 1.12$ (+0.57). The ensemble achieved 63.18 % (-1.52 %). As expected, the training time per epoch was reduced. For the GTX 980, it was reduced from 22.0 s of the baseline model to 15 s of the model with one less convolutional layer, one less Batch Normalization and one less activation layer. The inference time was also reduced from 6 ms

to 4 ms for 1 image and from 32 ms to 23 ms for 128 images. Due to the loss in accuracy of more then one percentage point of the mean model and the increased standard deviation of the models performance, at least two convolutional layers are on the $32\,\text{px} \times 32\,\text{px}$ feature map scale are recommendable for CIFAR-100.

Changing the baseline to have less filters but more layers is another option. This was tried for the first block at the $32\,\text{px} \times 32\,\text{px}$ feature map scale. The two convolutional layers (layers $1-4$ in Page 39) were replaced by two convolutional layers with 27 filters and one convolutional layer with 26 filters in the `convolution - BN - ELU` pattern. The model has 944 132 parameters. Compared to the baseline model, the time for inference was the same. This is unexpected, because the inference time changed when a layer was removed at this scale. The mean test accuracy was 63.66 % (+0.28) and the standard deviation was $\sigma = 1.03$ (+0.48). The ensemble achieved 64.91 % test accuracy (+0.21).

Having two nonlinearities at each feature map scale could be important to learn nonlinear transformations at that scale. As the baseline model does only have one nonlinearity at the 8×8 feature maps scale, another convolutional layer with 64 filters, Batch Normalization and ELU was added. To keep the number of parameters constant, layer 11 of the baseline model was reduced from 512 filters to 488 filters. The new model achieves a mean accuracy of 63.09 % (-0.29) with a standard deviation of $\sigma = 0.70$ (+0.15). The ensemble achieves an accuracy of 64.39 % (+0.31). This could indicate that having two convolutional layers is more important for layers close to the input than intermediate layer. Alternatively, the parameters could be more important in layer 11 than having a new convolutional layer after layer 9.

In order to control the hypothesis that having two convolutional layers are less important in the middle of a network, the second convolutional layer at the 16×16 feature map scale is removed. The first convolutional layer was increased from 32 filters to 59 filters, the second convolutional layer was increased from 32 filter s to 58 filters in order to keep the amount of parameters of the model constant. The adjusted model achieved 62.72 % (-0.66) mean test accuracy with a standard deviation of $\sigma = 0.84$ (+0.29). The ensemble achieved 63.88 % test accuracy (-0.66).

Even more extreme, if both convolutional layers are removed from the 16×16 feature map scale, the mean test accuracy drops to 61.21 % (-2.17) with a standard deviation of $\sigma = 0.51$ (-0.04). The ensemble achieves a test accuracy of 63.07 % (-1.63). Thus it is very important to have at least one convolutional layer at this feature map scale.

5.8. Batch Normalization

In [CUH15], the authors write that Batch Normalization does not improve ELU networks. Hence the effect of removing Batch Normalization from the baseline is investigated in this

experiment.

As before, 10 models are trained on CIFAR-100. The training setup and the model $m_{\text{no-bn}}$ are identical to the baseline model m, except that in $m_{\text{no-bn}}$ the Batch Normalization layers are removed.

One notable difference is the training time: While m needs $21\,\text{ms}$ per epoch in average on a GTX 980, $m_{\text{no-bn}}$ only needs $21\,\text{ms}$ per epoch. The number of epochs used for training, however, also increased noticeably from 149 epochs to 178 epochs in average. The standard deviation of trained epochs is 17.3 epochs for the baseline model and 23.4 epochs for $m_{\text{no-bn}}$.

The mean accuracy of $m_{\text{no-bn}}$ is $62.86\,\%$ and hence 0.52 percentage points worse. The standard deviation between models increased from 0.55 to 0.61. This is likely a result of the early stopping policy and the differences in training epochs. This can potentially be fixed by retraining the models which stopped earlier than the model which was trained for the biggest amount of epochs. The ensemble test accuracy is $63.88\,\%$ and hence 0.82 percentage points worse than the baseline.

The filter weight range and distribution is approximately the same as Figure 5.6 and Figure 5.2, but the distribution of bias weights changed noticeably: While the bias weights of the baseline are spread out in the first layer and much more concentrated in subsequent layers (see Figure 5.3), the model without Batch Normalization has rather concentrated weights in the first layers and only the bias weights of the last layer is spread out (see Figure A.2).

Another model $m'_{\text{no-bn}}$ which has one more filter in the convolutional layer 1, 3, 5, and 7 to compensate for the loss of parameters in Batch Normalization. The mean test accuracy of 10 such models is $62.87\,\%$ which is 0.51 percentage points worse than the baseline. The ensemble of $m'_{\text{no-bn}}$ achieves $64.33\,\%$ which is 0.37 percentage points worse than the baseline. The mean training time was $14\,\text{s}$ per epoch and 157.4 epochs with a standard deviation of 20.7 epochs.

Hence it is not advisable to remove Batch Normalization for the final model. It could, however, be possible to remove Batch Normalization for the experiments to iterate quicker through different ideas if the relative performance changes behave the same with or without Batch Normalization.

5.9. Batch size

The mini-batch size $m \in \mathbb{N}_{\geq 1}$ influences

- **Epochs until convergence**: The smaller m, the more often the model is updated in one epoch. Those updates, however, are based on fewer samples of the dataset. Hence the gradients of different mini-batches can noticeably differ. In the literature, this is referred to as gradient noise [KMN+16].

- **Training time per epoch**: The smaller the batch size, the higher the training time per epoch as the hardware is not optimally utilized.

- **Resulting model quality**: The choice of the hyperparameter m influences the accuracy of the classifier when training is finished. [KMN+16] supports the view that smaller m result in less sharp minima. Hence smaller m lead to better generalization.

Empiric evaluation results can be found in Table 5.9. Those results confirm the claim of [KMN+16] that lower batch sizes generalize better.

m	Training time	Epochs	Mean total training time	Single model Accuracy	std	Ensemble Accuracy
8	$118 \frac{s}{epoch}$	**81 − 153**	$14\,131\,s$	$61.93\,\%$	$\sigma = 1.03$	$65.68\,\%$
16	$62 \frac{s}{epoch}$	$103 − 173$	$8349\,s$	**64.16 %**	$\sigma = 0.81$	**66.98 %**
32	$35 \frac{s}{epoch}$	$119 − 179$	$5171\,s$	$64.11\,\%$	$\sigma = 0.75$	$65.89\,\%$
64	$25 \frac{s}{epoch}$	$133 − 195$	**2892 s**	$63.38\,\%$	$\boldsymbol{\sigma = 0.55}$	$64.70\,\%$
128	$18 \frac{s}{epoch}$	$145 − 239$	$3126\,s$	$62.23\,\%$	$\sigma = 0.73$	$63.55\,\%$

Table 5.9.: Training time per epoch and single model test set accuracy (mean and standard deviation) of baseline models trained with different mini-batch sizes m on GTX 970 GPUs on CIFAR-100.

5.10. Bias

Figure 5.3 suggests that the bias is not important for the layers 11, 13 and 15. Hence a model $m_{\text{no-bias}}$ is created which is identical to the baseline model m, except that the bias of layers 11, 13 and 15 is removed.

The mean test accuracy of 10 trained $m_{\text{no-bias}}$ is $63.74\,\%$ which is an improvement of 0.36 percentage points over the baseline. The ensemble achieves a test accuracy of $65.13\,\%$ which is 0.43 percentage points better than the baseline. Hence the bias can safely be removed.

Removing the biases did not have a noticeable effect on the filter weight range, the filter weight distribution or the distribution of the remaining biases. Also, the γ and β parameters of the Batch Normalization layers did not noticeably change.

5.11. Learned Color Space Transformation

In [MSM16] it is described that placing one convolutional layer with 10 filters of size 1×1 directly after the input and then another convolutional layer with 3 filters of size 1×1 acts as a learned transformation in another color space and boosts the accuracy.

This approach was evaluated on CIFAR-100 by adding a convolutional layer with ELU activation and 10 filters followed by another convolutional layer with ELU activation and 3 filters. The mean accuracy of 10 models was $63.31\,\%$ with a standard deviation of 1.37. The standard deviation is noticeable higher than the standard deviation of the baseline model (0.55) and the accuracy also decreased by 0.07 percentage points. The accuracy of the ensemble is at $64.77\,\%$ and hence 0.07 percentage points higher than the accuracy of the baseline models.

The inference time for 1 image and for 128 images did not change compared to the baseline. The training time per epoch increased from $26\,\mathrm{s}$ to $30\,\mathrm{s}$ on the GTX 970.

Hence it is not advisable to use the learned color space transformation.

5.12. Pooling

An alternative to max pooling with stride 2 with a 2×2 kernel is using a 3×3 kernel with stride 2.

This approach was evaluated on CIFAR-100 by replacing all max pooling layers with the 3×3 kernel max pooling (and `SAME` padding). The mean accuracy of 10 models was $63.32\,\%$ (-0.06) and the standard deviation was 0.57 $(+0.02)$. The ensemble achieved $65.15\,\%$ test accuracy $(+0.45)$.

The training time per epoch decreased from $20.5\,\mathrm{s}$-$21.1\,\mathrm{s}$ to $18.6\,\mathrm{s}$ (mean of 10 training runs) on the Nvidia GTX 970. The time for inference increased from $25\,\mathrm{ms}$ to $26\,\mathrm{ms}$ for a batch of 128 images.

5.13. Activation Functions

Nonlinear, differentiable activation functions are important for neural networks to allow them to learn nonlinear decision boundaries. One of the simplest and most widely used activation functions for CNNs is ReLU [KSH12], but others such as ELU [CUH15], parametrized rectified linear unit (PReLU) [HZRS15b], softplus [ZYL+15] and softsign [BDLB09] have been proposed. The baseline uses ELU.

Activation functions differ in the range of values and the derivative. The definitions and other comparisons of eleven activation functions are given in Table B.3.

Theoretical explanations why one activation function is preferable to another in some scenarios are the following:

- **Vanishing Gradient**: Activation functions like tanh and the logistic function saturate outside of the interval $[-5, 5]$. This means weight updates are very small for preceding neurons, which is especially a problem for very deep or recurrent networks as described in [BSF94]. Even if the neurons learn eventually, learning is slower [KSH12].

- **Dying ReLU**: The dying ReLU problem is similar to the vanishing gradient problem. The gradient of the ReLU function is 0 for all non-positive values. This means if all elements of the training set lead to a negative input for one neuron at any point in the training process, this neuron does not get any update and hence does not participate in the training process. This problem is addressed in [MHN13].

- **Mean unit activation**: Some publications like [CUH15, IS15] claim that mean unit activations close to 0 are desirable. They claim that this speeds up learning by reducing the bias shift effect. The speedup of learning is supported by many experiments. Hence the possibility of negative activations is desirable.

Those considerations are listed in Table 5.10 for 11 activation functions. Besides the theoretical properties, empiric results are provided in Tables 5.11 and 5.12. The baseline network was adjusted so that every activation function except the one of the output layer was replaced by one of the 11 activation functions.

As expected, PReLU and ELU performed best. Unexpected was that the logistic function, tanh and softplus performed worse than the identity and it is unclear why the pure-softmax network performed so much better than the logistic function. One hypothesis why the logistic function performs so bad is that it cannot produce negative outputs. Hence the logistic$^-$ function was developed:

$$\text{logistic}^-(x) = \frac{1}{1 + e^{-x}} - 0.5$$

The logistic$^-$ function has the same derivative as the logistic function and hence still suffers from the vanishing gradient problem. The network with the logistic$^-$ function achieves an accuracy which is $11.30\,\%$ better than the network with the logistic function, but is still $5.54\,\%$ worse than the ELU.

Similarly, ReLU was adjusted to have a negative output:

$$\text{ReLU}^-(x) = \max(-1, x) = \text{ReLU}(x + 1) - 1$$

The results of ReLU$^-$ are much worse on the training set, but perform similar on the test

set. The result indicates that the possibility of hard zero and thus a sparse representation is either not important or similar important as the possibility to produce negative outputs. This contradicts [GBB11, SMGS14].

A key difference between the logistic$^-$ function and ELU is that ELU does neither suffers from the vanishing gradient problem nor is its range of values bound. For this reason, the S2ReLU activation function, defined as

$$\text{S2ReLU}(x) = ReLU(\frac{x}{2} + 1) - ReLU(-\frac{x}{2} + 1) = \begin{cases} -\frac{x}{2} + 1 & \text{if } x \leq -2 \\ x & \text{if } -2 \leq x \leq 2 \\ \frac{x}{2} + 1 & \text{if } x > -2 \end{cases}$$

This function is similar to SReLUs as introduced in [JXF$^+$16]. The difference is that S2ReLU does not introduce learnable parameters. The S2ReLU was designed to be symmetric, be the identity close to zero and have a smaller absolute value than the identity farther away. It is easy to compute and easy to implement.

Those results — not only the absolute values, but also the relative comparison — might depend on the network architecture, the training algorithm, the initialization and the dataset. Results for MNIST can be found in Table 5.13 and for HASYv2 in Table A.2. For both datasets, the logistic function has a much shorter training time and a noticeably lower test accuracy.

Function	Vanishing Gradient	Negative Activation possible	Bound activation
Identity	No	Yes	No
Logistic	Yes	No	Yes
Logistic$^-$	Yes	Yes	Yes
Softmax	Yes	Yes	Yes
tanh	Yes	Yes	Yes
Softsign	Yes	Yes	Yes
ReLU	Yes[1]	No	Half-sided
Softplus	No	No	Half-sided
S2ReLU	No	Yes	No
LReLU/PReLU	No	Yes	No
ELU	No	Yes	No

Table 5.10.: Properties of activation functions.

[1] The dying ReLU problem is similar to the vanishing gradient problem.

Function	Single model				Ensemble of 10	
	Training set		Test set		Training set	Test set
Identity	66.25 %	$\boldsymbol{\sigma = 0.77}$	56.74 %	$\sigma = 0.51$	68.77 %	58.78 %
Logistic	51.87 %	$\sigma = 3.64$	46.54 %	$\sigma = 3.22$	61.19 %	54.58 %
Logistic⁻	66.49 %	$\sigma = 1.99$	57.84 %	$\sigma = 1.15$	69.04 %	60.10 %
Softmax	75.22 %	$\sigma = 2.41$	59.49 %	$\sigma = 1.25$	78.87 %	63.06 %
Tanh	67.27 %	$\sigma = 2.38$	55.70 %	$\sigma = 1.44$	70.21 %	58.10 %
Softsign	66.43 %	$\sigma = 1.74$	55.75 %	$\sigma = 0.93$	69.78 %	58.40 %
ReLU	78.62 %	$\sigma = 2.15$	62.18 %	$\sigma = 0.99$	81.81 %	64.57 %
ReLU⁻	76.01 %	$\sigma = 2.31$	62.87 %	$\sigma = 1.08$	78.18 %	64.81 %
Softplus	66.75 %	$\sigma = 2.45$	56.68 %	$\sigma = 1.32$	71.27 %	60.26 %
S2ReLU	63.32 %	$\sigma = 1.69$	56.99 %	$\sigma = 1.14$	65.80 %	59.20 %
LReLU	74.92 %	$\sigma = 2.49$	61.86 %	$\sigma = 1.23$	77.67 %	64.01 %
PReLU	**80.01 %**	$\sigma = 2.03$	62.16 %	$\sigma = 0.73$	**83.50 %**	**64.79 %**
ELU	76.64 %	$\sigma = 1.48$	**63.38 %**	$\sigma = 0.55$	78.30 %	64.70 %

Table 5.11.: Training and test accuracy of adjusted baseline models trained with different activation functions on CIFAR-100. For LReLU, $\alpha = 0.3$ was chosen.

Function	Inference per		Training time	Epochs	Mean total training time
	1 Image	128			
Identity	8 ms	42 ms	$31\,\frac{\text{s}}{\text{epoch}}$	108 − **148**	3629 s
Logistic	6 ms	**31 ms**	$24\,\frac{\text{s}}{\text{epoch}}$	**101** − 167	**2234 s**
Logistic⁻	6 ms	**31 ms**	$\mathbf{22}\,\frac{\text{s}}{\textbf{epoch}}$	133 − 255	3421 s
Softmax	7 ms	37 ms	$33\,\frac{\text{s}}{\text{epoch}}$	127 − 248	5250 s
Tanh	6 ms	**31 ms**	$23\,\frac{\text{s}}{\text{epoch}}$	125 − 211	3141 s
Softsign	6 ms	**31 ms**	$23\,\frac{\text{s}}{\text{epoch}}$	122 − 205	3505 s
ReLU	6 ms	**31 ms**	$23\,\frac{\text{s}}{\text{epoch}}$	118 − 192	3449 s
Softplus	6 ms	**31 ms**	$24\,\frac{\text{s}}{\text{epoch}}$	**101** − 165	2718 s
S2ReLU	**5 ms**	32 ms	$26\,\frac{\text{s}}{\text{epoch}}$	108 − 209	3231 s
LReLU	7 ms	34 ms	$25\,\frac{\text{s}}{\text{epoch}}$	109 − 198	3388 s
PReLU	7 ms	34 ms	$28\,\frac{\text{s}}{\text{epoch}}$	131 − 215	3970 s
ELU	6 ms	**31 ms**	$23\,\frac{\text{s}}{\text{epoch}}$	146 − 232	3692 s

Table 5.12.: Training time and inference time of adjusted baseline models trained with different activation functions on GTX 970 GPUs on CIFAR-100. It was expected that the identity is the fastest function. This result is likely an implementation specific problem of Keras 2.0.4 or Tensorflow 1.1.0.

| Function | Single model | | Ensemble | Epochs | |
	Accuracy	std	Accuracy	Range	Mean
Identity	99.45 %	$\sigma = 0.09$	99.63 %	55 – 77	62.2
Logistic	97.27 %	$\sigma = 2.10$	99.48 %	**37** – 76	**54.5**
Softmax	99.60 %	$\boldsymbol{\sigma = 0.03}$	99.63 %	44 – 73	55.6
Tanh	99.40 %	$\sigma = 0.09$	99.57 %	56 – 80	67.6
Softsign	99.40 %	$\sigma = 0.08$	99.57 %	72 – 101	84.0
ReLU	**99.62 %**	$\sigma = 0.04$	**99.73 %**	51 – 94	71.7
Softplus	99.52 %	$\sigma = 0.05$	99.62 %	62 – **70**	68.9
PReLU	99.57 %	$\sigma = 0.07$	**99.73 %**	44 – 89	71.2
ELU	99.53 %	$\sigma = 0.06$	99.58 %	45 – 111	72.5

Table 5.13.: Test accuracy of adjusted baseline models trained with different activation functions on MNIST.

5.14. Label smoothing

Ensembles consisting of n models trained by the same procedure on the same data but initialized with different weights and trained with a different order of the training data perform consistently better than single models. One drawback of ensembles in applications such as self-driving cars is that they increase the computation by a factor of n. One idea why they improve the test accuracy is by reducing the variance.

The idea of label smoothing is to use the ensemble prediction of the training data as labels for another classifier. For every element x of the training set, the one-hot encoded target $t(x)$ is smoothed by the ensemble prediction $y_E(x)$

$$t'(x) = \alpha \cdot t(x) + (1 - \alpha)y_E(x)$$

where $\alpha \in [0, 1]$ is the smoothing factor.

There are three reasons why label smoothing could be beneficial:

- **Training speed**: The ensemble prediction contains more information about the image than binary class decisions. Classifiers in computer vision predict how similar the input looks to other input of the classes they are trained on. By smoothing the labels, the information that one image could also belong to another class is passed to the optimizer. In early stages of the optimization this could lead to a lower loss on the non-smoothed validation set.

- **Higher accuracy**: Using smoothed labels for the optimization could lead to a higher accuracy of the base-classifier due to a smoothed error surface. It might be less likely

that the classifier gets into bad local minima.

- **Label noise**: Depending on the way how the labels are obtained, it might not always be clear which label is the correct one. Also, labeling errors can be present in training datasets. Those errors severely harm the training. By smoothing the labels errors could be relaxed.

10 models m_{smooth} are trained with the $\alpha = 0.5$ smoothed labels from the prediction of an ensemble of 10 baseline models. The mean accuracy of the models trained on the smoothed training set labels was 63.61% $(+0.23\%)$ and the standard deviation was $\sigma = 0.72$ $(+0.17\%)$. The ensemble of 10 m_{smooth} models achieved 64.79% accuracy $(+0.09\%)$. Hence the effect of this kind of label smoothing on the final accuracy is questionable.

The training speed didn't noticeably change either: The number of trained epochs ranged from 144 to 205, the mean number of epochs was 177. The baseline training ranged from 146 to 232 epochs with a mean of 174 epochs. After 10, 30 and 80 epochs both training methods accuracy differed by less than one percentage point. Hence it is unlikely that label smoothing has a positive effect on the training speed.

Hinton et al. called this method *distillation* in [HVD15]. Hinton et al. used smooth and hard labels for training, this work only used smoothed labels.

5.15. Optimized Classifier

In comparison to the baseline classifier, the following changes are applied to the optimized classifier:

- **Remove the bias for the last layers**: For all layers which output a 1×1 feature map, the bias is removed

- **Increase the max pooling kernel to** 3×3

- **More filters in the first layers**

The detailed architecture is given in Table 5.14 and visualized in Figure 5.16. The evaluation is given in Table 5.15 and the timing comparison is given in Table 5.16.

#	Type	Filters @ Patch size / stride	Parameters	FLOPs	Output size
	Input		0	0	3 @ 32 × 32
1	Convolution	69 @ 3 × 3 × 3 / 1	1 932	3 744 768	**69** @ **32** × **32**
2	BN + ELU		138	353 418	**69** @ **32** × **32**
3	Convolution	69 @ 3 × 3 × 32 / 1	42 918	37 684 096	**69** @ **32** × **32**
4	BN + ELU		138	353 418	**69** @ **32** × **32**
	Max pooling	2 × 2 / 2	0	40 960	32 @ 16 × 16
5	Convolution	64 @ 3 × 3 × 32 / 1	39 808	20 332 544	64 @ 16 × 16
6	BN + ELU		128	82 048	64 @ 16 × 16
7	Convolution	64 @ 3 × 3 × 64 / 1	36 928	**18 857 984**	64 @ 16 × 16
8	BN + ELU		128	82 048	64 @ 16 × 16
	Max pooling	2 × 2 / 2		20 480	64 @ 8 × 8
9	Convolution	64 @ 3 × 3 × 64 / 1	36 928	4 714 496	64 @ 8 × 8
10	BN + ELU		128	20 608	64 @ 8 × 8
	Max pooling	2 × 2 / 2		5 120	64 @ 4 × 4
11	Convolution (v)	512 @ 4 × 4 × 64 / 1	**524 288**	1 048 064	512 @ 1 × 1
12	BN + ELU		1 024	3 584	512 @ 1 × 1
	Dropout 0.5		0	0	512 @ 1 × 1
13	Convolution	512 @ 1 × 1 × 512 / 1	262 144	523 776	512 @ 1 × 1
14	BN + ELU		1 024	3 584	512 @ 1 × 1
	Dropout 0.5		0	0	512 @ 1 × 1
15	Convolution	k @ 1 × 1 × 512 / 1	$512 \cdot k$	$512 \cdot k$	k @ 1 × 1
	Global avg Pooling	1 × 1	0	k	k @ 1 × 1
16	BN + Softmax		$2k$	$7k$	k @ 1 × 1
$\sum$			$514k$ +947 654	$520k$ +87 870 996	$179\,200 + 2k$

Table 5.14.: Optimized architecture with 3 input channels of size 32×32. All convolutional layers use `SAME` padding, except for layer 11 which used `VALID` padding in order to decrease the feature map size to 1×1. If the input feature map is bigger than 32×32, for each power of two there are two `Convolution + BN + ELU` blocks and one `Max pooling` block added. This is the framed part in the table.
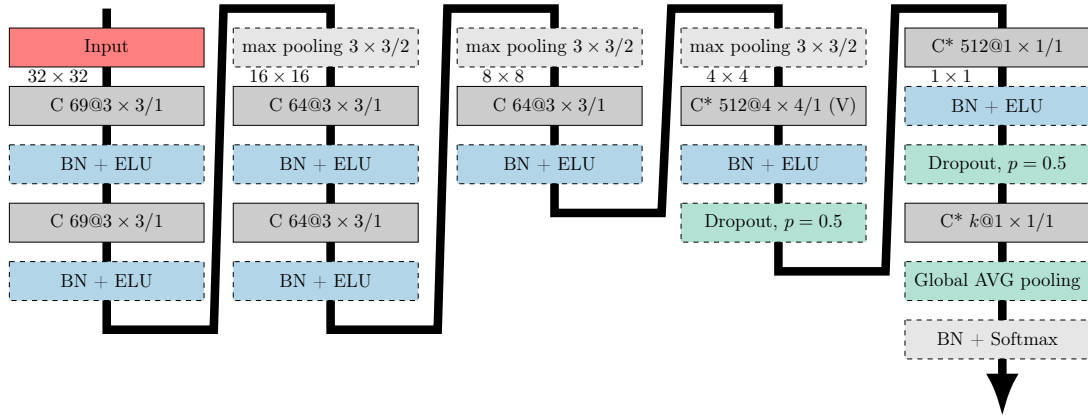
Figure 5.16.: Architecture of the optimized model. `C` $32@3 \times 3/1$ is a convolutional layer with 32 filters of kernel size 3×3 with stride 1. The * indicates that no bias is used.

Dataset	Single Model Accuracy				Ensemble of 10	
	Training Set		Test Set		Training Set	Test Set
Asirra	95.83 %	$\sigma = 4.70$	90.75 %	$\sigma = 4.73$	98.78 %	93.09 %
CIFAR-10	94.58 %	$\sigma = 0.70$	87.92 %	$\sigma = 0.46$	96.47 %	89.86 %
CIFAR-100	77.96 %	$\sigma = 2.18$	64.42 %	$\sigma = 0.73$	81.44 %	67.03 %
GTSRB	100.00 %	$\sigma = 0.00$	99.28 %	$\sigma = 0.10$	100.00 %	99.51 %
HASYv2	88.79 %	$\sigma = 0.45$	85.36 %	$\sigma = 0.15$	89.36 %	85.92 %
MNIST	99.88 %	$\sigma = 0.10$	99.48 %	$\sigma = 0.13$	99.99 %	99.67 %
STL-10	95.43 %	$\sigma = 3.57$	75.09 %	$\sigma = 2.39$	98.54 %	78.66 %
SVHN	99.08 %	$\sigma = 0.07$	96.37 %	$\sigma = 0.12$	99.50 %	97.47 %

Table 5.15.: Optimized model accuracy on eight datasets. The single model actuary is the 10 models used in the ensemble. The empirical standard deviation σ of the accuracy is also given. CIFAR-10, CIFAR-100 and STL-10 models use test-time transformations. None of the models uses unlabeled data or data from other datasets. For MNIST, GTSRB, SVHN and HASY, no test time transformations are used.

Network	GPU	Tensorflow	Inference per		Training
			1 Image	128 images	time / epoch
Optimized	Default	Intel i7-4930K	5 ms	432 ms	386 s
Optimized	Optimized	Intel i7-4930K	4 ms	307 ms	315 s
Optimized	Default	GeForce 940MX	4 ms	205 ms	192 s
Optimized	Default	GTX 970	6 ms	41 ms	35 s
Optimized	Default	GTX 980	3 ms	35 ms	27 s
Optimized	Default	GTX 980 Ti	6 ms	36 ms	26 s
Optimized	Default	GTX 1070	2 ms	24 ms	21 s
Optimized	Default	Titan Black	4 ms	46 ms	43 s

Table 5.16.: Speed comparison of the optimized model on CIFAR-10. The baseline model is evaluated on six Nvidia GPUs and one CPU. The weights for DenseNet-40-12 are taken from [Maj17]. Weights the baseline model can be found at [Tho17b]. The optimized Tensorflow build makes use of SSE4.X, AVX, AVX2 and FMA instructions.

5.16. Early Stopping vs More Data

A separate validation set is necessary for two reasons: (1) Early stopping and (2) preventing overfitting due to many experiments. To prevent overfitting, a different dataset can be used. For example, all decisions about hyperparameters in this thesis are based on CIFAR-100, but the network is finally trained and evaluated with the same hyperparameters on all datasets.[2] The validation set can hence be removed if early stopping is removed. Instead, the validation data is used in a first run to determine the number of epochs necessary for training. In a second training run the validation data is added to the training set. The number of used epochs for the second run is given in Table 5.17.

Dataset	Mean epochs	Train data	classes	average data / class
Asirra	60	15 075	2	7538
MNIST	41	54 000	10	5400
SVHN	45	543 949	10	54 395
CIFAR-10	84	45 000	10	4500
HASYv2	92	136 116	369	369
GTSRB	97	35 288	43	821
STL-10	116	4500	10	450
CIFAR-100	155	45 000	100	450

Table 5.17.: Mean number of training epochs for the optimized model. For comparison, the total amount of used training data, the number of classes of the dataset and the average amount of data per class is given.

Alternatively, the model can be trained with early stopping (ES) purely on the training loss. All three methods – early stopping on the validation set accuracy, early stopping on the training loss and training a fixed number of epochs are evaluated. While having more data helped with Asirra and CIFAR-100, the results as shown in Table 5.18 on the other datasets are only marginally different. For CIFAR-10, training with more data did not improve the results when the number of epochs is fixed, but notably improved the results when the training loss was used as the early stopping criterion.

5.17. Regularization

Stronger regularization might even improve the results when using the training loss as an early stopping criterion. ℓ_2 regularization with a weighting factor of $\lambda = 0.0001$ is used in all other experiments. While the accuracy as shown in Table 5.19 does not show a clear pattern, the number of epochs increases with lower model regularization (see Table 5.20).

---

[2]Except data augmentation and test time transformations.
[3]Only 1 model is trained due to the long training time of 581 epochs and 12 hours for this model.
[4]Only 3 models are in this ensemble due to the long training time of more than 8 hours per model.

| Dataset | Early Stopping | | Fixed epochs |
	val. acc	train loss	
Asirra	93.09 %	96.01 %[3]	96.01 %
CIFAR-10	89.86 %	91.75 %	88.88 %
CIFAR-100	67.03 %	71.01 %	69.08 %
HASYv2	85.92 %	82.89 %[4]	85.05 %
MNIST	99.67 %	99.64 %	99.57 %
STL-10	78.66 %	83.25 %	78.64 %

Table 5.18.: Comparisons of trained optimized models with early stopping on the validation accuracy compared training setups without a validation set and thus more training data. The second column uses the training loss as a stopping criterion, the third column uses a fixed number of epochs which is equal to the mean number of training epochs of the models with early stopping on the validation set accuracy.

| λ | Single Model Accuracy | | | | Ensemble of 10 | |
	Training Set		Test Set		Training Set	Test Set
$\lambda = 0.01$	73.83 %	$\sigma = 1.78$	58.94 %	$\sigma = 1.33$	87.78 %	69.98 %
$\lambda = 0.001$	82.86 %	$\sigma = 0.89$	63.03 %	$\sigma = 0.67$	91.86 %	71.02 %
$\lambda = 0.0001$	77.96 %	$\sigma = 2.18$	64.42 %	$\sigma = 0.73$	81.44 %	67.03 %

Table 5.19.: Different choices of ℓ_2 model regularization applied to the optimized model.

λ	min	max	mean	std
$\lambda = 0.01$	457	503	404.6	37.2
$\lambda = 0.001$	516	649	588.4	41.6
$\lambda = 0.0001$	579	833	696.1	79.1

Table 5.20.: Training time in epochs of models with early stopping on training loss by different choices of ℓ_2 model regularization applied to the optimized model.

6. Conclusion and Outlook

This master thesis gave an extensive overview over the design patterns of CNNs in Chapter 2, the methods how CNNs can be analyzed and the principle directions of topology learning algorithms in Chapter 3.

Confusion Matrix Ordering (CMO), originally developed as a method to make visualizations of confusion matrices easier to read (see Figure 5.13), was introduced as a class clustering algorithm in Chapter 4 and evaluated in Sections 4.2 and 5.4. The important insights are:

- Ordering the classes in the confusion matrix allows to display the relevant parts even for several hundred classes.

- A hierarchy of classifiers based on the classes does not improve the results on CIFAR-100. There are three possible reasons for this:

    - $32\,\mathrm{px} \times 32\,\mathrm{px}$ is too low dimensional

    - 100 classes are not enough for this approach

    - More classes are always easier to distinguish if each new class comes with more data. One reason why this might be the case is that distinguishing the object from background has similar properties even for different classes.

- Label smoothing had only a minor effect on the accuracy and no effect on the training time when a single base classifier was used to train with the smoothed labels by an ensemble of base classifiers.

A baseline model was defined and evaluated on eight publicly available datasets. The baselines topology and training setup are described in detail as well as its behavior during training and properties of the weights of the trained model.

The influence of various hyperparameters is examined in Sections 5.5 to 5.12 for CIFAR-100. The insights of those experiments are:

- Averaging ensembles of 10 base classifiers of the same architecture and trained with the same setup consistently improve the accuracy. The amount of improvement depends on the base classifiers, but the ensemble tends to improve the test accuracy by about one percentage point.

- Wider networks learn in fewer epochs. This, however, does not mean that the

71

wall-clock time is lower due to increased computation in forward- and backward passes.

- Batch Normalization increases the training time noticeably. For the described ELU baseline model it also increases accuracy, which contradicts [CUH15].

- The lower the batch size, the longer the time for each epoch of training and the less epochs need to be trained. Higher accuracy by lower batch sizes was empirically confirmed. The batch size, however, can also be too low.

- An analysis of the weights of the baseline indicated that the bias of layers close to the output layer can be removed. This was experimentally confirmed.

- It could not be confirmed that learned color space transformation, as described in [MSM16], improves the network. Neither with ELU nor with leaky rectified linear unit (LReLU) and $\alpha = 0.3$.

- It could be confirmed that ELU networks gives better results than any other activation function on CIFAR-100. For the character datasets MNIST and HASYv2, however, ReLU, LReLU, PReLU, Softplus and ELU all performed similar.

- Changing the activation functions to the identity had very little impact on the HASYv2 and MNIST classifiers. Note that those networks are still able to learn nonlinear decision boundaries due to max-pooling and `SAME` padding. For CIFAR-100, however, the accuracy drops by 6.64 % when ELU is replaced by the identity.

Based on the results of those experiments, an optimized classifier was developed and evaluated on all eight datasets.

The state of the art of STL-10 was improved from 74.80 % [ZMGL15] to 78.66 % without using the unlabeled part of the dataset. The state of the art of HASYv2 was improved from 81.00 % [Tho17a] to 85.92 %, for GTSRB the state of the art was improved from 99.46 % [SL11] to 99.51 %, for Asirra it was improved from 82.7 % [Gol08] to 93.09 %.[1] This was mainly achieved by the combination of ELU, Dropout, ensembles, training data augmentation and test-time transformations. The removal of the bias of layers close to the output and re-usage of those parameters in layers close to the input as well as using 3×3 pooling instead of 2×2 pooling improved the baseline.

While writing this masters thesis, several related questions could not be answered:

- Deeper CNNs have generally higher accuracy, if trained long enough and if overfitting is not a problem. But at which subsampling-level does having more layers have the biggest effect? Can this question be answered before a deeper network is trained?

- Is label smoothing helpful for noisy labels?

---

[1]The baseline is better than the optimized model on Asirra and on HASYv2.

- How does the choice of activation functions influence residual architectures? Could the results be the same for different activation functions in architectures with hundreds of layers?

- The results for the pooling kernel were inconclusive. Larger pooling kernels might be advantageous as well as fractional max pooling [Gra15].

- Why is the mean weight update (see Figure 5.8) not decreasing? Is this an effect that can and should be fixed?

- Why is softmax so much better than the logistic function? Can the reason be used to further improve ELU?

Besides those questions, the influence of optimizers on time per epoch, epochs until convergence, total training time, memory consumption, accuracy of the models and standard deviation of the models was not evaluated. This, and the stopping criterion for training might be crucial for the models quality.

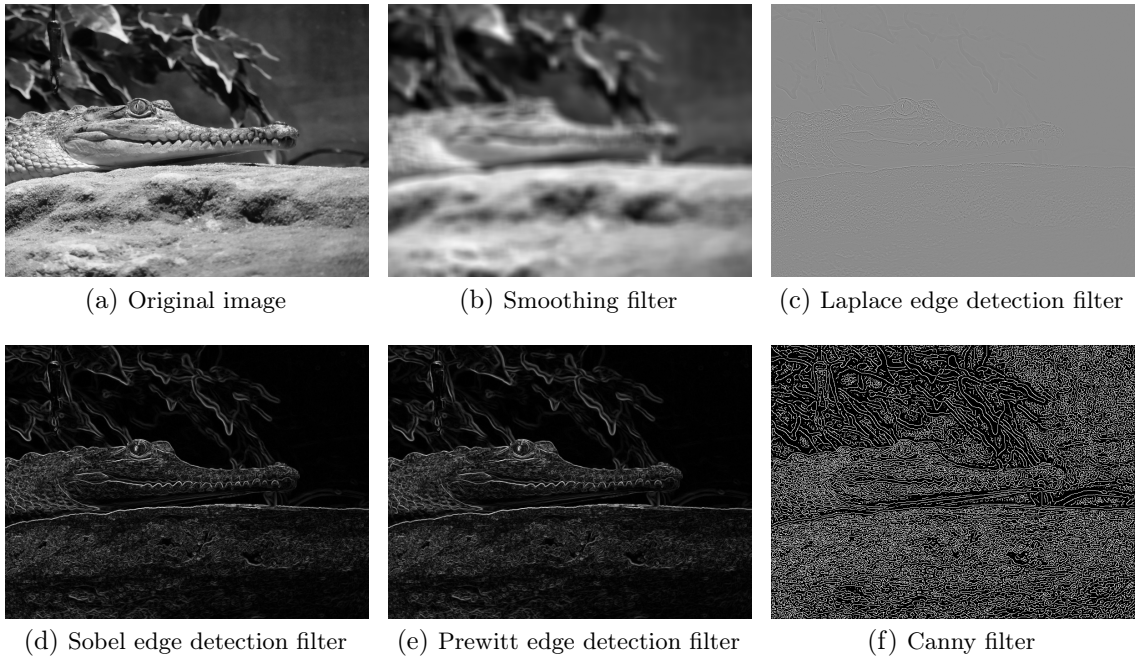# A. Figures, Tables and Algorithms

(a) Original image   (b) Smoothing filter   (c) Laplace edge detection filter

(d) Sobel edge detection filter   (e) Prewitt edge detection filter   (f) Canny filter

Figure A.1.: Examples of image filters. Best viewed in electronic form.

| Layer | 99-percentile interval | |
	filter	bias
1	[-0.50, 0.48]	[-0.06, 0.07]
3	[-0.21, 0.19]	[-0.07, 0.07]
5	[-0.20, 0.17]	[-0.07, 0.05]
7	[-0.15, 0.14]	[-0.05, 0.06]
9	[-0.14, 0.15]	[-0.04, 0.03]
11	[-0.08, 0.08]	[-0.00, 0.00]
13	[-0.08, 0.08]	[-0.00, 0.00]
15	[-0.10, 0.11]	[-0.01, 0.01]

Table A.1.: 99-percentile intervals for filter weights and bias weights by layer of a baseline model trained on CIFAR-100.
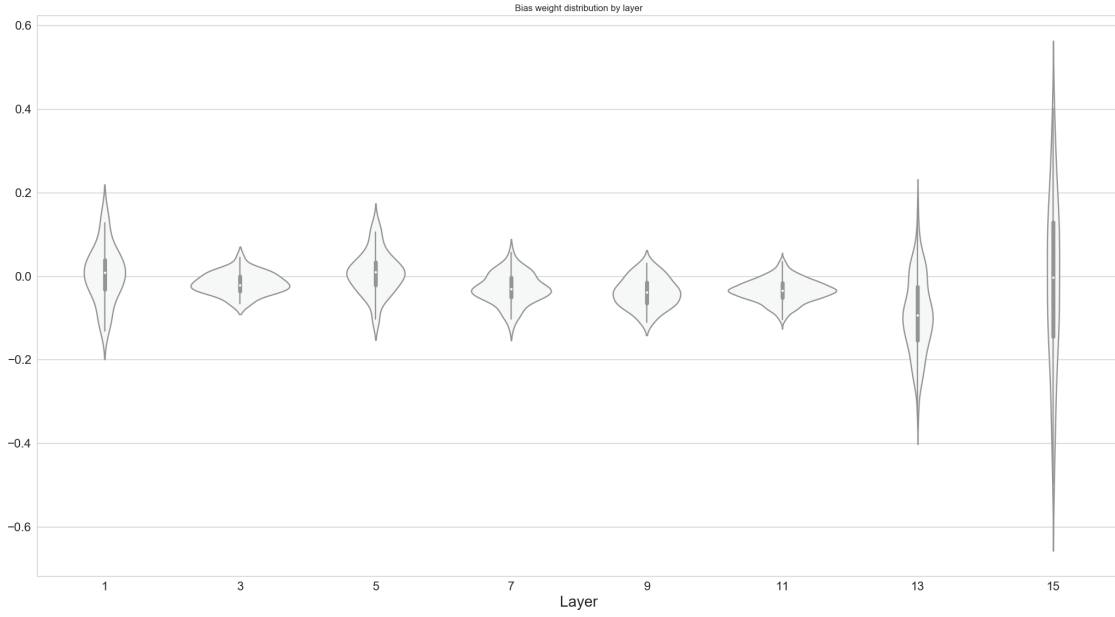
Figure A.2.: The distribution of bias weights of a model without batch normalization trained on CIFAR-100.

Algorithm 1 Simulated Annealing for minimizing Equation (4.1).

Require: $C \in \mathbb{N}^{n \times n}$, steps $\in \mathbb{N}$, $T \in \mathbb{R}^+$, $c \in (0, 1)$

  procedure SIMULATEDANNEALING(C, steps, T, c)

    bestScore $\leftarrow$ ACCURACY(C)

    bestC $\leftarrow C$

    for $i = 0$; $i <$ steps; $i \leftarrow i + 1$ **do**

      $p \leftarrow$ RANDOMFLOAT($0, 1$)

      if $p < 0.5$ **then**   ▷ Swap rows

        $i \leftarrow$ RANDOMINTEGER($1, \ldots, n$)

        $j \leftarrow$ RANDOMINTEGER($1, \ldots, n$) $\setminus \{\, i \,\}$

        $p \leftarrow$ RANDOMUNIFORM($0, 1$)

        $C' \leftarrow$ SWAP(C, i, j)

        $s \leftarrow$ ACCURACY(C')

        if $p < \exp(\frac{s - \text{bestScore}}{T})$ **then**

          $C \leftarrow C'$

          if $s >$ bestScore **then**

            bestScore $\leftarrow s$

            bestC $\leftarrow C$

        $T \leftarrow T \cdot c$

      else   ▷ Move Block

        $s \leftarrow$ RANDOMINTEGER($1, \ldots, n$)   ▷ Block start

        $e \leftarrow$ RANDOMINTEGER($s, \ldots, n$)   ▷ Block end

        $i \leftarrow$ RANDOMINTEGER($1, \ldots, n - (e - s)$)   ▷ Block insert position

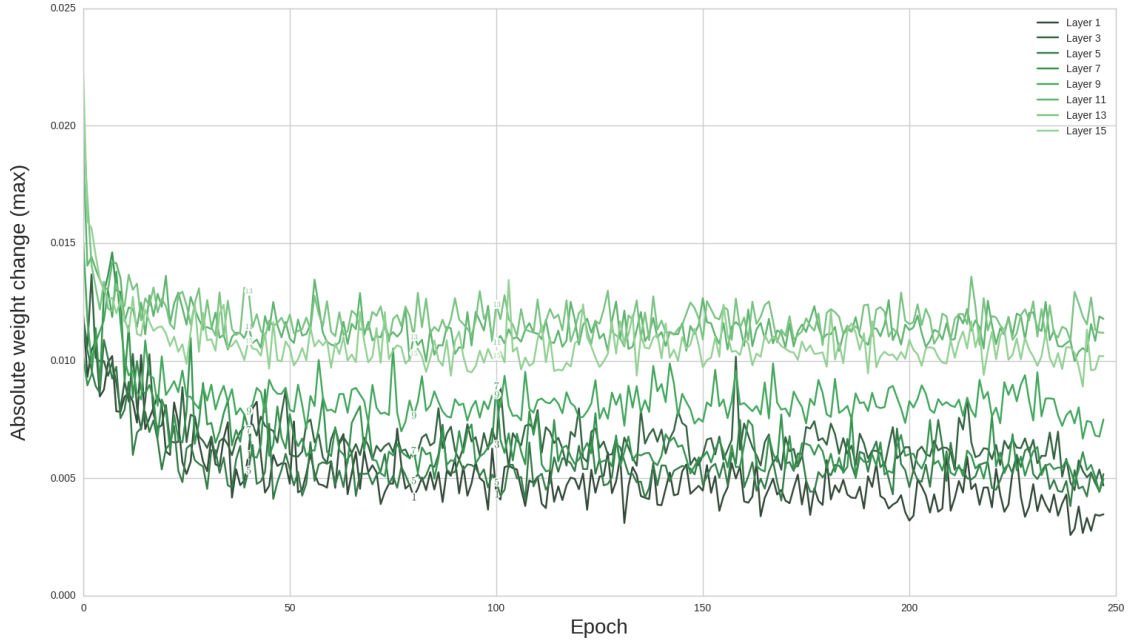   Move Block (s, $\ldots$, e) to position i

    return bestM

Figure A.3.: Maximum weight updates between epochs by layer. The model is the baseline model, but with layer 5 reduced to 3 filters.

Function	Single model				Ensemble of 10		Epochs	
	Training set		Test set		Train	Test	Range	Mean
Identity	87.92 %	$\sigma = 0.40$	84.69 %	$\sigma = 0.08$	88.59 %	85.43 %	92 − 140	114.5
Logistic	81.46 %	$\sigma = 5.08$	79.67 %	$\sigma = 4.85$	86.38 %	84.60 %	**58 − 91**	**77.3**
Softmax	88.19 %	$\sigma = 0.31$	84.70 %	$\sigma = 0.15$	88.69 %	85.43 %	124 − 171	145.8
Tanh	88.41 %	$\sigma = 0.36$	84.46 %	$\sigma = 0.27$	89.24 %	85.45 %	89 − 123	108.7
Softsign	88.00 %	$\sigma = 0.47$	84.46 %	$\sigma = 0.23$	88.77 %	85.33 %	77 − 119	104.1
ReLU	88.93 %	$\sigma = 0.46$	**85.35 %**	$\sigma = 0.21$	89.35 %	85.95 %	96 − 132	102.8
Softplus	88.42 %	$\boldsymbol{\sigma = 0.29}$	85.16 %	$\sigma = 0.15$	88.90 %	85.73 %	108 − 143	121.0
LReLU	88.61 %	$\sigma = 0.41$	85.21 %	$\boldsymbol{\sigma = 0.05}$	89.07 %	85.83 %	87 − 117	104.5
PReLU	**89.62 %**	$\sigma = 0.41$	**85.35 %**	$\sigma = 0.17$	**90.10 %**	86.01 %	85 − 111	100.5
ELU	89.49 %	$\sigma = 0.42$	**85.35 %**	$\sigma = 0.10$	89.94 %	**86.03 %**	73 − 113	92.4

Table A.2.: Test accuracy of adjusted baseline models trained with different activation functions on HASYv2. For LReLU, $\alpha = 0.3$ was chosen.
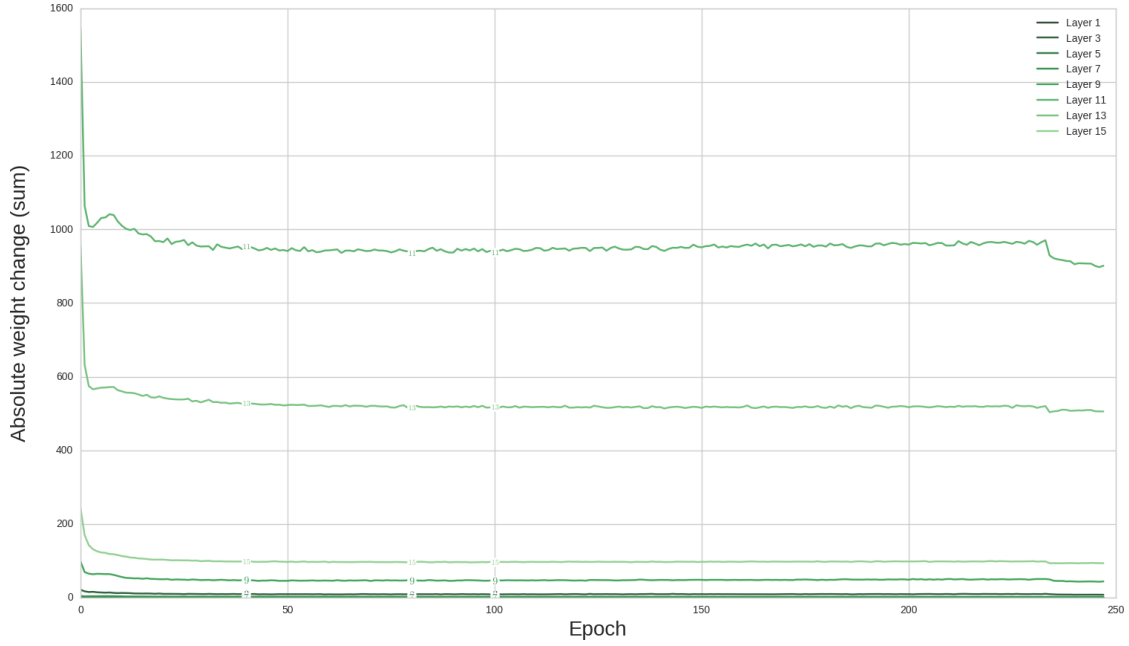
Figure A.4.: Sum of weight updates between epochs by layer. The model is the baseline model, but with layer 5 reduced to 3 filters.

Function	Single model				Ensemble of 10		Epochs	
	Training set		Test set		Train	Test	Range	Mean
Identity	87.49 %	$\sigma = 2.50$	69.86 %	$\sigma = 1.41$	89.78 %	71.90 %	51 – 65	53.4
Logistic	45.32 %	$\sigma = 14.88$	40.85 %	$\sigma = 12.56$	51.06 %	45.49 %	38 – 93	74.6
Softmax	87.90 %	$\sigma = 3.58$	67.91 %	$\sigma = 2.32$	91.51 %	70.96 %	108 – 150	127.5
Tanh	85.38 %	$\sigma = 4.04$	67.65 %	$\sigma = 2.01$	90.47 %	71.29 %	48 – 92	65.2
Softsign	88.57 %	$\sigma = 4.00$	69.32 %	$\sigma = 1.68$	93.04 %	72.40 %	55 – 117	83.2
ReLU	94.35 %	$\sigma = 3.38$	71.01 %	$\sigma = 1.63$	98.20 %	74.85 %	52 – 98	75.5
Softplus	83.03 %	$\sigma = 2.07$	68.28 %	$\sigma = 1.74$	93.04 %	75.99 %	56 – 89	68.9
LReLU	93.83 %	$\sigma = 3.89$	74.66 %	$\sigma = 2.11$	97.56 %	78.08 %	52 – 120	80.1
PReLU	95.53 %	$\sigma = 1.92$	71.69 %	$\sigma = 1.37$	98.17 %	74.69 %	59 – 101	78.8
ELU	95.42 %	$\sigma = 3.57$	75.09 %	$\sigma = 2.39$	98.54 %	78.66 %	66 – 72	67.2

Table A.3.: Test accuracy of adjusted baseline models trained with different activation functions on STL-10. For LReLU, $\alpha = 0.3$ was chosen.

B. Hyperparameters

Hyperparameters are parameters of models which are not optimized automatically (e.g., by gradient descent), but by methods like random search [BB12], grid search [LBOM98] or manual search.

B.1. Preprocessing

Preprocessing used to be of major importance in machine learning. However, with the availability of data sets with hundreds of examples per class and the possibility of CNNs to learn features themselves, most models today rely on raw pixel values. The only common preprocessing is size normalization. In order to get a fixed input-size for a CNN, the following procedure can be used:

- Take one or multiple crops of the image which have the desired aspect ratio.

- Scale the crop(s) to the desired size.

- In training, all crops can be used independently. In testing, all crops can be passed through the network and the output probability distributions can get fusioned, for example by averaging.

Other preprocessing methods are:

- Color space transformations (RGB, HSV, etc.)

- Mean subtraction

- Standardization of pixel-values to $[0, 1]$ by dividing through 255 (used by [HLW16])

- Dimensionality reduction

    - Principal component analysis (PCA): An unsupervised linear transformation which can be learned in the first hidden layer. It is hence doubtful if PCA improves the network.

    - Linear discriminant analysis (LDA)

- Zero Components Analysis (ZCA) whitening (used by [KH09])

B.2. Data augmentation

Data augmentation techniques aim at making artificially more data from real data items by applying invariances. For computer vision, they include:

Name	Augmentation Factor	Used by
Horizontal flip	2	[KSH12, WYS$^+$15]
Vertical flip	2	[DWD15][1]
Rotation	~ 40 ($\delta = 20$)	[DSRB14]
Scaling	~ 14 ($\delta \in [0.7, 1.4]$)	[DSRB14]
Crops	$32^2 = 1024$	[KSH12, WYS$^+$15]
Shearing		[Gra15]
GANs		[BCW$^+$17]
Brightness	~ 20 ($\delta \in [0.5, 1.5]$)	[How13]
Hue	51 ($\delta = 0.1$)	[MRM15, DSRB14]
Saturation	~ 20 ($\delta = 0.5$)	[DSRB14]
Contrast	~ 20 ($\delta \in [0.5, 1.5]$)	[How13]
Channel shift		[KSH12]

Table B.1.: Overview of data augmentation techniques. The augmentation factor is calculated for typical situations. For example, the augmentation factor for random crops is calculated for 256 px × 256 px images which are cropped to 224 px × 224 px.

Taking several scales if the original is of higher resolution than desired is another technique. Combinations of the techniques above can also be applied. Please note that the order of operations does matter in many cases and hence the order is another augmentation factor.

Less common, but also reasonable are:

- Adding noise

- Elastic deformations

- Color casting (used by [WYS$^+$15])

- Vignetting (used by [WYS$^+$15])

- Lens distortion (used by [WYS$^+$15])

---

[1] Vertical flipping combined with 180° rotation is equivalent to horizontal flipping

B.3. Initialization

Weight initializations are usually chosen to be small and centered around zero. One way to characterize many initialization schemes is by

$$w \sim \alpha \cdot \mathcal{U}[-1, 1] + \beta \cdot \mathcal{N}(0, 1) + \gamma \text{ with } \alpha, \beta, \gamma \geq 0$$

Table B.2 shows six commonly used weight initialization schemes. Several schemes use the same idea, that unit-variance is desired for each layer as the training converges faster [IS15].

Name	α	β	γ	Reference
Constant	$\alpha = 0$	$\beta = 0$	$\gamma \geq 0$	used by [ZF14]
Xavier/Glorot uniform	$\alpha = \sqrt{\frac{6}{n_{in}+n_{out}}}$	$\beta = 0$	$\gamma = 0$	[GB10]
Xavier/Glorot normal	$\alpha = 0$	$\beta = \left(\frac{2}{(n_{in}+n_{out})}\right)^2$	$\gamma = 0$	[GB10]
He	$\alpha = 0$	$\beta = \frac{2}{n_{in}}$	$\gamma = 0$	[HZRS15b]
Orthogonal	—	—	$\gamma = 0$	[SMG13]
LSUV	—	—	$\gamma = 0$	[MM15]

Table B.2.: Weight initialization schemes of the form $w \sim \alpha \cdot \mathcal{U}[-1, 1] + \beta \cdot \mathcal{N}(0, 1) + \gamma$.
   n_{in}, n_{out} are the number of units in the previous layer and the next layer. Typically, biases are initialized with constant 0 and weights by one of the other schemes to prevent unit-coadaptation. However, dropout makes it possible to use constant initialization for all parameters.
   LSUV and Orthogonal initialization cannot be described with this simple pattern.

B.4. Objective function

For classification tasks, the cross-entropy

$$E_{CE}(W) = -\sum_{x \in X} \sum_{k=1}^{K} [t_k^x \log(o_k^x) + (1 - t_k^x) \log(1 - o_k^x)]$$

is by far the most commonly used objective function (e.g., used by [ZF14]). In this equation, X is the set of training examples, K is the number of classes, $t_k^x \in \{0, 1\}$ indicates if the training example x is of class k, o_k^x is the output of the classifier for the training example x and class k.

However, regularization terms weighted with a constant $\lambda \in (0, +\infty)$ are sometimes added:

- LASSO: ℓ_1 (e.g., used in [HPTD15])

- Weight decay: ℓ_2 (e.g., $\lambda = 0.0005$ as in [MSM16])

- Orthogonality regularization ($|(W^T \cdot W - I)|$, see [VTKP17])

B.5. Optimization Techniques

Most relevant optimization techniques for CNNs are based on SGD, which updates the weights according to the rule

$$w_{ji} \leftarrow w_{ji} + \Delta w_{ji} \text{ with } \Delta w_{ji} = -\eta \frac{\partial E_x}{\partial w_{ji}}$$

where $\eta \in (0, 1)$, typically 0.01 (e.g., [MSM16]), is called the *learning rate*.

A slight variation of SGD is mini-batch gradient descent with the mini-batch B (typically mini-batch sizes are $|B| \in \{32, 64, 128, 256, 512\}$, e.g. [ZF14]). Larger mini-batch sizes lead to sharp minima and thus poor generalization [KMN+16]. Smaller mini-batch sizes lead to longer training times due to computational overhead and to more training steps due to gradient noise.

$$w_{ji} \leftarrow w_{ji} + \Delta w_{ji} \text{ with } \Delta w_{ji} = -\eta \frac{\partial E_B}{\partial w_{ji}}$$

Nine variations which adjust the learning rate during training are:

- Momentum:

$$w_{ji}^{(t+1)} \leftarrow w_{ji}^{(t)} + \Delta w_{ji}^{(t+1)} \text{ with } \Delta w_{ji}^{(t+1)} = -\eta \frac{\partial E_B}{\partial w_{ji}} + \alpha \Delta w_{ji}^{(t)}$$

  with $\alpha \in [0, 1]$, typically 0.9 (e.g., [ZF14, MSM16])

- Adagrad [DHS11]

- RProp and the mini-batch version RMSProp [TH12]

- Adadelta [Zei12]

- Power Scheduling [Xu11]: $\eta(t) = \eta(0)(1 + a \cdot t)^{-c}$, where $t \in \mathbb{N}_0$ is the training step, a, c are constants.

- Performance Scheduling [SHY+13]: Measure the error on the cross validation set and decrease the learning rate when the algorithms improvement is below a threshold.

- Exponential Decay Learning Rate [SHY+13]: $\eta(t) = \eta(0) \cdot 10^{-\frac{t}{k}}$ where $t \in \mathbb{N}_0$ is the training step, $\eta(0)$ is the initial learning rate, $k \in \mathbb{N}_{\geq 1}$ is the number of training steps until the learning rate is decreased by $\frac{1}{10}$th.

- Newbob Scheduling [new00]: Start with Performance Scheduling, then use Exponential Decay Scheduling.

- Adam and AdaMax [KB14]

- Nadam [Doz15]

Some of those are explained in [Rud16].

Other first-order gradient optimization methods are:

- Quickprop [Fah88]

- Nesterov Accellerated Momentum (NAG) [Nes83]

- Conjugate Gradient method [Cha92]: Combines a line search for the step size with the gradients direction.

Higher-order gradient methods like Newtons method or quasi-Newton methods like BFGS and L-BFGS need the inverse of the Hessian matrix which is intractable for today's CNNs.

However, there are alternatives which do not use gradient information:

- Genetic algorithms such as NeuroEvolution of Augmenting Topologies (NEAT) [SM02]

- Simulated Annealing [vLA87]

- Twiddle: A local hill-climbing algorithm explained by Sebastian Thrun and described on [Tho14b]

There are also approaches which learn the optimization algorithm [ADG+16, LM16].

B.6. Network Design

CNNs have the following hyperparameters:

- **Depth**: The number of layers
- **Width**: The number of filters per layer
- **Layer and block connectivity graph**
- **Layer and block hyperparameters**:
  - Activation Functions as shown in Table B.3
  - For more, see Sections 2.2 and 2.3.

Name	Function $\varphi(x)$	Range of Values	$\varphi'(x)$	Used by
Sign function[†]	$\begin{cases} +1 & \text{if } x \geq 0 \\ -1 & \text{if } x < 0 \end{cases}$	$\{-1, 1\}$	0	[KS02]
Heaviside step function[†]	$\begin{cases} +1 & \text{if } x > 0 \\ 0 & \text{if } x < 0 \end{cases}$	$\{0, 1\}$	0	[MP43]
Logistic function	$\frac{1}{1+e^{-x}}$	$[0, 1]$	$\frac{e^x}{(e^x+1)^2}$	[DJ99]
Tanh	$\frac{e^x - e^{-x}}{e^x + e^{-x}} = \tanh(x)$	$[-1, 1]$	$\text{sech}^2(x)$	[LBBH98, Tho14a]
ReLU[†]	$\max(0, x)$	$[0, +\infty)$	$\begin{cases} 1 & \text{if } x > 0 \\ 0 & \text{if } x < 0 \end{cases}$	[KSH12]
LReLU[†2] (PReLU)	$\varphi(x) = \max(\alpha x, x)$	$(-\infty, +\infty)$	$\begin{cases} 1 & \text{if } x > 0 \\ \alpha & \text{if } x < 0 \end{cases}$	[MHN13, HZRS15b]
Softplus	$\log(e^x + 1)$	$(0, +\infty)$	$\frac{e^x}{e^x+1}$	[DBB$^+$01, GBB11]
ELU	$\begin{cases} x & \text{if } x > 0 \\ \alpha(e^x - 1) & \text{if } x \leq 0 \end{cases}$	$(-\infty, +\infty)$	$\begin{cases} 1 & \text{if } x > 0 \\ \alpha e^x & \text{otherwise} \end{cases}$	[CUH15]
Softmax[‡]	$o(\mathbf{x})_j = \frac{e^{x_j}}{\sum_{k=1}^{K} e^{x_k}}$	$[0, 1]^K$	$o(\mathbf{x})_j \cdot \frac{\sum_{k=1}^{K} e^{x_k} - e^{x_j}}{\sum_{k=1}^{K} e^{x_k}}$	[KSH12, Tho14a]
Maxout[‡]	$o(\mathbf{x}) = \max_{x \in \mathbf{x}} x$	$(-\infty, +\infty)$	$\begin{cases} 1 & \text{if } x_i = \max \mathbf{x} \\ 0 & \text{otherwise} \end{cases}$	[GWFM$^+$13]

Table B.3.: Overview of activation functions. Functions marked with † are not differentiable at 0 and functions marked with ‡ operate on all elements of a layer simultaneously. The hyperparameters $\alpha \in (0, 1)$ of Leaky ReLU and ELU are typically $\alpha = 0.01$. Other activation function like randomized leaky ReLUs exist [XWCL15], but are far less commonly used.
Some functions are smoothed versions of others, like the logistic function for the Heaviside step function, tanh for the sign function, softplus for ReLU.
Softmax is the standard activation function for the last layer of a classification network as it produces a probability distribution. See Figure B.1 for a plot of some of them.

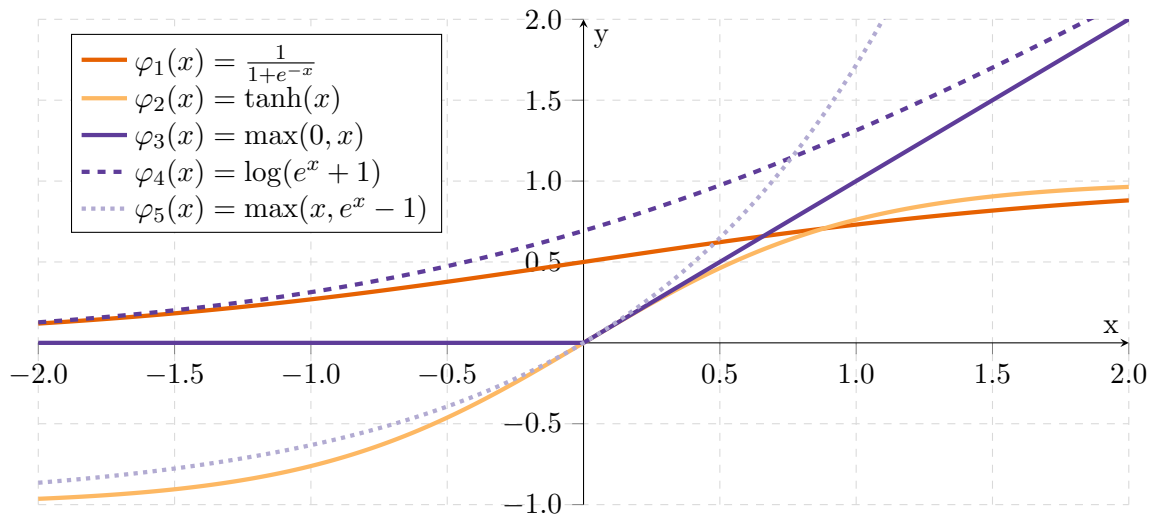[2]α is a hyperparameter in leaky ReLU, but a learnable parameter in the parametric ReLU function.

Figure B.1.: Activation functions plotted in $[-2, +2]$. tanh and ELU are able to produce negative numbers. The image of ELU, ReLU and Softplus is not bound on the positive side, whereas tanh and the logistic function are always below 1.

B.7. Regularization

Regularization techniques aim to make the fitted function smoother and reduce overfitting. Regularization techniques are:

- ℓ_1, ℓ_2, and Orthogonality regularization: See Appendix B.4

- Max-norm regularization (e.g. used ins [SHK+14])

- Dropout (introduced in [SHK+14]), DropConnect (see [WZZ+13]), Stochastic Depth (see [HSL+16])

- Feature scale clipping (see [ZF14])

- Data augmentation (according to [ZBH+16])

- Global average pooling (according to [ZKL+15])

- Dense-Sparse-Dense training (see [HPN+16])

- Soft targets (see [HVD15])

C. Calculating Network Characteristics

C.1. Parameter Numbers

- A fully connected layer with n nodes, k inputs has $n \cdot (k+1)$ parameters. The $+1$ is due to the bias.

- A convolutional layer i with k_i filters of size $n \times m$ being applied to k_{i-1} feature maps has $k_i \cdot k_{i-1}(n \cdot m + 1)$ parameters. The $+1$ is due to the bias.

- A fully connected layer with n nodes after k feature maps of size $m_1 \times m_2$ has $n \cdot (k \cdot m_1 \cdot m_2 + 1)$ parameters.

- A dense block with a depth of L, a growth rate of n and 3×3 filters has $L + n \cdot 3^2 + 3^2 \cdot n^2 \sum_{i=0}^{L}(L-i) = L + 9n + 9n^2 \frac{L^2-L}{2}$ parameters.

According to [HPTD15], AlexNet has 60 million parameters which is roughly the number calculated in Table D.2.

C.2. FLOPs

The FLOPs of a layer depend on the implementation, the compiler and the hardware. Hence the following number are only giving rough estimates.

In the following, n_φ denotes the number of FLOPs to compute the non-linearity φ. For simplicity, $n_\varphi = 5$ was chosen.

- A fully connected layer with n nodes and k inputs has to calculate $\varphi(W \cdot x + b)$ with $W \in \mathbb{R}^{n \times k}$, $x \in \mathbb{R}^{k \times 1}$, $b \in \mathbb{R}^{n \times 1}$. It hence needs about $n \cdot (k + (k-1) + 1) = 2nk$ additions / multiplications before the non-linearity φ is calculated. The total number of FLOPs is $2 \cdot n \cdot k + n \cdot n_\varphi$.
- In the following, biases are ignored. A convolutional layer with k_i filters of size $n \times m$ being applied to k_{i-1} filter maps of size $w \times h$ results in k_i filter maps of size $w \times h$ if padding is applied. For each element of each filter map, $n \cdot m \cdot k_{i-1}$ multiplications and $(n \cdot m \cdot k_{i-1} - 1)$ additions have to be made. This results in $(2nmk_{i-1} - 1) \cdot (k_i \cdot w \cdot h)$ operations. The total number of FLOPs is $(2 \cdot n \cdot m \cdot k_{i-1} - 1) \cdot (k_i \cdot w \cdot h) + k_i \cdot w \cdot h \cdot n_\varphi$. This is, of course, a naive way of calculating a convolution. There are other ways of calculating convolutions [LG16].

- A fully connected layer with n nodes after k feature maps of size $w \times h$ needs $2n(k \cdot w \cdot h)$ FLOPs. The total number of FLOPs is $2n \cdot (k \cdot w \cdot h) + n \cdot n_\varphi$.
- As Dropout is only calculated during training, the number of FLOPs was set to 0.
- The number of FLOPs for max pooling is dominated by the number of positions to which the pooling kernel is applied. For a feature map of size $w \times h$ a max pooling filter with stride s gets applied $\frac{w \cdot h}{s^2}$. The number of FLOPs per application depends on the kernel size. A 2×2 kernel is assumed to need 5 FLOPs.
- The number of FLOPs for Batch Normalization is the same as the number of its parameters.

Here are some references which give information for the FLOPs:

- AlexNet
    - 1.5B in total [HPTD15].
    - 725M in total [KPY$^+$15].
    - 3300M in total in Table D.2
- VGG-16:
    - 15484M in total [HPTD15].
    - 31000M in total in Table D.3.
- GoogleNet: 1566M in total [HPTD15].

One can see that the numbers are by a factor of 2 up to a factor of 4 different for the same network.

C.3. Memory Footprint

The memory footprint of CNNs determines when networks can be used at all and if they can be trained efficiently. In order to be able to train CNNs efficiently, one weight update step has to fit in the memory of the GPU. This includes the following:

- **Activations**: All activations of one mini-batch in order to calculate the gradients in the backward pass. This is the number of floats in the feature maps of all weight layers combined.

- **Weights**

- **Optimization algorithm**: The optimization algorithm introduces some overhead. For example, Adam stores two parameters per weights.

At inference time, every two consecutive layers have to fit into memory. When the forward pass of layer A to layer B is calculated, the memory can be freed if no skip connections are used.

D. Common Architectures

In the following, some of the most important CNN architectures are explained. Understanding the development of these architectures helps understanding critical insights the machine learning community got in the past years for convolutional networks for image recognition.

It starts with LeNet-5 from 1998, continues with AlexNet from 2012, VGG-16 D from 2014, the Inception modules v1 to v3 as well as ResNets in 2015. The recently developed Inception-v4 is also covered.

The summation row gives the sum of all floats for the output size column. This allows conclusions about the maximum mini-batch size which can be in memory for training.

D.1. LeNet-5

One of the first CNNs used was LeNet-5 [LBBH98]. LeNet-5 uses two times the common pattern of a single convolutional layer with tanh as a non-linear activation function followed by a pooling layer and three fully connected layers. One fully connected layer is used to get the right output dimension, another one is necessary to allow the network to learn a non-linear combination of the features of the feature maps.

Its exact architecture is shown in Figure D.1 and described in Table D.1. It reaches a test error rate of $0.8\,\%$ on MNIST.
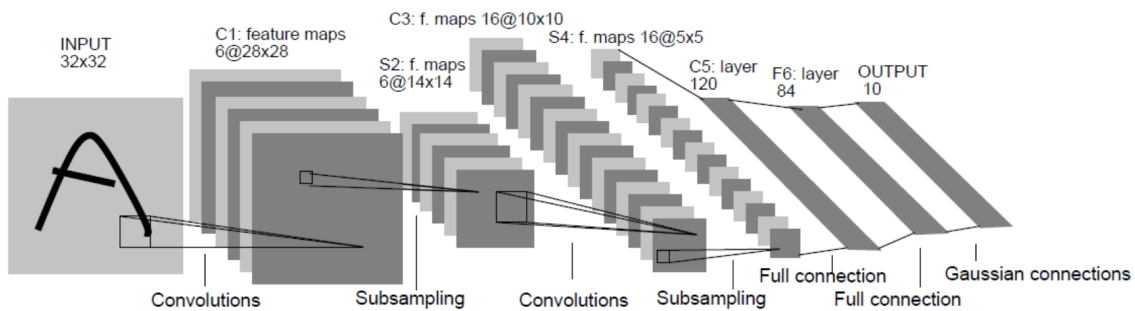
Figure D.1.: Architecture of LeNet-5 as shown in [LBBH98].

#	Type	Filters @ Patch size / stride	Parameters	FLOPs	Output size
	Input		0	0	$1@32 \times 32$
1	Convolution	$6@5 \times 5 \times 1 / 1$	156	307 800	$\mathbf{6@28 \times 28}$
2	Scaled average pooling	$2 \times 2 \quad / 2$	2	336	$6@14 \times 14$
3	Convolution	$16@5 \times 5 \times 6 / 1$	2 416	**942 400**	$16@10 \times 10$
4	Scaled average pooling	$2 \times 2 \quad / 2$	2	1 600	$16@\ 5 \times\ 5$
5	Fully Connected	120 neurons	**48 120**	240 000	120
6	Fully Connected	84 neurons	10 164	20 580	84
7	Fully Connected (output)	10 neurons	850	1 730	10
$\sum$			61 710	15 144 446	9118

Table D.1.: LeNet-5 architecture: After layers 1, 3, 5 and 6 the tanh activation function is applied. After layer 7, the softmax function is applied. One can see that convolutional layer need much fewer parameters, but an order of magnitude more FLOPs per parameter than fully connected layers.

D.2. AlexNet

The first CNN which achieved major improvements on the ImageNet dataset was AlexNet [KSH12]. Its architecture is shown in Figure D.2 and described in Table D.2. It has about $60 \cdot 10^6$ parameters. A trained AlexNet can be downloaded at www.cs.toronto.edu/g̃uerzhoy/tf_alexnet. Note that the uncompressed size is at least $60\,965\,224$ floats $\cdot\, 32\, \frac{\text{bit}}{\text{float}} \approx 244\,\text{MB}$.
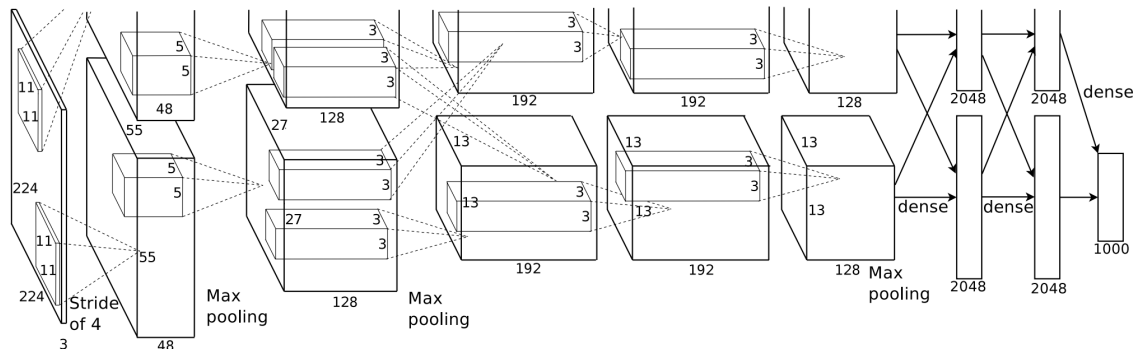

Figure D.2.: Architecture of AlexNet as shown in [KSH12]: Convolutional Layers are followed by pooling layers multiple times. At the end, a fully connected network is applied. Conceptually, it is identical to the architecture of LeNet-5 (see Figure D.1).

#	Type	Filters @ Patch size / stride	Parameters	FLOPs	Output size
	Input				3 @ 224 × 224
1	Convolution	96 @ 11 × 11 × 3 / 4	34 944	211 M	**96 @ 55 × 55**
	LCN			12 M	**96 @ 55 × 55**
2	Max pooling	3 × 3 / 2	0	301 k	96 @ 27 × 27
3	Convolution	256 @ 5 × 5 × 48 / 1	307 456	**448 M**	256 @ 13 × 13
	LCN			3 M	256 @ 13 × 13
4	Max pooling	3 × 3 / 2	0	50 k	256 @ 13 × 13
5	Convolution	384 @ 3 × 3 × 256 / 1	885 120	299 M	384 @ 13 × 13
7	Convolution	384 @ 3 × 3 × 192 / 1	663 936	224 M	384 @ 13 × 13
9	Convolution	256 @ 3 × 3 × 192 / 1	442 624	150 M	256 @ 13 × 13
10	Max pooling	3 × 3 / 2	0	50 k	256 @ 6 × 6
11	FC	4096 neurons	**37 752 832**	75 M	4096
12	FC	4096 neurons	16 781 312	34 M	4096
13	FC	1000 neurons	4 097 000	8 M	1000
$\sum$			60 965 224	3300 M	1 122 568

Table D.2.: AlexNet architecture: One special case of AlexNet is grouping of convolutions due to computational restrictions at the time of its development. This also reduces the number of parameters and allows parallel computation on separate GPUs. However, to make the architecture easier to compare, this grouping was ignored for the parameter count. The FLOPs are taken from [HPTD15] and combined with rough estimates for Local Contrast Normalization and max pooling.

The calculated number of parameters was checked against the downloaded version. It also has 60 965 224 parameters.

D.3. VGG-16 D

Another widespread architecture is the VGG-16 (D) [SZ14]. VGG comes from the **V**isual **G**eometry **G**roup in Oxford which developed this architecture. It has **16** layers which can learn parameters. A major difference compared to AlexNet is that VGG-16 uses only 3×3 filters and is much deeper. A visualization of the architecture is shown in Figure D.3 and a detailed textual description is given in Table D.3.

A trained VGG-16 D for Tensorflow can be downloaded at `https://github.com/machrisaa/` `tensorflow-vgg`. Note that the uncompressed size is at least $138\,357\,544$ floats $\cdot\, 32 \frac{\text{bit}}{\text{float}} \approx$ 520 MB. The downloaded Numpy binary file `npz` needs 553 MB without compression and 514 MB with compression.
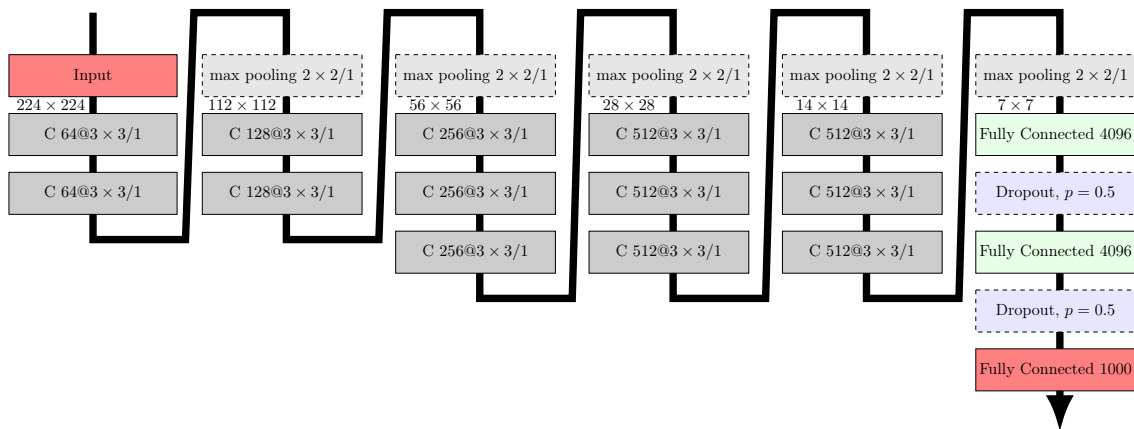
Figure D.3.: Architecture of VGG-16 D. `C` $512@3 \times 3/1$ is a convolutional layer with 512 filters of kernel size 3×3 with stride 1. All convolutional layers use `SAME` padding.

#	Type	Filters @ Patch size / stride	Parameters	FLOPs	Output size
	Input				3 @ 224 × 224
1	Convolution	64 @ 3 × 3 × 3 / 1	1 792	186 M	**64 @ 224 × 224**
2	Convolution	64 @ 3 × 3 × 64 / 1	36 928	**3712 M**	**64 @ 224 × 224**
	Max pooling	2 × 2 / 2	0	2 M	64 @ 112 × 112
3	Convolution	128 @ 3 × 3 × 64 / 1	73 856	1856 M	128 @ 112 × 112
4	Convolution	128 @ 3 × 3 × 128 / 1	147 584	3705 M	128 @ 112 × 112
	Max pooling	2 × 2 / 2	0	1 M	128 @ 56 × 56
5	Convolution	256 @ 3 × 3 × 128 / 1	295 168	1853 M	256 @ 56 × 56
6	Convolution	256 @ 3 × 3 × 256 / 1	590 080	3703 M	256 @ 56 × 56
7	Convolution	256 @ 3 × 3 × 256 / 1	590 080	3703 M	256 @ 56 × 56
	Max pooling	2 × 2 / 2	0	<1 M	256 @ 28 × 28
8	Convolution	512 @ 3 × 3 × 256 / 1	1 180 160	1851 M	512 @ 28 × 28
9	Convolution	512 @ 3 × 3 × 512 / 1	2 359 808	3701 M	512 @ 28 × 28
10	Convolution	512 @ 3 × 3 × 512 / 1	2 359 808	3701 M	512 @ 28 × 28
	Max pooling	2 × 2 / 2	0	<1 M	512 @ 14 × 14
11	Convolution	512 @ 3 × 3 × 512 / 1	2 359 808	925 M	512 @ 14 × 14
12	Convolution	512 @ 3 × 3 × 512 / 1	2 359 808	925 M	512 @ 14 × 14
13	Convolution	512 @ 3 × 3 × 512 / 1	2 359 808	925 M	512 @ 14 × 14
	Max pooling	2 × 2 / 2	0	<1 M	512 @ 7 × 7
14	FC	4096 neurons	**102 764 544**	206 M	4096
	Dropout		0	0	4096
15	FC	4096 neurons	16 781 312	34 M	4096
	Dropout		0	0	4096
16	FC	1000 neurons	4 097 000	8 M	1000
∑			138 357 544	31 000 M	15 245 800

Table D.3.: VGG-16 D architecture: The authors chose to give only layers a number which have learnable parameters. All convolutions are zero padded to prevent size changes and use ReLU activation functions. The channels mean is subtracted from each pixel as a preprocessing step $(-103.939, -116.779, -123.68)$. As Dropout is only calculated during training time, the number of FLOPs is 0. The dropout probability is 0.5. The calculated number of parameters was checked against the downloaded version. It also has 138 357 544 parameters.

D.4. GoogleNet, Inception v2 and v3

The large number of parameters and operations is a problem when such models should get applied in practice to thousands of images. In order to reduce the computational cost while maintaining the classification quality, GoogleNet [SLJ+15] and the Inception module were developed. The Inception module essentially only computes 1×1 filters, 3×3 filters and 5×5 filters in parallel, but applied bottleneck 1×1 filters before to reduce the number of parameters. It is shown in Figure D.4.
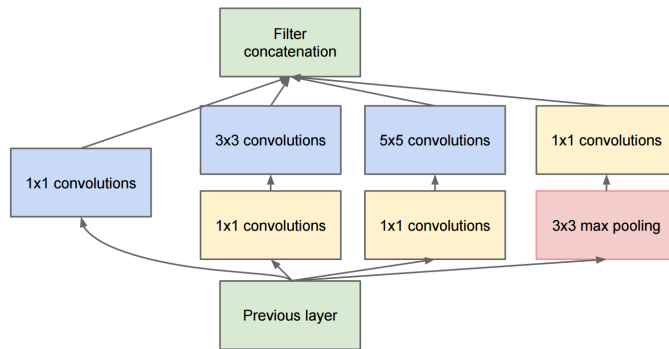
Figure D.4.: Inception module
Image source: [SLJ+15]

Compared to GoogleNet, Inception v2 [SVI+15] removed the 5×5 filters and replaced them by two successive layers of 3×3 filters. A visualization of an Inception v2 module is given in Figure D.5. Additionally, Inception v2 applies successive asymmetric filters to approximate symmetric filters with fewer parameters. The authors call this approach *filter factorization.*

Inception v3 introduced Batch Normalization to the network [SVI+15].
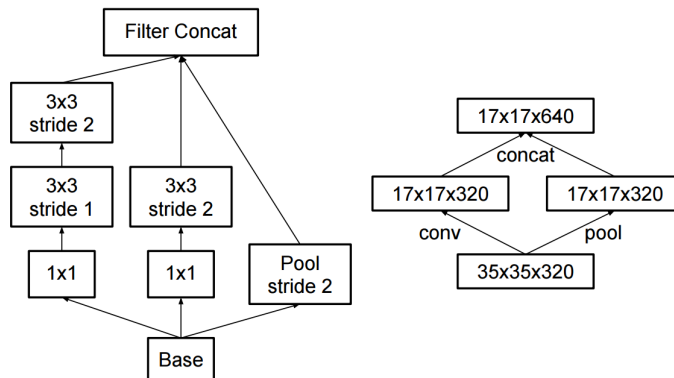
Figure D.5.: Inception v2 module
Image source: [SVI+15]

D.5. Inception-v4

Inception-v4 as described in [SIV16] consists of four main building blocks: The stem, Inception A, Inception B and Inception C. To quote the authors: Inception-v4 is a deeper, wider and more uniform simplified architecture than Inception-v3. The stem, Reduction A and Reduction B use max-pooling, whereas Inception A, Inception B and Inception C use average pooling. The stem, module B and module C use separable convolutions.

#	×	Type	Parameters	Output size
		Input		3 @ 299 × 299
1		Stem	605 728	384 @ 35 × 35
2	4×	Inception A	317 632	384 @ 35 × 35
3		Reduction A	2 306 112	1024 @ 17 × 17
4	7×	Inception B	2 936 256	1024 @ 17 × 17
5		Reduction B	2 747 392	1536 @ 8 × 8
6	3×	Inception C	4 553 088	1536 @ 8 × 8
		Global Average Pooling	0	1536 @ 1 × 1
		Dropout (p=0.8)	0	1536 @ 1 × 1
7		Softmax	1 537 000	1000
$\sum$			42 679 816	

Table D.4.: Inception-v4 network.

96

E. Datasets

Well-known benchmark datasets for classification problems in computer vision are listed in Table E.1. The best results known to me are given in Table E.2. However, every semantic segmentation dataset (e.g., PASCAL VOC) can also be used to benchmark image classifiers using Algorithm 2.

Database	Image Resolution (width × height)	Number of Images	Number of Classes	Channels	Data source
MNIST	28 px × 28 px	70 000	10	1	[YL98, LBBH98]
HASYv2	32 px × 32 px	168 233	369	1	[Tho17a]
SVHN	32 px × 32 px	630 420	10	3	[NWC$^+$11b], [NWC$^+$11a]
CIFAR-10	32 px × 32 px	60 000	10	3	[Kri, KH09]
CIFAR-100	32 px × 32 px	60 000	100	3	[Kri, KH09]
STL-10	96 px × 96 px	13 000	10	3	[CLN11, CLN10]
Caltech-101	(80 px − 3481 px) ×(92 px − 3999 px)	9144	102	3	[FFP03, FFFP06]
Caltech-256	(75 px − 7913 px) ×(75 px − 7913 px)	30 607	257	3	[Gri06, GG07]
ILSVRC 2012[1]	(8 px − 9331 px) ×(10 px − 6530 px)	$1.2 \cdot 10^6$	1000	3	[Ima12, RDS$^+$14]
Places365[2]	(290px − 3158px) ×(225px − 2630px)	$1.8 \cdot 10^6$	365	3	[Zho16, ZKL$^+$16]
GTSRB	(25 px − 266 px) ×(25 px − 232 px)	51 839	43	3	[SSSI, SSSI12]
Asirra[3]	(4 px − 500 px) ×(4 px − 500 px)	25 000	2	3	[Asi17, EDHS07]
Graz-02	480 px × 640 px and 640 px × 480 px	1096	3	3	[Mar08, MS07]

Table E.1.: An overview over publicly available image databases for classification. The number of images row gives the sum of the training and the test images. Some datasets, like SVHN, have additional unlabeled data which is not given in this table.

---

[1]ImageNet Large Scale Visual Recognition Competition
[2]The dimensions are only calculated for the validation set.
[3]Asirra is a CAPTCHA created by Microsoft and was used in the "Cats vs Dogs" competition on Kaggle

Dataset	Model type / name	Result	Score	Achieved / Claimed by
MNIST	—	0.21 %	error	[WZZ+13]
HASYv2	TF-CNN	81.00 %	accuracy	[Tho17a]
SVHN	DenseNet ($k = 24$)	1.59 %	error	[HLW16]
CIFAR-10	DenseNet-BC ($k = 40$)	3.46 %	error	[HLW16]
CIFAR-100	WRN-28-10	16.21 %	error	[LH16]
STL-10	SWWAE-4layer	74.80 %	accuracy	[ZMGL15]
Caltech-101	SPP-net (pretrained)	93.42 %±0.5 %	accuracy	[HZRS14]
Caltech-256	ZF-Net (pretrained)	74.2 %±0.3 %	accuracy	[ZF14]
ImageNet 2012	ResNet ensemble	3.57 %	Top-5 error	[HZRS15a]
GTSRB	MCDNN	99.46 %	accuracy	[SL11]
Asirra	SVM	82.7 %	accuracy	[Gol08]
Graz-02	Optimal NBNN	78.98 %	accuracy	[BMDP10]

Table E.2.: An overview over state of the art results achieved in computer vision datasets.

Algorithm 2 Create a classification dataset from a semantic segmentation dataset

---

Require: Semantic segmentation dataset (D_S)

   procedure CREATEDATASET(Annotated dataset D_S)

      $D_C \leftarrow$ LIST

      $w \leftarrow$ desired image width

      $h \leftarrow$ desired image height

      for Image and associated label (x, y) in D_S **do**

         $i \leftarrow$ RANDINT$(0, L.\text{width} - w)$

         $j \leftarrow$ RANDINT$(0, L.\text{height} - h)$

         $c_L \leftarrow$ CROP$(y, (i, j), (i + w, j + h))$

         if at least 50% of s are of one class **then**

            $c_I \leftarrow$ CROP$(x, (i, j), (i + w, j + h))$

            $D.$APPEND$((c_I, c_L))$

      return (D_C)

F. List of Tables

G. List of Figures

H. Bibliography

[AAB⁺16] M. Abadi, A. Agarwal *et al.*, "Tensorflow: Large-scale machine learning on heterogeneous distributed systems," *arXiv preprint arXiv:1603.04467*, Mar. 2016. [Online]. Available: https://arxiv.org/abs/1603.04467

[ABKS99] M. Ankerst, M. M. Breunig *et al.*, "OPTICS: Ordering points to identify the clustering structure," in *ACM Sigmod record*, vol. 28, no. 2. ACM, 1999, pp. 49–60.

[ADG⁺16] M. Andrychowicz, M. Denil *et al.*, "Learning to learn by gradient descent by gradient descent," in *Advances in Neural Information Processing Systems 29 (NIPS)*, D. D. Lee, M. Sugiyama *et al.*, Eds. Curran Associates, Inc., Mar. 2016, pp. 3981–3989. [Online]. Available: http://papers.nips.cc/paper/6461-learning-to-learn-by-gradient-descent-by-gradient-descent.pdf

[AM15] M. T. Alexander Mordvintsev, Christopher Olah, "Inceptionism: Going deeper into neural networks," Jun. 2015. [Online]. Available: https://research.googleblog.com/2015/06/inceptionism-going-deeper-into-neural.html

[Asi17] "Kaggle cats and dogs dataset," Oct. 2017. [Online]. Available: https://www.microsoft.com/en-us/download/details.aspx?id=54765

[BB12] J. Bergstra and Y. Bengio, "Random search for hyper-parameter optimization," *Journal of Machine Learning Research*, vol. 13, no. Feb, pp. 281–305, Feb. 2012. [Online]. Available: http://jmlr.csail.mit.edu/papers/volume13/bergstra12a/bergstra12a.pdf

[BCW⁺17] J. Bao, D. Chen *et al.*, "CVAE-GAN: Fine-grained image generation through asymmetric training," *arXiv preprint arXiv:1703.10155*, Mar. 2017. [Online]. Available: https://arxiv.org/abs/1703.10155

[BDLB09] J. Bergstra, G. Desjardins *et al.*, "Quadratic polynomials learn better image features," Département d'Informatique et de Recherche Opérationnelle, Université de Montréal, Tech. Rep. 1337, 2009.

[BGNR16] B. Baker, O. Gupta *et al.*, "Designing neural network architectures using reinforcement learning," *arXiv preprint arXiv:1611.02167*, Nov. 2016. [Online]. Available: https://arxiv.org/abs/1611.02167

[BM93]   U. Bodenhausen and S. Manke, *Automatically Structured Neural Networks For Handwritten Character And Word Recognition*. London: Springer London, Sep. 1993, pp. 956–961. [Online]. Available: http://dx.doi.org/10.1007/978-1-4471-2063-6_283

[BMDP10]   R. Behmo, P. Marcombes *et al.*, "Towards optimal naive Bayes nearest neighbor," in *European Conference on Computer Vision (ECCV)*. Springer, 2010, pp. 171–184.

[BPL10]   Y.-L. Boureau, J. Ponce, and Y. LeCun, "A theoretical analysis of feature pooling in visual recognition," in *International Conference on Machine Learning (ICML)*, no. 27, 2010, pp. 111–118. [Online]. Available: http://yann.lecun.com/exdb/publis/pdf/boureau-icml-10.pdf

[BSF94]   Y. Bengio, P. Simard, and P. Frasconi, "Learning long-term dependencies with gradient descent is difficult," *IEEE transactions on neural networks*, vol. 5, no. 2, pp. 157–166, 1994.

[Cha92]   C. Charalambous, "Conjugate gradient algorithm for efficient training of artificial neural networks," *IEEE Proceedings G-Circuits, Devices and Systems*, vol. 139, no. 3, pp. 301–310, 1992. [Online]. Available: http://ieeexplore.ieee.org/document/143326/

[Cho15]   F. Chollet, "Keras," https://github.com/fchollet/keras, 2015.

[CLN10]   A. Coates, H. Lee, and A. Y. Ng, "An analysis of single-layer networks in unsupervised feature learning," *Ann Arbor*, vol. 1001, no. 48109, p. 2, 2010. [Online]. Available: http://cs.stanford.edu/~acoates/papers/coatesleeng_aistats_2011.pdf

[CLN11]   A. Coates, H. Lee, and A. Y. Ng, "STL-10 dataset," 2011. [Online]. Available: http://cs.stanford.edu/~acoates/stl10

[CMS12]   D. Ciregan, U. Meier, and J. Schmidhuber, "Multi-column deep neural networks for image classification," in *Conference on Computer Vision and Pattern Recognition (CVPR)*. IEEE, Feb. 2012, pp. 3642–3649. [Online]. Available: https://arxiv.org/abs/1202.2745v1

[CUH15]   D.-A. Clevert, T. Unterthiner, and S. Hochreiter, "Fast and accurate deep network learning by exponential linear units (ELUs)," *arXiv preprint arXiv:1511.07289*, Nov. 2015. [Online]. Available: https://arxiv.org/abs/1511.07289

[CWV+14]   S. Chetlur, C. Woolley *et al.*, "cuDNN: Efficient primitives for deep learning," *arXiv preprint arXiv:1410.0759*, Oct. 2014. [Online]. Available: https://arxiv.org/abs/1410.0759

[DBB+01] C. Dugas, Y. Bengio *et al.*, "Incorporating second-order functional knowledge for better option pricing," in *Advances in Neural Information Processing Systems 13 (NIPS)*, T. K. Leen, T. G. Dietterich, and V. Tresp, Eds. MIT Press, 2001, pp. 472–478. [Online]. Available: http://papers.nips.cc/paper/1920-incorporating-second-order-functional-knowledge-for-better-option-pricing.pdf

[DDFK16] S. Dieleman, J. De Fauw, and K. Kavukcuoglu, "Exploiting cyclic symmetry in convolutional neural networks," *arXiv preprint arXiv:1602.02660*, Feb. 2016. [Online]. Available: https://arxiv.org/abs/1602.02660

[DHS11] J. Duchi, E. Hazan, and Y. Singer, "Adaptive subgradient methods for online learning and stochastic optimization," *Journal of Machine Learning Research*, vol. 12, no. Jul, pp. 2121–2159, 2011. [Online]. Available: http://www.jmlr.org/papers/volume12/duchi11a/duchi11a.pdf

[DHS16] J. Dai, K. He, and J. Sun, "Instance-aware semantic segmentation via multi-task network cascades," in *Conference on Computer Vision and Pattern Recognition (CVPR)*. IEEE, 2016, pp. 3150–3158. [Online]. Available: https://arxiv.org/abs/1512.04412

[DJ99] W. Duch and N. Jankowski, "Survey of neural transfer functions," *Neural Computing Surveys*, vol. 2, no. 1, pp. 163–212, 1999. [Online]. Available: ftp://ftp.icsi.berkeley.edu/pub/ai/jagota/vol2_6.pdf

[Doz15] T. Dozat, "Incorporating Nesterov momentum into Adam," Stanford University, Tech. Rep., 2015. [Online]. Available: http://cs229.stanford.edu/proj2015/054_report.pdf

[DSRB14] A. Dosovitskiy, J. T. Springenberg *et al.*, "Discriminative unsupervised feature learning with convolutional neural networks," in *Advances in Neural Information Processing Systems 27 (NIPS)*, Z. Ghahramani, M. Welling *et al.*, Eds. Curran Associates, Inc., 2014, pp. 766–774. [Online]. Available: http://papers.nips.cc/paper/5548-discriminative-unsupervised-feature-learning-with-convolutional-neural-networks.pdf

[DWD15] S. Dieleman, K. W. Willett, and J. Dambre, "Rotation-invariant convolutional neural networks for galaxy morphology prediction," *Monthly notices of the royal astronomical society*, vol. 450, no. 2, pp. 1441–1459, 2015.

[EDHS07] J. Elson, J. J. Douceur *et al.*, "Asirra: A CAPTCHA that exploits interest-aligned manual image categorization," in *ACM Conference on Computer and Communications Security (CCS)*, no. 14. Association for Computing Machinery, Inc., Oct. 2007. [Online].

Available: https://www.microsoft.com/en-us/research/publication/asirra-a-captcha-that-exploits-interest-aligned-manual-image-categorization/

[EKS+96]   M. Ester, H.-P. Kriegel *et al.*, "A density-based algorithm for discovering clusters in large spatial databases with noise." in *Kdd*, vol. 96, no. 34, 1996, pp. 226–231.

[ES03]   A. E. Eiben and J. E. Smith, *Introduction to evolutionary computing*. Springer, 2003, vol. 53. [Online]. Available: https://dx.doi.org/10.1007/978-3-662-44874-8

[Fah88]   S. E. Fahlman, "An empirical study of learning speed in back-propagation networks," 1988. [Online]. Available: http://repository.cmu.edu/cgi/viewcontent.cgi?article=2799&context=compsci

[FFFP06]   L. Fei-Fei, R. Fergus, and P. Perona, "One-shot learning of object categories," *IEEE transactions on pattern analysis and machine intelligence*, vol. 28, no. 4, pp. 594–611, Apr. 2006. [Online]. Available: http://vision.stanford.edu/documents/Fei-FeiFergusPerona2006.pdf

[FFP03]   R. F. Fei-Fei and P. Perona, "Caltech 101," 2003. [Online]. Available: http://www.vision.caltech.edu/Image_Datasets/Caltech101/Caltech101.html

[FGMR10]   P. F. Felzenszwalb, R. B. Girshick *et al.*, "Object detection with discriminatively trained part-based models," *IEEE transactions on pattern analysis and machine intelligence*, vol. 32, no. 9, pp. 1627–1645, 2010.

[FL89]   S. E. Fahlman and C. Lebiere, "The cascade-correlation learning architecture," 1989. [Online]. Available: http://repository.cmu.edu/compsci/1938/

[GB10]   X. Glorot and Y. Bengio, "Understanding the difficulty of training deep feedforward neural networks." in *Aistats*, vol. 9, 2010, pp. 249–256. [Online]. Available: http://jmlr.org/proceedings/papers/v9/glorot10a/glorot10a.pdf

[GBB11]   X. Glorot, A. Bordes, and Y. Bengio, "Deep sparse rectifier neural networks." in *Aistats*, vol. 15, no. 106, 2011, p. 275. [Online]. Available: http://www.jmlr.org/proceedings/papers/v15/glorot11a/glorot11a.pdf

[GDDM14]   R. Girshick, J. Donahue *et al.*, "Rich feature hierarchies for accurate object detection and semantic segmentation," in *Conference on Computer Vision and Pattern Recognition (CVPR)*. IEEE, 2014, pp. 580–587. [Online]. Available: https://arxiv.org/abs/1311.2524

[GG07]   P. P. Greg Griffin, Alex Holub, "Caltech-256 object category dataset," Apr. 2007. [Online]. Available: http://authors.library.caltech.edu/7694/

[GG16]   Y. Gal and Z. Ghahramani, "Bayesian convolutional neural networks with Bernoulli approximate variational inference," *arXiv preprint arXiv:1506.02158*, Jan. 2016. [Online]. Available: https://arxiv.org/abs/1506.02158v6

[GJ02]   M. R. Garey and D. S. Johnson, *Computers and intractability*. wh freeman New York, 2002, vol. 29.

[GJS76]   M. R. Garey, D. S. Johnson, and L. Stockmeyer, "Some simplified NP-complete graph problems," *Theoretical computer science*, vol. 1, no. 3, pp. 237–267, 1976.

[Gol08]   P. Golle, "Machine learning attacks against the Asirra CAPTCHA," in *ACM conference on Computer and communications security (CCS)*, no. 15. ACM, 2008, pp. 535–542.

[Gra15]   B. Graham, "Fractional max-pooling," *arXiv preprint arXiv:1412.6071*, May 2015. [Online]. Available: https://arxiv.org/abs/1412.6071

[Gri06]   A. P. Griffin, G. Holub, "Caltech 256," 2006. [Online]. Available: http://www.vision.caltech.edu/Image_Datasets/Caltech256/

[GWFM+13] I. J. Goodfellow, D. Warde-Farley *et al.*, "Maxout networks." *ICML*, vol. 28, no. 3, pp. 1319–1327, 2013. [Online]. Available: http://www.jmlr.org/proceedings/papers/v28/goodfellow13.pdf

[HAE16]   M. Huh, P. Agrawal, and A. A. Efros, "What makes ImageNet good for transfer learning?" *arXiv preprint arXiv:1608.08614*, Aug. 2016. [Online]. Available: https://arxiv.org/abs/1608.08614

[Han89]   S. J. Hanson, "Meiosis networks." in *NIPS*, 1989, pp. 533–541. [Online]. Available: http://papers.nips.cc/paper/227-meiosis-networks.pdf

[Har15]   M. Harris, "New features in CUDA 7.5," Jul. 2015. [Online]. Available: https://devblogs.nvidia.com/parallelforall/new-features-cuda-7-5/

[HLW16]   G. Huang, Z. Liu, and K. Q. Weinberger, "Densely connected convolutional networks," *arXiv preprint arXiv:1608.06993*, Aug. 2016. [Online]. Available: https://arxiv.org/abs/1608.06993v1

[HM16]   M. Hardt and T. Ma, "Identity matters in deep learning," *arXiv preprint arXiv:1611.04231*, Nov. 2016. [Online]. Available: https://arxiv.org/abs/1611.04231

[How13]   A. G. Howard, "Some improvements on deep convolutional neural network based image classification," *arXiv preprint arXiv:1312.5402*, Dec. 2013. [Online]. Available: https://arxiv.org/abs/1312.5402

[HPK11]   J. Han, J. Pei, and M. Kamber, *Data mining: concepts and techniques.* Elsevier, 2011.

[HPN+16]   S. Han, J. Pool *et al.*, "DSD: Regularizing deep neural networks with dense-sparse-dense training flow," *arXiv preprint arXiv:1607.04381*, Jul. 2016. [Online]. Available: https://arxiv.org/abs/1607.04381

[HPTD15]   S. Han, J. Pool *et al.*, "Learning both weights and connections for efficient neural network," in *Advances in Neural Information Processing Systems 28 (NIPS)*, C. Cortes, N. D. Lawrence *et al.*, Eds. Curran Associates, Inc., Jun. 2015, pp. 1135–1143. [Online]. Available: http://papers.nips.cc/paper/5784-learning-both-weights-and-connections-for-efficient-neural-network.pdf

[HSK+12]   G. E. Hinton, N. Srivastava *et al.*, "Improving neural networks by preventing co-adaptation of feature detectors," *arXiv preprint arXiv:1207.0580*, Jul. 2012. [Online]. Available: https://arxiv.org/abs/1207.0580

[HSL+16]   G. Huang, Y. Sun *et al.*, "Deep networks with stochastic depth," *arXiv preprint arXiv:1603.09382*, Mar. 2016. [Online]. Available: https://arxiv.org/abs/1603.09382

[HSW93]   B. Hassibi, D. G. Stork, and G. J. Wolff, "Optimal brain surgeon and general network pruning," in *International Conference on Neural Networks.* IEEE, 1993, pp. 293–299. [Online]. Available: http://ee.caltech.edu/Babak/pubs/conferences/00298572.pdf

[HVD15]   G. Hinton, O. Vinyals, and J. Dean, "Distilling the knowledge in a neural network," *arXiv preprint arXiv:1503.02531*, Mar. 2015. [Online]. Available: https://arxiv.org/abs/1503.02531

[HZRS14]   K. He, X. Zhang *et al.*, "Spatial pyramid pooling in deep convolutional networks for visual recognition," in *European Conference on Computer Vision (ECCV).* Springer, 2014, pp. 346–361. [Online]. Available: https://arxiv.org/abs/1406.4729

[HZRS15a]   K. He, X. Zhang *et al.*, "Deep residual learning for image recognition," *arXiv preprint arXiv:1512.03385*, Dec. 2015. [Online]. Available: https://arxiv.org/abs/1512.03385v1

[HZRS15b]   K. He, X. Zhang *et al.*, "Delving deep into rectifiers: Surpassing human-level performance on imagenet classification," in *International Conference on Computer Vision (ICCV)*, Feb. 2015, pp. 1026–1034. [Online]. Available: https://arxiv.org/abs/1502.01852

[Ima12]   "Imagenet large scale visual recognition challenge 2012 (ILSVRC2012),"

2012. [Online]. Available: http://www.image-net.org/challenges/LSVRC/2012/nonpub-downloads

[IS15]   S. Ioffe and C. Szegedy, "Batch normalization: Accelerating deep network training by reducing internal covariate shift," *arXiv preprint arXiv:1502.03167*, Feb. 2015. [Online]. Available: https://arxiv.org/abs/1502.03167

[JXF+16]   X. Jin, C. Xu *et al.*, "Deep learning with s-shaped rectified linear activation units," in *Thirtieth AAAI Conference on Artificial Intelligence*, Dec. 2016. [Online]. Available: https://arxiv.org/abs/1512.07030

[Kar11]   A. Karpathy, "Lessons learned from manually classifying CIFAR-10," Apr. 2011. [Online]. Available: http://karpathy.github.io/2011/04/27/manually-classifying-cifar10/

[KB14]   D. Kingma and J. Ba, "Adam: A method for stochastic optimization," *arXiv preprint arXiv:1412.6980*, Dec. 2014. [Online]. Available: https://arxiv.org/abs/1412.6980

[KH09]   A. Krizhevsky and G. Hinton, "Learning multiple layers of features from tiny images," Apr. 2009. [Online]. Available: https://www.cs.toronto.edu/~kriz/learning-features-2009-TR.pdf

[KMN+16]   N. S. Keskar, D. Mudigere *et al.*, "On large-batch training for deep learning: Generalization gap and sharp minima," *arXiv preprint arXiv:1609.04836*, Sep. 2016. [Online]. Available: https://arxiv.org/abs/1609.04836

[Koc15]   T. Kocmánek, "HyperNEAT and novelty search for image recognition," Ph.D. dissertation, Master's thesis, Czech Technical University in Prague, 2015. [Online]. Available: http://kocmi.tk/photos/DiplomaThesis.pdf

[KPY+15]   Y.-D. Kim, E. Park *et al.*, "Compression of deep convolutional neural networks for fast and low power mobile applications," *arXiv preprint arXiv:1511.06530*, Nov. 2015. [Online]. Available: https://arxiv.org/abs/1511.06530

[KR09]   L. Kaufman and P. J. Rousseeuw, *Finding groups in data: an introduction to cluster analysis.* John Wiley & Sons, 2009, vol. 344.

[Kri]   A. Krizhevsky, "The CIFAR-10 dataset." [Online]. Available: https://www.cs.toronto.edu/~kriz/cifar.html

[KS02]   V. Kurkova and M. Sanguineti, "Comparison of worst case errors in linear and neural network approximation," *IEEE Transactions on Information Theory*, vol. 48, no. 1, pp. 264–275, Jan. 2002. [Online]. Available: http://ieeexplore.ieee.org/abstract/document/971754/

[KSH12]   A. Krizhevsky, I. Sutskever, and G. E. Hinton, "Imagenet classification with deep convolutional neural networks," in *Advances in Neural Information Processing Systems 25 (NIPS)*, F. Pereira, C. J. C. Burges *et al.*, Eds.   Curran Associates, Inc., 2012, pp. 1097–1105. [Online]. Available: http://papers.nips.cc/paper/4824-imagenet-classification-with-deep-convolutional-neural-networks.pdf

[KSlB$^+$10]   K. Kavukcuoglu, P. Sermanet *et al.*, "Learning convolutional feature hierarchies for visual recognition," in *Advances in Neural Information Processing Systems 23 (NIPS)*, J. D. Lafferty, C. K. I. Williams *et al.*, Eds.   Curran Associates, Inc., 2010, pp. 1090–1098. [Online]. Available: http://papers.nips.cc/paper/4133-learning-convolutional-feature-hierarchies-for-visual-recognition.pdf

[LAE$^+$16]   W. Liu, D. Anguelov *et al.*, "SSD: Single shot multibox detector," in *European Conference on Computer Vision (ECCV)*.   Springer, 2016, pp. 21–37. [Online]. Available: https://arxiv.org/abs/1512.02325

[Las17]   "Noise layers," Jan. 2017. [Online]. Available: http://lasagne.readthedocs.io/en/latest/modules/layers/noise.html#lasagne.layers.DropoutLayer

[LBBH98]   Y. LeCun, L. Bottou *et al.*, "Gradient-based learning applied to document recognition," *Proceedings of the IEEE*, vol. 86, no. 11, pp. 2278–2324, Nov. 1998. [Online]. Available: http://yann.lecun.com/exdb/publis/pdf/lecun-01a.pdf

[LBH15]   Y. LeCun, Y. Bengio, and G. Hinton, "Deep learning," *Nature*, vol. 521, no. 7553, pp. 436–444, May 2015. [Online]. Available: http://www.nature.com/nature/journal/v521/n7553/abs/nature14539.html

[LBOM98]   Y. A. LeCun, L. Bottou *et al.*, *Efficient BackProp*, ser. Lecture Notes in Computer Science.   Berlin, Heidelberg: Springer Berlin Heidelberg, 1998, vol. 1524, pp. 9–50. [Online]. Available: http://dx.doi.org/10.1007/3-540-49430-8

[LDS$^+$89]   Y. LeCun, J. S. Denker *et al.*, "Optimal brain damage." in *NIPs*, vol. 2, 1989, pp. 598–605. [Online]. Available: http://yann.lecun.com/exdb/publis/pdf/lecun-90b.pdf

[Le13]   Q. V. Le, "Building high-level features using large scale unsupervised learning," in *International conference on acoustics, speech and signal processing*.   IEEE, 2013, pp. 8595–8598. [Online]. Available: http://ieeexplore.ieee.org/stamp/stamp.jsp?arnumber=6639343

[LG16]   A. Lavin and S. Gray, "Fast algorithms for convolutional neural networks," in

Conference on Computer Vision and Pattern Recognition (CVPR). IEEE, Sep. 2016, pp. 4013–4021. [Online]. Available: https://arxiv.org/abs/1509.09308

[LGT16]   C.-Y. Lee, P. W. Gallagher, and Z. Tu, "Generalizing pooling functions in convolutional neural networks: Mixed, gated, and tree," in *International Conference on Artificial Intelligence and Statistics*, 2016. [Online]. Available: https://arxiv.org/abs/1509.08985v2

[LH16]   I. Loshchilov and F. Hutter, "SGDR: stochastic gradient descent with warm restarts," *Learning*, Aug. 2016. [Online]. Available: https://arxiv.org/abs/1608.03983

[LJD+16]   L. Li, K. Jamieson *et al.*, "Hyperband: A novel bandit-based approach to hyperparameter optimization," *arXiv preprint arXiv:1603.06560*, Mar. 2016. [Online]. Available: https://arxiv.org/abs/1603.06560

[LM16]   K. Li and J. Malik, "Learning to optimize," *arXiv preprint arXiv:1606.01885*, Jun. 2016. [Online]. Available: https://arxiv.org/abs/1606.01885

[LSD15]   J. Long, E. Shelhamer, and T. Darrell, "Fully convolutional networks for semantic segmentation," in *Conference on Computer Vision and Pattern Recognition (CVPR)*. IEEE, Mar. 2015, pp. 3431–3440. [Online]. Available: https://arxiv.org/abs/1411.4038v2

[LX17]   A. Y. Lingxi Xie, "Genetic CNN," *arXiv preprint arXiv:1703.01513*, Mar. 2017. [Online]. Available: https://arxiv.org/abs/1703.01513

[Maj17]   S. Majumdar, "Densenet," GitHub, Feb. 2017. [Online]. Available: https://github.com/titu1994/DenseNet

[Mar08]   M. Marszałek, "INRIA annotations for Graz-02 (IG02)," Oct. 2008. [Online]. Available: http://lear.inrialpes.fr/people/marszalek/data/ig02/

[MDA15]   D. Maclaurin, D. Duvenaud, and R. Adams, "Gradient-based hyperparameter optimization through reversible learning," in *International Conference on Machine Learning (ICML)*, 2015, pp. 2113–2122.

[MH08]   L. v. d. Maaten and G. Hinton, "Visualizing data using t-SNE," *Journal of Machine Learning Research*, vol. 9, no. Nov, pp. 2579–2605, 2008.

[MHN13]   A. L. Maas, A. Y. Hannun, and A. Y. Ng, "Rectifier nonlinearities improve neural network acoustic models," in *Proc. ICML*, vol. 30, no. 1, 2013. [Online]. Available: https://web.stanford.edu/~awni/papers/relu_hybrid_icml2013_final.pdf

[MM15]   D. Mishkin and J. Matas, "All you need is a good init," *arXiv*

preprint arXiv:1511.06422, Nov. 2015. [Online]. Available: https: //arxiv.org/abs/1511.06422

[MP43]   W. S. McCulloch and W. Pitts, "A logical calculus of the ideas immanent in nervous activity," *The bulletin of mathematical biophysics*, vol. 5, no. 4, pp. 115–133, 1943.

[MRM15]   N. McLaughlin, J. M. D. Rincon, and P. Miller, "Data-augmentation for reducing dataset bias in person re-identification," in *International Conference on Advanced Video and Signal Based Surveillance (AVSS)*, no. 12, Aug. 2015, pp. 1–6. [Online]. Available: http://ieeexplore.ieee.org/abstract/document/7301739/

[MS07]   M. Marszalek and C. Schmid, "Accurate object localization with shape masks," in *Conference on Computer Vision and Pattern Recognition (CVPR)*. IEEE, 2007, pp. 1–8. [Online]. Available: http://ieeexplore.ieee.org/document/4270110/

[MSM16]   D. Mishkin, N. Sergievskiy, and J. Matas, "Systematic evaluation of CNN advances on the ImageNet," *arXiv preprint arXiv:1606.02228*, Jun. 2016. [Online]. Available: https://arxiv.org/abs/1606.02228

[MV16]   A. Mahendran and A. Vedaldi, "Visualizing deep convolutional neural networks using natural pre-images," *International Journal of Computer Vision*, pp. 1–23, Apr. 2016. [Online]. Available: https://arxiv.org/abs/1512.02017

[NDRT13]   N. Natarajan, I. S. Dhillon *et al.*, "Learning with noisy labels," in *Advances in Neural Information Processing Systems 26 (NIPS)*, C. J. C. Burges, L. Bottou *et al.*, Eds. Curran Associates, Inc., 2013, pp. 1196–1204. [Online]. Available: http://papers.nips.cc/paper/5073-learning-with-noisy-labels.pdf

[Nes83]   Y. Nesterov, "A method of solving a convex programming problem with convergence rate o (1/k2)," in *Soviet Mathematics Doklady*, vol. 27, no. 2, 1983, pp. 372–376.

[new00]   "The training performed by qnstrn," Aug. 2000. [Online]. Available: http://www1.icsi.berkeley.edu/Speech/faq/nn-train.html

[Ng16]   A. Ng, "Nuts and bolts of building ai applications using deep learning," NIPS Talk, Dec. 2016.

[NH92]   S. J. Nowlan and G. E. Hinton, "Simplifying neural networks by soft weight-sharing," *Neural computation*, vol. 4, no. 4, pp. 473–493, 1992. [Online]. Available: https://www.cs.toronto.edu/~hinton/absps/sunspots.pdf

[NH02]   R. T. Ng and J. Han, "CLARANS: A method for clustering objects for spatial

data mining," *IEEE transactions on knowledge and data engineering*, vol. 14, no. 5, pp. 1003–1016, 2002.

[NWC⁺11a] Y. Netzer, T. Wang *et al.*, "Reading digits in natural images with unsupervised feature learning," in *NIPS workshop on deep learning and unsupervised feature learning*, vol. 2011, no. 2, 2011, p. 5. [Online]. Available: http://ufldl.stanford.edu/housenumbers/nips2011_housenumbers.pdf

[NWC⁺11b] Y. Netzer, T. Wang *et al.*, "The street view house numbers (SVHN) dataset," 2011. [Online]. Available: http://ufldl.stanford.edu/housenumbers/

[NYC16] A. Nguyen, J. Yosinski, and J. Clune, "Multifaceted feature visualization: Uncovering the different types of features learned by each neuron in deep neural networks," *arXiv preprint arXiv:1602.03616*, May 2016. [Online]. Available: https://arxiv.org/abs/1602.03616

[OHIL16] J. Ortigosa-Hernández, I. Inza, and J. A. Lozano, "Towards competitive classifiers for unbalanced classification problems: A study on the performance scores," *arXiv preprint arXiv:1608.08984*, Aug. 2016. [Online]. Available: https://arxiv.org/abs/1608.08984

[PMW⁺15] N. Papernot, P. McDaniel *et al.*, "Distillation as a defense to adversarial perturbations against deep neural networks," *arXiv preprint arXiv:1511.04508*, Nov. 2015. [Online]. Available: https://arxiv.org/abs/1511.04508

[Pre98] L. Prechelt, *Early Stopping - But When?* Berlin, Heidelberg: Springer Berlin Heidelberg, 1998, pp. 55–69. [Online]. Available: http://dx.doi.org/10.1007/3-540-49430-8_3

[RDS⁺14] O. Russakovsky, J. Deng *et al.*, "Imagenet large scale visual recognition challenge," *arXiv preprint arXiv:1409.0575*, vol. 115, no. 3, pp. 211–252, Sep. 2014. [Online]. Available: https://arxiv.org/abs/1409.0575

[RFB15] O. Ronneberger, P. Fischer, and T. Brox, "U-net: Convolutional networks for biomedical image segmentation," in *International Conference on Medical Image Computing and Computer-Assisted Intervention.* Springer, 2015, pp. 234–241. [Online]. Available: https://arxiv.org/abs/1505.04597

[RLS10] S. Risi, J. Lehman, and K. O. Stanley, "Evolving the placement and density of neurons in the hyperneat substrate," in *Conference on Genetic and evolutionary computation*, no. 12. ACM, 2010, pp. 563–570.

[RSG16] M. T. Ribeiro, S. Singh, and C. Guestrin, ""why should i trust you?": Explaining the predictions of any classifier," *arXiv preprint arXiv:1602.04938*, Feb. 2016. [Online]. Available: https://arxiv.org/abs/1602.04938

[Rud16]   S. Ruder, "An overview of gradient descent optimization algorithms," *arXiv preprint arXiv:1609.04747*, Sep. 2016. [Online]. Available: https://arxiv.org/abs/1609.04747

[SCL12]   P. Sermanet, S. Chintala, and Y. LeCun, "Convolutional neural networks applied to house numbers digit classification," in *International Conference on Pattern Recognition (ICPR)*, no. 21. IEEE, Apr. 2012, pp. 3288–3291. [Online]. Available: https://arxiv.org/abs/1204.3968

[SDG09]   K. O. Stanley, D. B. D'Ambrosio, and J. Gauci, "A hypercube-based encoding for evolving large-scale neural networks," *Artificial life*, vol. 15, no. 2, pp. 185–212, 2009. [Online]. Available: http://ieeexplore.ieee.org/document/6792316/

[SEZ+13]   P. Sermanet, D. Eigen *et al.*, "Overfeat: Integrated recognition, localization and detection using convolutional networks," *arXiv preprint arXiv:1312.6229*, Feb. 2013. [Online]. Available: https://arxiv.org/abs/1312.6229v4

[SHK+14]   N. Srivastava, G. E. Hinton *et al.*, "Dropout: a simple way to prevent neural networks from overfitting." *Journal of Machine Learning Research*, vol. 15, no. 1, pp. 1929–1958, 2014. [Online]. Available: https://www.cs.toronto.edu/~hinton/absps/JMLRdropout.pdf

[SHY+13]   A. Senior, G. Heigold *et al.*, "An empirical study of learning rates in deep neural networks for speech recognition," in *International Conference on Acoustics, Speech and Signal Processing*. IEEE, 2013, pp. 6724–6728. [Online]. Available: http://ieeexplore.ieee.org/document/6638963/?arnumber=6638963

[SIV16]   C. Szegedy, S. Ioffe, and V. Vanhoucke, "Inception-v4, inception-resnet and the impact of residual connections on learning," *arXiv preprint arXiv:1602.07261*, Feb. 2016. [Online]. Available: https://arxiv.org/abs/1602.07261

[SKP15]   F. Schroff, D. Kalenichenko, and J. Philbin, "Facenet: A unified embedding for face recognition and clustering," in *Conference on Computer Vision and Pattern Recognition (CVPR)*. IEEE, Mar. 2015, pp. 815–823. [Online]. Available: https://arxiv.org/abs/1503.03832

[SL11]   P. Sermanet and Y. LeCun, "Traffic sign recognition with multi-scale convolutional networks," in *International Joint Conference on Neural Networks (IJCNN)*, Jul. 2011, pp. 2809–2813. [Online]. Available: http://ieeexplore.ieee.org/document/6033589/

[SLJ+15]   C. Szegedy, W. Liu *et al.*, "Going deeper with convolutions," in *Conference on Computer Vision and Pattern Recognition (CVPR)*. IEEE, Sep. 2015, pp. 1–9. [Online]. Available: https://arxiv.org/abs/1409.4842

[SM02]   K. O. Stanley and R. Miikkulainen, "Evolving neural networks through

augmenting topologies," *Evolutionary computation*, vol. 10, no. 2, pp. 99–127, 2002. [Online]. Available: http://www.mitpressjournals.org/doi/abs/10.1162/106365602320169811

[SMG13]   A. M. Saxe, J. L. McClelland, and S. Ganguli, "Exact solutions to the nonlinear dynamics of learning in deep linear neural networks," *arXiv preprint arXiv:1312.6120*, Dec. 2013. [Online]. Available: https://arxiv.org/abs/1312.6120

[SMGS14] R. K. Srivastava, J. Masci *et al.*, "Understanding locally competitive networks," *arXiv preprint arXiv:1410.1165*, Oct. 2014. [Online]. Available: https://arxiv.org/abs/1410.1165

[SSSI]   J. Stallkamp, M. Schlipsing *et al.*, "The german traffic sign recognition benchmark." [Online]. Available: http://benchmark.ini.rub.de/?section=gtsrb&subsection=news

[SSSI12] J. Stallkamp, M. Schlipsing *et al.*, "Man vs. computer: Benchmarking machine learning algorithms for traffic sign recognition," *Neural Networks*, no. 0, pp. –, 2012. [Online]. Available: http://www.sciencedirect.com/science/article/pii/S0893608012000457

[SV16]   S. Saxena and J. Verbeek, "Convolutional neural fabrics," *arXiv preprint arXiv:1606.02492*, 2016. [Online]. Available: https://arxiv.org/abs/1606.02492

[SVI+15] C. Szegedy, V. Vanhoucke *et al.*, "Rethinking the inception architecture for computer vision," *arXiv preprint arXiv:1512.00567*, Dec. 2015. [Online]. Available: https://arxiv.org/abs/1512.00567v3

[SVZ13]   K. Simonyan, A. Vedaldi, and A. Zisserman, "Deep inside convolutional networks: Visualising image classification models and saliency maps," *arXiv preprint arXiv:1312.6034*, Dec. 2013. [Online]. Available: https://arxiv.org/abs/1312.6034

[SZ14]   K. Simonyan and A. Zisserman, "Very deep convolutional networks for large-scale image recognition," *arXiv preprint arXiv:1409.1556*, Sep. 2014. [Online]. Available: https://arxiv.org/abs/1409.1556

[SZS+13] C. Szegedy, W. Zaremba *et al.*, "Intriguing properties of neural networks," *arXiv preprint arXiv:1312.6199*, Dec. 2013. [Online]. Available: https://arxiv.org/abs/1312.6199v4

[TF-16a] "MNIST for ML beginners," Dec. 2016. [Online]. Available: https://www.tensorflow.org/tutorials/mnist/beginners/

[tf-16b]   "tf.nn.dropout," Dec. 2016. [Online]. Available: https://www.tensorflow.org/api_docs/python/nn/activation_functions_#dropout

[TH12]   T. Tieleman and G. Hinton, "Lecture 6.5-rmsprop: Divide the gradient by a running average of its recent magnitude," *COURSERA: Neural Networks for Machine Learning*, vol. 4, no. 2, 2012. [Online]. Available: http://www.cs.toronto.edu/~tijmen/csc321/slides/lecture_slides_lec6.pdf

[Tho14a]   M. Thoma, "On-line recognition of handwritten mathematical symbols," Karlsruhe, Germany, Nov. 2014. [Online]. Available: http://martin-thoma.com/write-math

[Tho14b]   M. Thoma, "The Twiddle algorithm," Sep. 2014. [Online]. Available: https://martin-thoma.com/twiddle/

[Tho16]   M. Thoma, "A survey of semantic segmentation," *arXiv preprint arXiv:1602.06541*, Feb. 2016. [Online]. Available: https://arxiv.org/abs/1602.06541

[Tho17a]   M. Thoma, "The HASYv2 dataset," *arXiv preprint arXiv:1701.08380*, Jan. 2017. [Online]. Available: https://arxiv.org/abs/1701.08380

[Tho17b]   M. Thoma, "Master thesis (blog post)," Apr. 2017. [Online]. Available: https://martin-thoma.com/msthesis

[VH13]   P. Verbancsics and J. Harguess, "Generative neuroevolution for deep learning," *arXiv preprint arXiv:1312.5355*, Dec. 2013. [Online]. Available: https://arxiv.org/abs/1312.5355

[vLA87]   P. J. M. van Laarhoven and E. H. L. Aarts, *Simulated annealing*. Dordrecht: Springer Netherlands, 1987, pp. 7–15. [Online]. Available: http://dx.doi.org/10.1007/978-94-015-7744-1_2

[VTKP17]   E. Vorontsov, C. Trabelsi *et al.*, "On orthogonality and learning recurrent networks with long term dependencies," *arXiv preprint arXiv:1702.00071*, Jan. 2017. [Online]. Available: https://arxiv.org/abs/1702.00071

[WHH+89]   A. Waibel, T. Hanazawa *et al.*, "Phoneme recognition using time-delay neural networks," *IEEE transactions on acoustics, speech, and signal processing*, vol. 37, no. 3, pp. 328–339, Aug. 1989. [Online]. Available: http://ieeexplore.ieee.org/document/21701/

[Wil92]   R. J. Williams, "Simple statistical gradient-following algorithms for connectionist reinforcement learning," *Machine learning*, vol. 8, no. 3-4, pp. 229–256, 1992.

[WWQ13]   X. Wang, L. Wang, and Y. Qiao, *A Comparative Study of Encoding, Pooling and Normalization Methods for Action Recognition.*   Berlin, Heidelberg: Springer Berlin Heidelberg, Nov. 2013, no. 11, pp. 572–585. [Online]. Available: http://dx.doi.org/10.1007/978-3-642-37431-9_44

[WYS$^+$15]   R. Wu, S. Yan *et al.*, "Deep image: Scaling up image recognition," *arXiv preprint arXiv:1501.02876*, vol. 7, no. 8, Jul. 2015. [Online]. Available: https://arxiv.org/abs/1501.02876v4

[WZZ$^+$13]   L. Wan, M. Zeiler *et al.*, "Regularization of neural networks using dropconnect," in *International Conference on Machine Learning (ICML)*, no. 30, 2013, pp. 1058–1066. [Online]. Available: http://www.matthewzeiler.com/pubs/icml2013/icml2013.pdf

[XGD$^+$16]   S. Xie, R. Girshick *et al.*, "Aggregated residual transformations for deep neural networks," *arXiv preprint arXiv:1611.05431*, Nov. 2016. [Online]. Available: https://arxiv.org/abs/1611.05431v1

[Xu11]   W. Xu, "Towards optimal one pass large scale learning with averaged stochastic gradient descent," *arXiv preprint arXiv:1107.2490*, Jul. 2011. [Online]. Available: https://arxiv.org/abs/1107.2490

[XWCL15]   B. Xu, N. Wang *et al.*, "Empirical evaluation of rectified activations in convolutional network," *arXiv preprint arXiv:1505.00853*, May 2015. [Online]. Available: https://arxiv.org/abs/1505.00853

[XXE12]   H. Xiao, H. Xiao, and C. Eckert, "Adversarial label flips attack on support vector machines." in *ECAI*, 2012, pp. 870–875. [Online]. Available: https://www.sec.in.tum.de/assets/Uploads/ecai2.pdf

[XZY$^+$14]   T. Xiao, J. Zhang *et al.*, "Error-driven incremental learning in deep convolutional neural network for large-scale image classification," in *International Conference on Multimedia*, no. 22.   ACM, 2014, pp. 177–186.

[YL98]   C. J. B. Yann LeCun, Corinna Cortes, "The MNIST database of handwritten digits," 1998. [Online]. Available: http://yann.lecun.com/exdb/mnist/

[ZBH$^+$16]   C. Zhang, S. Bengio *et al.*, "Understanding deep learning requires rethinking generalization," *arXiv preprint arXiv:1611.03530*, Nov. 2016. [Online]. Available: https://arxiv.org/abs/1611.03530

[ZCZL16]   S. Zhai, Y. Cheng *et al.*, "Doubly convolutional neural networks," in *Advances in Neural Information Processing Systems 29 (NIPS)*, D. D. Lee, M. Sugiyama *et al.*, Eds.   Curran Associates, Inc., Oct. 2016, pp. 1082–1090. [Online]. Available: http://papers.nips.cc/paper/6340-doubly-convolutional-neural-networks.pdf

[ZDGD14]   N. Zhang, J. Donahue *et al.*, "Part-based R-CNNs for fine-grained category detection," in *European Conference on Computer Vision (ECCV)*. Springer, Jul. 2014, pp. 834–849. [Online]. Available: https://arxiv.org/abs/1407.3867

[Zei12]   M. D. Zeiler, "Adadelta: an adaptive learning rate method," *arXiv preprint arXiv:1212.5701*, Dec. 2012. [Online]. Available: https://arxiv.org/abs/1212.5701v1

[ZF13]   M. D. Zeiler and R. Fergus, "Stochastic pooling for regularization of deep convolutional neural networks," *arXiv preprint arXiv:1301.3557*, Jan. 2013. [Online]. Available: https://arxiv.org/abs/1301.3557v1

[ZF14]   M. D. Zeiler and R. Fergus, "Visualizing and understanding convolutional networks," in *European Conference on Computer Vision (ECCV)*. Springer, Nov. 2014, pp. 818–833. [Online]. Available: https://arxiv.org/abs/1311.2901

[Zho16]   B. Zhou, "Places2 download," 2016. [Online]. Available: http://places2.csail.mit.edu/download.html

[ZK16]   S. Zagoruyko and N. Komodakis, "Wide residual networks," *arXiv preprint arXiv:1605.07146*, May 2016. [Online]. Available: https://arxiv.org/abs/1605.07146

[ZKL+15]   B. Zhou, A. Khosla *et al.*, "Learning deep features for discriminative localization," *arXiv preprint arXiv:1512.04150*, Dec. 2015. [Online]. Available: https://arxiv.org/abs/1512.04150

[ZKL+16]   B. Zhou, A. Khosla *et al.*, "Places: An image database for deep scene understanding," *arXiv preprint arXiv:1610.02055*, Oct. 2016. [Online]. Available: https://arxiv.org/abs/1610.02055

[ZL16]   B. Zoph and Q. V. Le, "Neural architecture search with reinforcement learning," *arXiv preprint arXiv:1611.01578*, Nov. 2016. [Online]. Available: https://arxiv.org/abs/1611.01578

[ZMGL15]   J. Zhao, M. Mathieu *et al.*, "Stacked what-where auto-encoders," *arXiv preprint arXiv:1506.02351*, Jun. 2015. [Online]. Available: https://arxiv.org/abs/1506.02351v1

[ZYL+15]   H. Zheng, Z. Yang *et al.*, "Improving deep neural networks using softplus units," in *International Joint Conference on Neural Networks (IJCNN)*, Jul. 2015, pp. 1–4.

I. Glossary

ANN artificial neural network. 4

ASO Automatic Structure Optimization. 29

CMO Confusion Matrix Ordering. 2, 35, 36, 51, 52, 71

CNN Convolutional Neural Network. 1, 3–6, 11, 13, 15, 21–23, 28, 29, 31, 33, 37, 54, 60, 71, 72, 79, 82–84, 88–91

ELU Exponential Linear Unit. 38, 57, 60–64, 72, 73, 77, 78, 84

ES early stopping. 68

FC Fully Connected. 91, 93

FLOP floating point operation. 27, 29, 87, 88, 90, 91, 93

GA genetic algorithm. 30

GAN Generative Adverserial Network. 80

GPU graphics processing unit. 37, 40, 59, 63, 67, 88, 91

HSV hue, saturation, value. 79

LCN Local Contrast Normalization. 91

LDA linear discriminant analysis. 79

LReLU leaky rectified linear unit. 63, 72, 77, 78, 84

MLP multilayer perceptron. 3–6, 28

NAG Nesterov Accellerated Momentum. 83

NEAT NeuroEvolution of Augmenting Topologies. 83

OBD Optimal Brain Damage. 29